Flood, R.D., Piper, D.J.W., Klaus, A., et al., 1995
Proceedings of the Ocean Drilling Program, Initial Reports, Vol. 155

20. SITE 944[1]

Shipboard Scientific Party[2]

HOLE 944A

Date occupied: 12 May 1994

Date departed: 16 May 1994

Time on hole: 3 days, 10 hr, 30 min

Position: 5°56.335′N, 47°45.469′E

Bottom felt (drill pipe measurement from rig floor, m): 3712.6

Distance between rig floor and sea level (m): 11.30

Water depth (drill pipe measurement from sea level, m): 3701.3

Penetration (m): 384.20

Number of cores (including cores having no recovery): 41

Total length of cored section (m): 384.20

Total core recovered (m): 208.01

Core recovery (%): 54

Oldest sediment cored:
Depth (mbsf): 384.20
Nature: Silty clay
Earliest age: Pleistocene

HOLE 944B

Date occupied: 16 May 1994

Date departed: 16 May 1994

Time on hole: 7 hr, 15 min

Position: 5°56.259′N, 47°45.606′E

Bottom felt (drill pipe measurement from rig floor, m): 3708.2

Distance between rig floor and sea level (m): 11.40

Water depth (drill pipe measurement from sea level, m): 3696.8

Penetration (m): 47.80

Number of cores (including cores having no recovery): 6

Total length of cored section (m): 47.80

Total core recovered (m): 46.81

Core recovery (%): 97

Oldest sediment cored:
Depth (mbsf): 47.80
Nature: Silty clay
Earliest age: Pleistocene

HOLE 944C

Date occupied: 16 May 1994

Date departed: 16 May 1994

Time on hole: 3 hr, 15 min

Position: 5°56.415′N, 47°45.339′E

Bottom felt (drill pipe measurement from rig floor, m): 3721.9

Distance between rig floor and sea level (m): 11.40

Water depth (drill pipe measurement from sea level, m): 3710.5

Penetration (m): 9.60

Number of cores (including cores having no recovery): 1

Total length of cored section (m): 9.60

Total core recovered (m): 9.60

Core recovery (%): 100

Oldest sediment cored:
Depth (mbsf): 9.60
Nature: Silty clay
Earliest age: Pleistocene

HOLE 944D

Date occupied: 16 May 1994

Date departed: 17 May 1994

Time on hole: 13 hr, 30 min

Position: 5°56.424′N, 47°45.332′E

Bottom felt (drill pipe measurement from rig floor, m): 3719.9

Distance between rig floor and sea level (m): 11.40

Water depth (drill pipe measurement from sea level, m): 3708.5

Penetration (m): 44.60

Number of cores (including cores having no recovery): 5

Total length of cored section (m): 44.60

Total core recovered (m): 43.37

Core recovery (%): 97

Oldest sediment cored:
Depth (mbsf): 44.60
Nature: Silty clay
Earliest age: Pleistocene

Principal results: Site 944 (near proposed Site AF-3) is located on the middle Amazon Fan, on the eastern levee of the Amazon Channel, down-fan from the Amazon-Brown avulsion point. The site is about 2 km from the channel axis and on the outside of a meander bend. It is one of a series of sites designed to understand the evolution of the Amazon Channel-levee System. It was also designed to sample the Unit R Debris Flow, the Middle

[1]Flood, R.D., Piper, D.J.W., Klaus, A., et al., 1995. *Proc. ODP, Init. Repts.*, 155: College Station, TX (Ocean Drilling Program).

[2]Shipboard Scientific Party is as given in the list of participants in the contents.

and Lower Levee complexes, and the equivalent of interglacial calcareous clays previously recovered up-fan at Sites 935 and 936. The site was expected to be more sandy than these previous sites, and Quad-combination and FMS logs were planned to better understand the geometry of sand beds and debris-flow deposits.

The site was selected from a *Conrad* seismic-reflection profile (C2514; 0557UTC on 4 Dec. 1984). We located Site 944 at a corresponding position on a *JOIDES Resolution* seismic-reflection profile (2020UTC on 11 May 1994).

Hole 944A was cored by APC to 97.1 mbsf, then by XCB to 384.2 mbsf, with total hole recovery of 208.1 m (54.1%). Hole 944B was offset 300 m to the southwest and cored to 47.8 mbsf and recovered 46.81 m (97.9%). Hole 944C was offset 300 m to the northeast of Hole 944A and failed to obtain a mud-line core (cored and recovered 9.6 m). Hole 944D, 20 m from Hole 944C, was cored to 44.6 mbsf, with total recovery of 43.37 m (97.2%). This hole was sampled in detail for pore-water and diagenetic-mineral studies. Hole 944A was logged from 74 to 384 mbsf.

Temperature measurements made in Hole 944A at 51 and 80 mbsf (ADARA) show a mean gradient of 39°C/km, with a steeper geothermal gradient at depth. There was gas expansion in many cores. Methane was found throughout the hole, but higher hydrocarbons were not detected.

Six lithologic units are recognized. Depths are based on a type section in Hole 944A.

Unit I (0–0.54 mbsf) is a Holocene, bioturbated, foraminifer-nannofossil clay, with up to 38% carbonate.

Unit II (0.54–191.60 mbsf) consists of mud with interbedded laminae and beds of silt and very fine sand. The mud has 2%–3% carbonate content. The unit is subdivided into four subunits. Subunit IIA (0.54–15.38 mbsf) comprises intensely bioturbated mud, stained to varying degrees by black hydrotroilite. Subunit IIB (15.38–37.42 mbsf) consists of mud with silt laminae. An interval of sediment deformation interpreted as a slump occurs from 32.4 to 36.9 mbsf. Subunit IIC (37.42–163.23) comprises mud with laminae of silt and thin beds of silt, and very fine, fine, and medium sand. The frequency of silt and sand beds fluctuates through the unit, but no very fine sand beds occur above 111 mbsf, and no medium sand above 143 mbsf. Moderate bioturbation is common. Two thin intervals of contorted or dipping beds occur at 44 and 57 mbsf. Wireline log data suggest that sand is common in the interval of poor recovery in the lower half of the subunit, notably at 122–128 mbsf and 158–180 mbsf. Subunit IID (182.00 to 191.60 mbsf) consists of mud with thin beds and laminae of silt and thin beds of fine sand. Log data suggest that this subunit forms a coarsening-upward sequence. Seismic correlation shows that Unit II corresponds to levees of the Amazon and Brown Channel-levee systems, and high-amplitude reflection packets (HARPs) associated with the Brown, Purple, and Orange systems, with some interbedded distal levee deposits of the Purple System.

Unit III (191.60–268.70 mbsf) consists of various types of mud that appear to occur as blocks and have been affected by soft-sediment deformation. Many carbonate-rich clasts are found in the upper and middle parts of the unit. This unit is interpreted as a mass-transport deposit that correlates seismically with the Unit R Debris Flow. Log data show generally rather uniform gamma-ray response, except for a washed-out interval at 226–233 mbsf. High resistivity from 218 to 226 mbsf corresponds to an interval with large numbers of carbonate-rich clasts in cores. Color-reflectance data suggest that the interval from 192 to 220 mbsf is compositionally different from the interval from 230 to 260 mbsf.

Unit IV (268.70–335.40 mbsf) consists of mud with laminae and thin beds of silt and sand. This unit correlates seismically with the Red Channel-levee System. Two subunits are distinguished on the basis of the occurrence of sand beds. Subunit IVA (268.70–293.07 mbsf) consists of bioturbated and color-banded mud with abundant laminae of silt. Subunit IVB (293.07–355.40 mbsf) consists of mud with numerous silt laminae and thin beds of silt and very fine sand. Only 1 m of core was recovered in the lower 47 m of this subunit, and logs suggest that the base of the subunit is at 352 mbsf. The borehole diameter is particularly large through this subunit, which affected the quality of log data. Log characteristics in general are similar to those in the lower part of Subunit IIC and suggest several coarsening-upward sequences within Subunit IVB, whereas Subunit IVA is more uniformly fine grained.

Unit V (355.40–357.53 mbsf) contains two short intervals of nannofossil-foraminifer-rich clay, with up to 17% carbonate content, passing both uphole and downhole into nannofossil-bearing clay. The entire unit suffered severe coring disturbance. Wireline log data suggest that this lithology extends uphole to about 352 mbsf.

Unit VI (357.53–384.20 mbsf) consists of mud with laminae and thin beds of silt. It correlates seismically with the levee of the Green Channel-levee System. Log data suggest a downhole increase in the abundance of silt.

Foraminifer and nannofossil abundances are generally high in Units I and V, and in some calcareous clasts in Unit III. Otherwise, nannofossils are almost absent, and foraminifers are in low abundance in Subunits IIA and IIB and Unit VI, and rare to absent in Subunits IIC and IID and Unit IV. *P. obliquiloculata* was not detected above the Unit III debris-flow deposit, but this could result from the low foraminifer abundance. Some clasts in Unit III contain well-preserved nannofossils of Zone CN15a, indicating that the debris-flow deposit is older than 85 ka. In Unit V, the well-preserved and abundant nannofossils, dominated by *Gephyrocapsa*, and foraminifers, including *G. tumida* and *G. tumida flexuosa*, indicate interglacial conditions. The nannofossils are of Zone CN14b (0.26–0.46 Ma) and are similar to those sampled at depth at Sites 935 and 936.

Short-wavelength oscillations in magnetic inclination, declination, and remanence intensity were detected throughout the APC cores, with generally 2–4 cycles per meter. These oscillations are interpreted as geomagnetic secular variation. No magnetic excursion was found in APC cores.

A detailed pore-water profile in Hole 944D showed that alkalinity peaks at 4.4 mbsf (22 mM), decreasing to 10 mM by 10 mbsf and then remaining approximately constant. Pore-water sulfate decreases to zero by 4.4 mbsf; at the same depth, phosphate peaks at 0.4 mM. Dissolved iron concentrations are variable. Pore-water geochemical profiles at this site change more rapidly with depth than at Sites 931 and 939.

Elevated total sulfur (0.5%–1.5%) was measured in the lower part of Unit III (debris flow) and the lower part of Unit V. Total organic carbon decreases from about 0.9% in Unit II to 0.7% in Unit VI. Log data show anomalously low values of velocity from 305 to 315 mbsf, which may indicate higher concentrations of gas in the formation. Cores from this interval had an unusual number of gas-filled voids. An interval from 17 to 22 mbsf shows almost constant water content and does not appear to have undergone normal compaction. Similar intervals were identified near the top of Sites 939 and 940. The detailed samples of reactive iron minerals taken at this site may help determine if these zones of constant water content are related to diagenesis.

Site 944 sampled a similar stratigraphic section to Site 936, but farther down-fan. Units II and IV, corresponding to levee and HARP sediment in the Upper and Middle Levee complexes, respectively, were sandier than in Site 936. The Unit III mass-transport deposit is thinner and has a higher proportion of decimeter- to meter-sized blocks compared with Site 936. As at Site 936, the carbonate-rich layer above the Lower Levee Complex is of interglacial origin, possibly isotopic Stage 9. At this site, the series of holes away from the levee crest shows substantial changes in silt bed thickness and abundance over distances of a few hundred meters, which, together with data from Site 943 in the adjacent channel, will permit analysis of turbidity-current flow dynamics and deposition.

SETTING AND OBJECTIVES

Introduction

Site 944 (proposed Site AF-3) was one of a series of sites designed to characterize the development of the most recently active channel of the Amazon Fan (the Amazon Channel). The deepest hole planned for this site penetrated the contact between the Amazon and Brown levees and the flank of the Brown levee, the high-amplitude reflection packets (HARPs) beneath the Brown Channel, the Unit R Debris Flow, the Red levee of the Middle Levee Complex, and terminated in the Green levee of the Lower Levee Complex (nomenclature from Manley and Flood, 1988). Short B and C holes were planned to offset Hole 944A 300 m on either side to study lateral sediment variability near the levee crest and to obtain closely spaced samples of pore water and diagenetic minerals.

Setting

Site 944 is located on the eastern (right) levee of the Amazon Channel, about 2 km from the channel axis and on the outside of a meander bend (Fig. 1 of "Site 943" chapter, this volume). Channel geometry and near-surface sedimentation patterns have been studied using multibeam bathymetric data and piston cores (Flood et al., 1991; Pirmez, 1994). The site was selected from a *Conrad* seismic profile (C2514; 0557UTC on 4 Dec. 1984). We located Site 944 at a similar position on our *JOIDES Resolution* profile (2020UTC on 11 May 1994; Fig. 3 of "Site 943" chapter, this volume).

The channel and levee at this site developed following the avulsion, up-fan, of the Amazon Channel from the Brown Channel. In seismic profiles over Site 944 (Fig. 3 of "Site 943" chapter, this volume), the most recent Amazon (right) levee is underlain by the Brown (left) levee, which in turn is underlain by a HARP. The HARP at this site should include sediment deposited as the Brown levee evolved, overlying sediment deposited prior to the Aqua-Brown avulsion. The record at this site needs to be compared with the records from Sites 939, 940, 935, 936, and 946 to characterize the growth of these most recent levees (see back-pocket foldout). The onsite 3.5-kHz profile (Fig. 2 of "Site 943" chapter, this volume) shows that the uppermost 34 ms of sediment is weakly laminated lying on top of a more reflective but diffuse layer. The upper layer may be related to the Amazon System, whereas the diffuse horizon may be the contact with the Brown levee.

Deeper units sampled at this site include the Unit R Debris Flow, sampled upslope at Sites 935 and 936; the Red levee of the Middle Levee Complex, sampled upslope at Site 936; and the Green levee of the Lower Levee Complex, also sampled at Site 936. At Site 936, the Red levee is located to the west of the Green levee. Between Sites 936 and 944, the Red levee has crossed over the Green levee and here lies to the east of the Green levee. At Site 936, the region east of the Red levee was characterized by a 50-m sandy interval that was not recovered well by coring. Site 944 samples the region west of the Red levee.

Objectives

The principal objectives at Site 944 were to:

1. Sample the Amazon levee deposits to characterize turbidity current dynamics and to compare the sediment record here with those of other near-channel sites, including Site 943 in the channel.
2. Sample the Amazon levee and Brown levee deposits downslope from the Brown avulsion to characterize levee evolution.
3. Sample the multiple HARP units that underlie the levee.
4. Characterize the downslope evolution of Unit R Debris Flow.
5. Sample the Middle and Lower Levee complexes to characterize levee facies.
6. Recover deep carbonate layers similar to those observed at Sites 935 and 936.

Additional objectives of the B and C holes were to characterize lateral sediment variability on the levee crest, and to sample pore water and diagenetic minerals in detail, for comparison with Site 939.

The logging objectives at Site 944 were to characterize the various sedimentary units drilled by their log response, particularly to establish thickness and patterns of sand beds that are poorly recovered by coring.

OPERATIONS

Transit: Site 943 to Site 944 (AF-20)

We moved the 1.5 nmi from Site 943 to Site 944 (AF-3) in dynamic positioning mode in about 2 hr. At 2200 hr 12 May, we deployed a beacon at 5°56.354′N, 47°45.473′W.

Hole 944A

We positioned the bit at 3702.0 mbrf and attempted to spud Hole 944A at 2330 hr 12 May, but the core was empty. We lowered the bit 5 m, to 3707.0 mbrf, and spudded Hole 944A at 0023 hr 13 May. The distance from sea level to rig floor, which depends on the ship's draft, was 11.32 m for Hole 944A and 11.41 m for Holes 944B, 944C, and 944D. Core 1H recovered 3.87 m, and the mud line was defined to be at 3712.6 mbrf. Cores 1H through 11H were taken from 3712.6 to 3809.7 m (0–97.1 mbsf) and recovered 86.92 m (89.5%; Table 1).

While taking Cores 10H and 11H, the core barrel only partially stroked, and an overpull of 40,000 to 50,000 lb was observed when extracting Cores 9H, 10H, and 11H from the sediment. Cores 3H through 11H were oriented using the Tensor tool. ADARA heat-flow measurements were taken during Cores 6H and 9H. Parts of Cores 10H, 30X, 31X, and 32X were disturbed as a result of either gas-induced extrusion of core from the liner onto the rig floor or collapsed core liners. One liner had to be pumped out of the core barrel.

XCB Cores 12X through 41X were taken from 3809.7 to 4096.8 m (97.1–384.2 mbsf), coring 287.1 m and recovering 121.17 m (42.2%). The overall APC/XCB recovery was 54.4%. The FCV was run in defeated (inactive) mode on alternate cores through Core 30X and from Cores 31X through 41X. The pump rate and pressure were increased while taking Cores 23X through 29X to increase the rate of penetration through the debris flow. Cores 34X through 38X were taken in soft material. It took less than 10 min to cut each core (sand) with 8-finger core catchers instead of the 8-finger/4-petal combination that had been used throughout most of the leg. Cores 39X and 40X were severely disturbed because the 4-petals were installed backwards. They would not fully retract; therefore, the core was trimmed and deformed by them.

In preparation for logging, we circulated a 20- and then a 30-barrel sepiolite and seawater mixture. While pulling the pipe up to 73.4 mbsf we experienced negligible overpull. We encountered 15 m of soft fill on the trip back to the bottom of the hole. The go-devil was dropped to open the lockable flapper valve, the bottom 310 m of hole was filled with sepiolite mud (8.8 parts per gallon), and the pipe was pulled back up to 92.0 mbsf for logging. At the end of each logging run, we pulled the bit up to 74 mbsf to obtain logs of the upper parts of the hole. We first ran the Quad combo in to 3437.0 mbrf (384.2 mbsf), and no fill was encountered. This logging run lasted about 5 hr. We then ran the FMS tool in to 3437.0 mbrf (384.2 mbsf), and once again we encountered no fill. This run lasted about 4.75 hr. The hole diameter ranged from 11 to 13 in. (28–33 cm) down to 305 mbsf, where it increased to 15 in. (38 cm). The bit cleared the seafloor at 0824 hr 16 May.

Hole 944B

We moved 300 m to the west-southwest (bearing 240°) of Hole 944A in dynamic positioning mode. We positioned the bit at 3699.0 mbrf and spudded Hole 944B at 1010 hr 16 May. Core 1H recovered 0.32 m, and the mud line was defined to be at 3708.2 mbrf. Although we recovered only a short core, it appears to have been a good mud-line core. In addition, the core liner was cracked while taking Core 1H. Cores 1H through 6H were taken from 3708.2 to 3756.0 m (0–47.8 mbsf), coring 47.8 m and recovering 46.81 m (97.9%). Parts of

Table 1. Site 944 coring summary.

Core	Date (1994)	Time (UTC)	Depth (mbsf)	Length cored (m)	Length recovered (m)	Recovery (%)
155-944A-						
1H	May 13	0440	0.0–3.9	3.9	3.87	99.2
2H	May 13	0550	3.9–13.4	9.5	5.59	58.8
3H	May 13	0645	13.4–22.9	9.5	10.23	107.7
4H	May 13	0745	22.9–32.4	9.5	0.42	4.4
5H	May 13	0835	32.4–41.9	9.5	10.19	107.2
6H	May 13	0950	41.9–51.4	9.5	9.65	101.0
7H	May 13	1100	51.4–60.9	9.5	10.15	106.8
8H	May 13	1240	60.9–70.4	9.5	9.46	99.6
9H	May 13	1355	70.4–79.9	9.5	10.43	109.8
10H	May 13	1515	79.9–89.4	9.5	9.20	96.8
11H	May 13	1625	89.4–97.1	7.7	7.73	100.0
12X	May 13	1740	97.1–104.9	7.8	6.35	81.4
13X	May 13	1855	104.9–114.5	9.6	7.71	80.3
14X	May 13	2005	114.5–124.1	9.6	0.00	0.0
15X	May 13	2110	124.1–133.8	9.7	0.59	6.1
16X	May 13	2235	133.8–143.4	9.6	6.94	72.3
17X	May 13	2340	143.4–153.1	9.7	1.18	12.1
18X	May 14	0105	153.1–162.7	9.6	0.32	3.3
19X	May 14	0210	162.7–172.4	9.7	0.53	5.5
20X	May 14	0320	172.4–182.0	9.6	0.00	0.0
21X	May 14	0510	182.0–191.6	9.6	3.03	31.5
22X	May 14	0710	191.6–201.2	9.6	8.77	91.3
23X	May 14	0850	201.2–210.9	9.7	8.21	84.6
24X	May 14	1055	210.9–220.5	9.6	9.62	100.0
25X	May 14	1240	220.5–230.1	9.6	9.87	103.0
26X	May 14	1440	230.1–239.7	9.6	7.26	75.6
27X	May 14	1640	239.7–249.4	9.7	0.10	1.0
28X	May 14	1900	249.4–259.0	9.6	6.24	65.0
29X	May 14	2055	259.0–268.7	9.7	0.00	0.0
30X	May 14	2230	268.7–278.3	9.6	9.61	100.0
31X	May 15	0000	278.3–288.0	9.7	9.25	95.3
32X	May 15	0135	288.0–297.6	9.6	9.67	101.0
33X	May 15	0255	297.6–307.3	9.7	7.82	80.6
34X	May 15	0415	307.3–316.9	9.6	1.00	10.4
35X	May 15	0540	316.9–326.6	9.7	0.02	0.2
36X	May 15	0745	326.6–336.2	9.6	0.00	0.0
37X	May 15	0915	336.2–345.9	9.7	0.00	0.0
38X	May 15	1050	345.9–355.4	9.5	0.42	4.4
39X	May 15	1255	355.4–364.9	9.5	2.40	25.2
40X	May 15	1535	364.9–374.5	9.6	0.62	6.5
41X	May 15	1755	374.5–384.2	9.7	3.56	36.7
Coring totals				384.2	208.0	54.10
155-944B-						
1H	May 16	1430	0.0–0.3	0.3	0.32	100.0
2H	May 16	1545	0.3–9.8	9.5	10.46	110.1
3H	May 16	1640	9.8–19.3	9.5	8.60	90.5
4H	May 16	1735	19.3–28.8	9.5	10.21	107.5
5H	May 16	1825	28.8–38.3	9.5	8.55	90.0
6H	May 16	1925	38.3–47.8	9.5	8.67	91.2
Coring totals				47.8	46.8	97.90
155-944C-						
1H	May 16	2252	0.0–9.6	9.6	9.60	100.0
Coring totals				9.6	9.6	100.00
155-944D-						
1H	May 16	2335	0.0–6.6	6.6	6.60	100.0
2H	May 17	0035	6.6–16.1	9.5	8.95	94.2
3H	May 17	0100	16.1–25.6	9.5	7.92	83.3
4H	May 17	0145	25.6–35.1	9.5	9.85	103.0
5H	May 17	0230	35.1–44.6	9.5	10.05	105.8
Coring totals				44.6	43.4	97.20

Note: An expanded version of this coring summary table that includes lengths and depths of sections, location of whole-round samples, and comments on sampling disturbance is included on the CD-ROM in the back pocket of this volume.

Cores 5H and 6H were disturbed as a result of split core liners. Cores 3H through 6H were oriented with the Tensor tool. No heat-flow measurements were taken. The bit cleared the seafloor at 1545 hr 16 May.

Hole 944C

We moved the ship 600 m east-northeast (060°) in dynamic positioning mode. We positioned the bit at 3720.0 mbrf and attempted to spud-in. A small amount of gray clay (probably from just below the mud line) was in the core catcher, and apparently whatever mud-line core had been in the liner had fallen out. We then positioned the bit at 3722.0 mbrf and spudded Hole 944C at 1835 hr 16 May. Core 1H recovered 9.60 m, and the mud line was defined to be at 3721.9 mbrf. However, it appeared that the mud line was not recovered, and we suspected that Core 1H was taken about 2.0 m below the mud line (about 2.0–11.6 mbsf). We decided to terminate Hole 944C, and the bit cleared the seafloor at 1900 hr 16 May.

Hole 944D

We did not move the ship, positioned the bit at 3717.0 mbrf, and spudded Hole 944D at 1915 hr 16 May. Core 1H recovered 6.60 m, and the mud line was defined to be at 3719.9 mbrf. APC Cores 1H through 5H were taken from 3717.0 to 3764.5 mbrf (0–44.6 mbsf) and recovered 43.37 m (97.2%). Parts of Cores 4H and 5H were disturbed as a result of either gas-induced extrusion of core from the liner onto the rig floor or collapsed core liners. The bit cleared the seafloor at 2305 hr and cleared the rig floor at 0823 hr 17 May. In preparation for the end of the leg, we inspected the bottom-hole assembly on the trip out.

LITHOSTRATIGRAPHY

Introduction

Hole 944A, located near the levee crest of the Amazon Channel on the middle fan, penetrated 384.20 mbsf through the Amazon levee, the Unit R debris-flow deposit, and the Red and Gold Channel-levee systems (Figs. 1 and 2). Only 54.10% of the cored sequence was recovered. Holes 944B and 944D were laterally offset 300 m from Hole 944A; both penetrated to approximately 50 mbsf. The lithologic interpretation of the site is based on Hole 944A. The intervals of poor core recovery, especially from 114 mbsf to 191 mbsf (Cores 944A-14X through -21X), from 240 mbsf to 269 mbsf (Cores 944A-27X through -29X), and from 307 mbsf to 384.2 mbsf (Cores 944A-34X through -41X), have been supplemented by downhole logging data to more precisely define lithostratigraphic boundaries. Expansion of methane gas during core recovery affected the sediment by disrupting the primary sedimentary structures in some silt and sand beds, and by producing void spaces within some of the core sections (see "Lithostratigraphy" section in the "Explanatory Notes" chapter, this volume).

Description of Lithostratigraphic Units

Unit I

Intervals: 155-944A-1H-1, 0–54 cm; 155-944B-1H-CC; 155-944D-1H, 0–35 cm
Age: Holocene
Depth: 0 to 0.54 mbsf

Unit I consists of 0.54 m of moderately burrowed foraminifer-nannofossil clay, which grades in color from yellowish brown (10YR 5/4; 0–0.21 mbsf) through light yellowish brown (10YR 6/4; 0.21–0.36 mbsf) to grayish brown (5Y 5/2; 0.36–0.52 mbsf). The unit contains three 0.5-cm-thick, diagenetic, dark brown (10YR 4/3) horizons at 0.21, 0.23, and 0.25 mbsf, as well as a semi-indurated, 1-cm-thick, very dark grayish-brown (2.5Y 3/2), iron-rich "crust" at 0.53–0.54 mbsf. Similar horizons and iron-rich "crusts" were analyzed previously and correlated throughout the Amazon Fan and adjacent Guiana Basin (Damuth, 1977; see "Introduction" chapter, this volume). The iron-rich "crust" marks the lower boundary of Unit I. The carbonate content at 0.07 mbsf is 38% and decreases to 25% at 0.42 mbsf (see "Organic Geochemistry" section, this chapter).

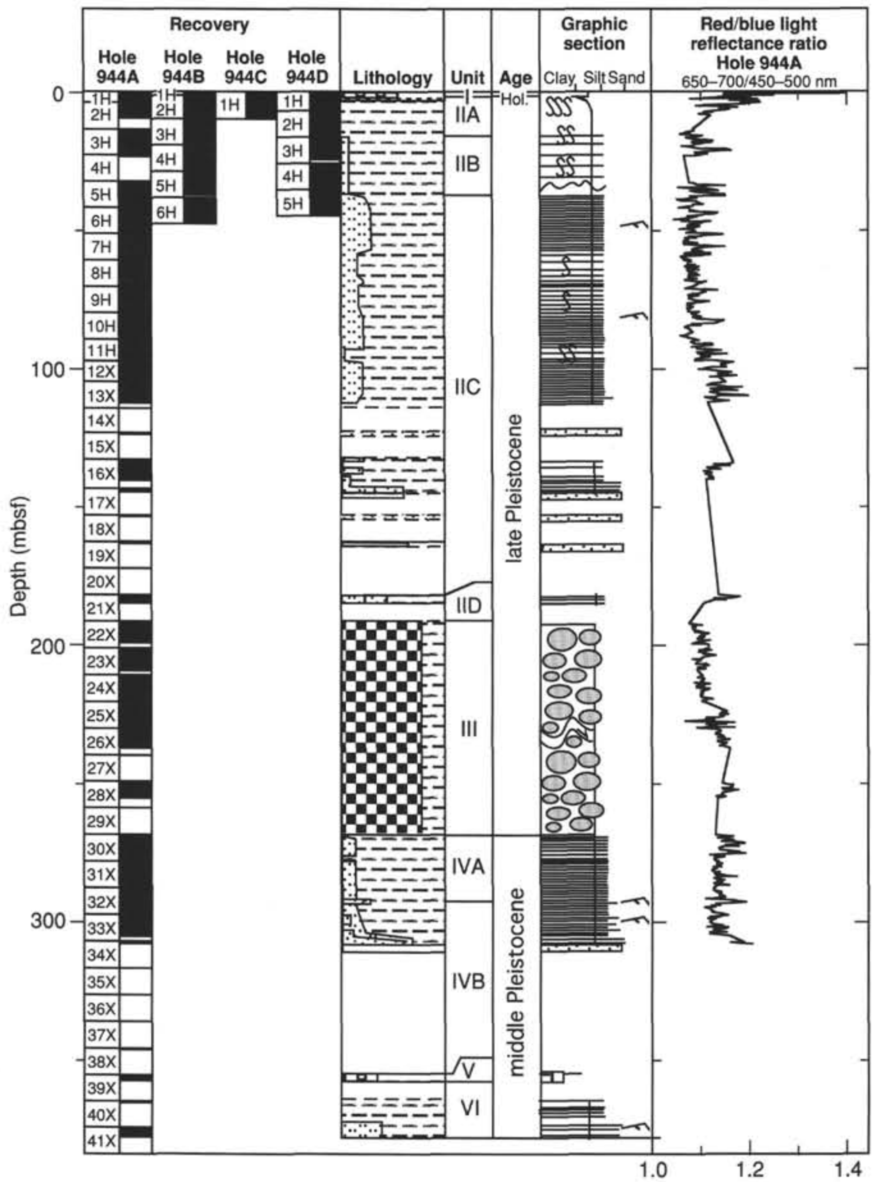

Figure 1. Composite stratigraphic section for Site 944 showing core recovery in all holes, simplified summary of lithology primarily for Hole 944A, depths of unit boundaries, age, a graphic section with generalized grain-size and bedding characteristics, and downhole variations in light-reflectance values. The lithologic symbols are explained in Figure 1 of the "Explanatory Notes" chapter, this volume.

Unit II

Intervals: 155-944A-1H-1, 54 cm, through -22X-1, 0 cm; 155-944B-1H-CC, 26 cm, through -6H-CC (bottom of the hole); 155-944C-1H-CC; 155-944D-1H-1, 35 cm, through -5H-CC (bottom of the hole)
Age: late Pleistocene
Depth: 0.54 to 191.60 mbsf

Unit II consists of about 190 m of olive gray (5Y 4/2) to very dark gray (5Y 3/1) terrigenous clay, silty clay, silt, and sand. A large proportion of the sediment is stained to varying degrees by diagenetic hydrotroilite, which imparts a black (N2/0) color to the sediment in the form of irregular patches and/or color bands and laminae (see "Introduction" chapter, this volume). The carbonate content of Unit II is low and averages 2.5%. Unit II has been subdivided into four subunits based on the occurrence and frequency of silty clay, silt laminae, and thin beds of sand (Figs. 1 and 2). Subunits IIA, IIB, and IIC are identified in Holes 944B and 944D, though the base of Subunit IIC was not recovered at either hole.

Subunit IIA

Subunit IIA extends from 0.54 to 15.38 mbsf (interval 944A-1H-1, 54 cm, through -3H-2, 48 cm), and consists of olive gray (5Y 4/2) clay that grades to dark gray (5Y 4/1) silty clay at approximately 1.50 mbsf. The subunit is moderately to heavily bioturbated and color mottled with black (N2/0) hydrotroilite. A few black (N2/0) laminae are present also.

Subunit IIB

Subunit IIB extends from 15.38 to 37.42 mbsf (interval 944A-3H-2, 94 cm, through -5H-4, 52 cm) and is characterized by very dark gray (5Y 3/1) silty clay that contains silt laminae. The boundary between Subunits IIA and IIB is placed at the uppermost occurrence of

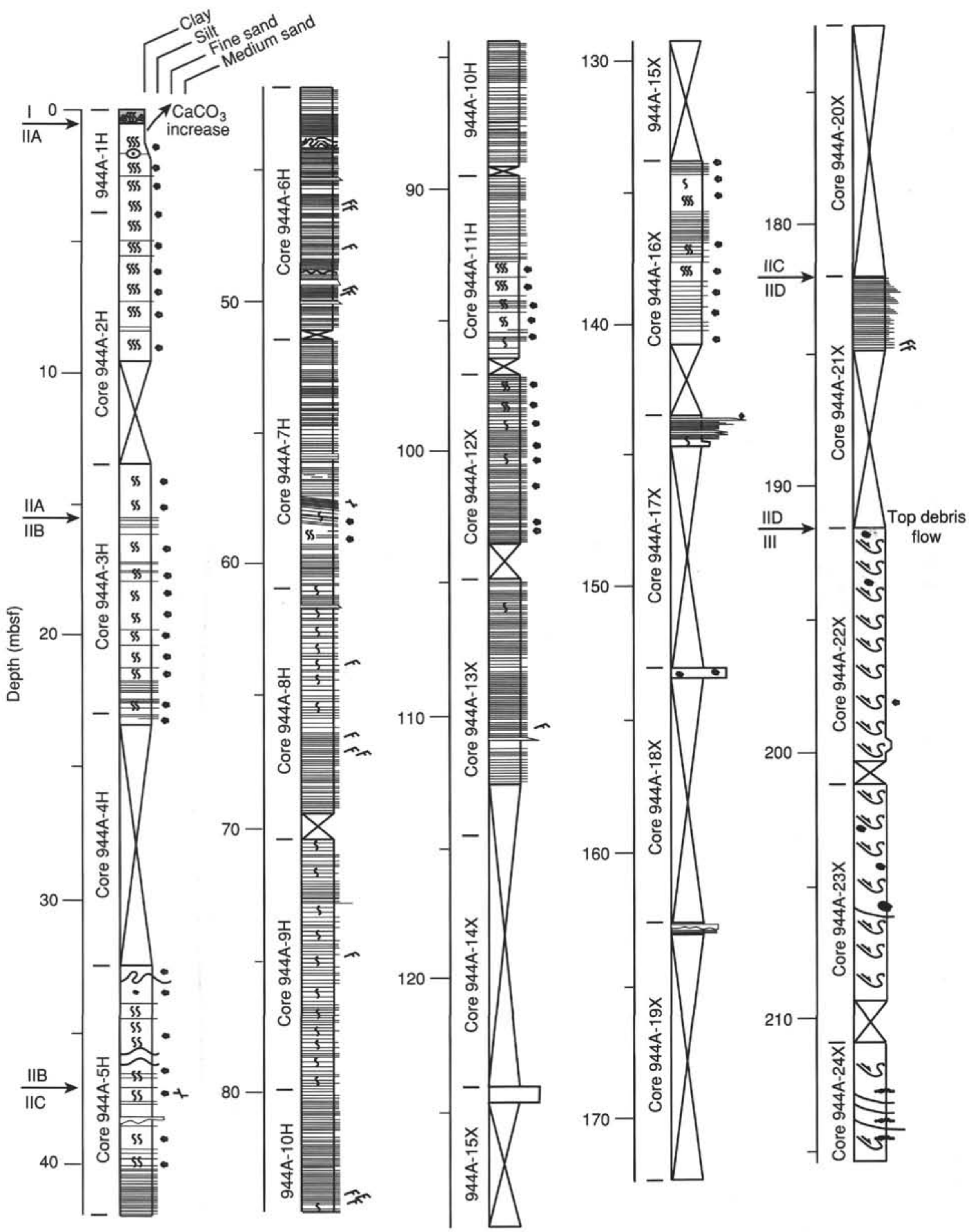

Figure 2. Graphic sedimentological columns for Site 944 showing grain-size variation (width of columns), bed thickness, and sedimentary structures; symbols and preparation of these columns are explained in the "Lithostratigraphy" section of the "Explanatory Notes" chapter, this volume. Arrows indicate the positions of unit and subunit boundaries. The upper part of the column is shown in the longitudinal profile of the foldout (back pocket, this volume) to show the down-fan changes in levee deposits. Void subtraction but no compression was applied to cores for which the ODP official recovery was less than 100%, although many of these cores also showed evidence for pervasive gas expansion.

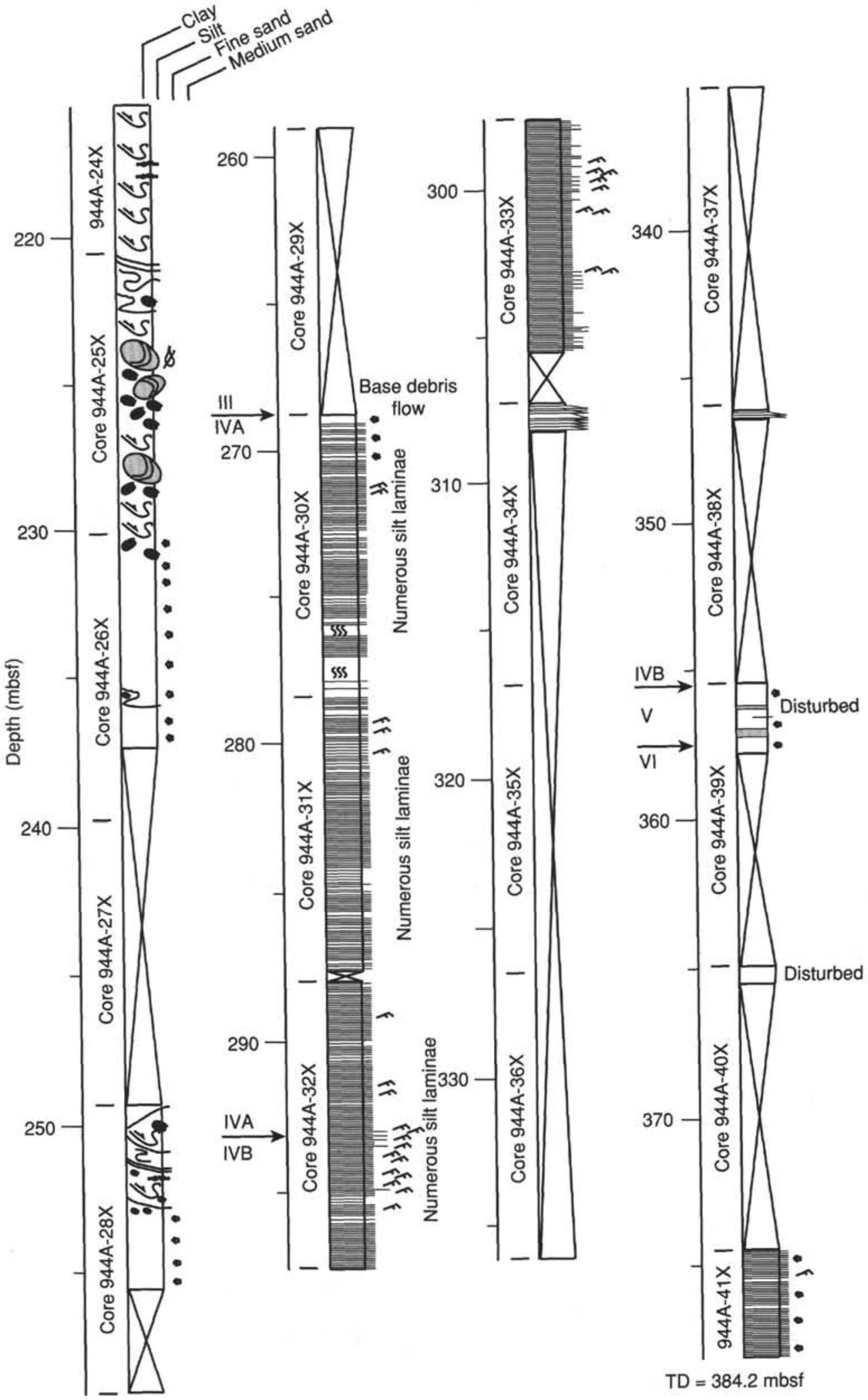

Figure 2 (continued).

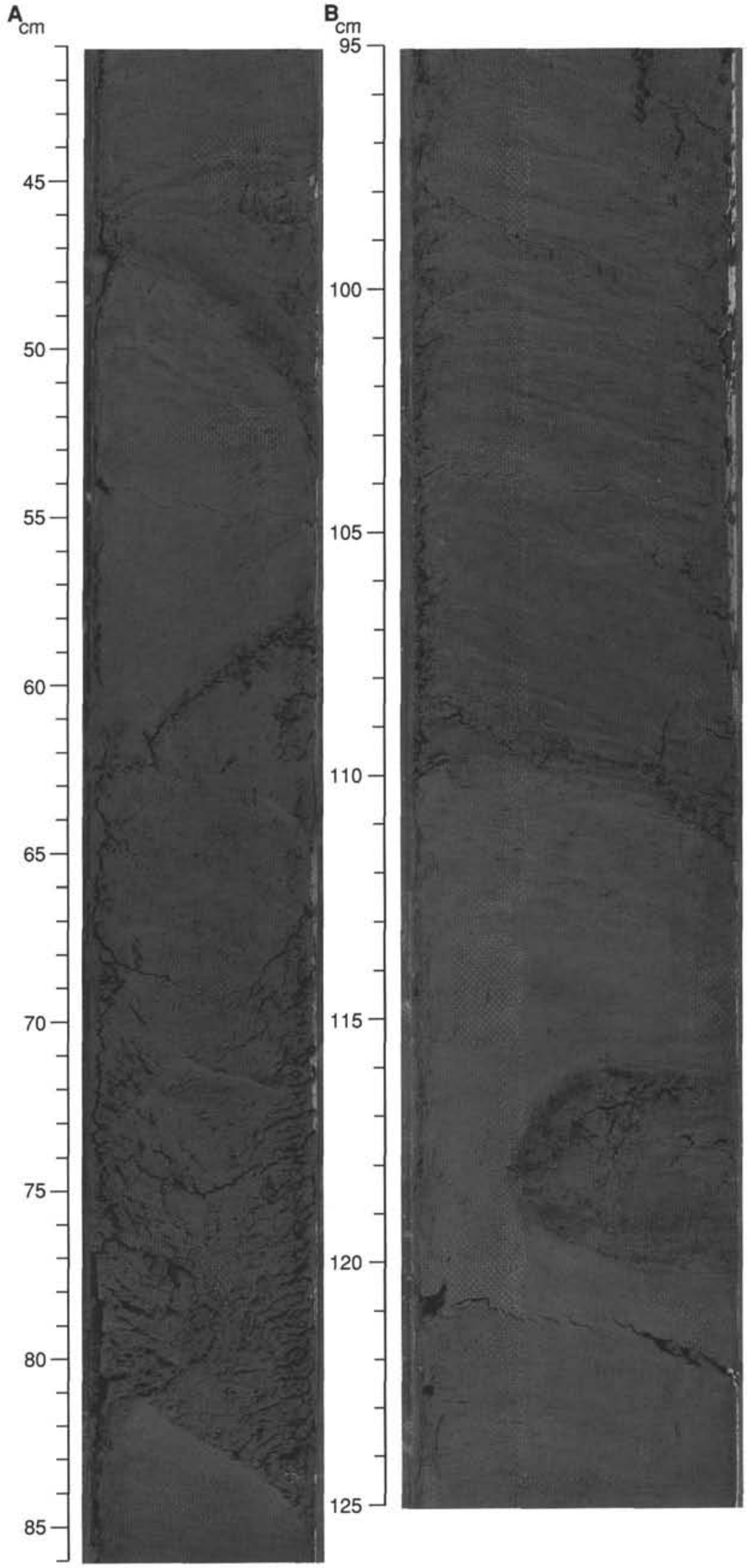

Figure 3. Contorted bedding highlighted by grain-size variation of primary sedimentary fabric from Subunit IIB. These features are interpreted as slumps within levee sequences. **A.** 155-944A-5H-1, 41–86 cm. **B.** 155-944A-5H-1, 95–125 cm.

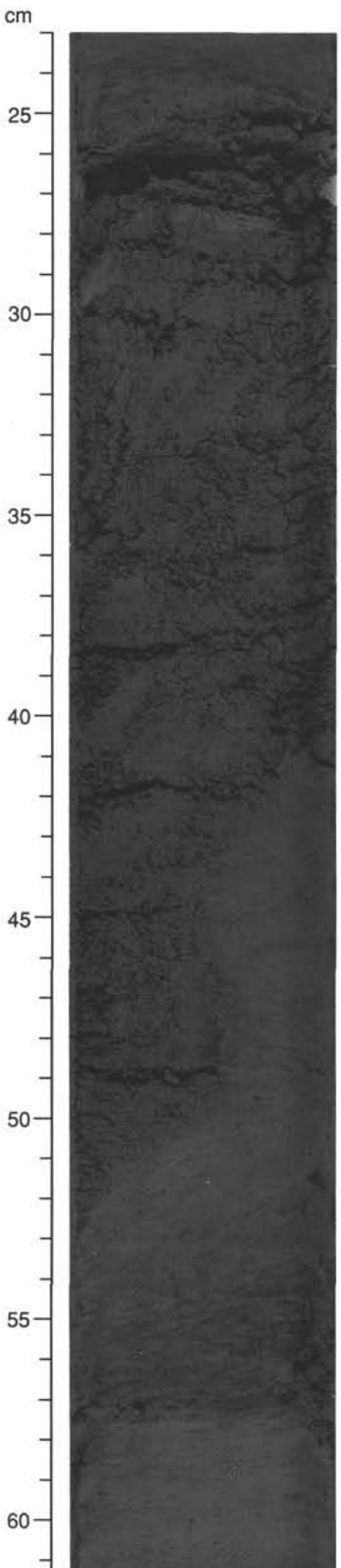

Figure 4. Contorted bedding highlighted by grain-size variation in sedimentary fabric in Subunit IIB. This feature is interpreted as a slump (155-944A-5H-5, 23–62 cm).

silt laminae. On average, between one and three silt laminae occur per meter of core. An interval of soft-sediment deformation, including folds (Figs. 3 and 4), occurs between 32.40 and 36.90 mbsf (Section 944A-5H-1 through -5H-3 at 150 cm).

Subunit IIC

Subunit IIC extends from 37.42 to 182.00 mbsf (interval 944A-5H-4, 52 cm, through -21X-1H, 0 cm) and consists of very dark gray (5Y 3/1) and dark olive gray (5Y 3/2) silty clay containing silt laminae and thin beds of silt, very fine, fine, and medium sand. The boundary between Subunits IIB and IIC is placed at the first thin bed that contains very fine sand. Two intervals of contorted bedding, interpreted as small-scale slumps, occur between 38.80 and 39.00 mbsf, and between 43.98 and 44.08 mbsf (Fig. 5). The interval between 57.53 and 57.71 mbsf contains dipping beds (Fig. 6), black (N2/0) color banding and mottling. Moderate levels of bioturbation are common throughout the subunit.

The frequency and occurrence of coarser grained laminae and thin beds fluctuate throughout Subunit IIC, ranging between five and 30 layers per meter, though no distinctive cycles related to the frequency of silt and fine sand deposition are apparent in the interval between 37 mbsf and 112 mbsf (Fig. 2). The first bed of very fine sand occurs at 110.97 mbsf (Section 944A-13X-5, at 11 cm) and of coarse to medium sand at 143.63 mbsf (Section 944A-17X-1, at 23 cm). Some of the beds in this interval are T_{bcde} turbidites (Bouma, 1962). The interval between 112 mbsf and the base of the subunit at 185 mbsf has very low recovery. An 18-cm-thick interval of disturbed very fine sand was recovered between 124.39 and 124.57 mbsf. A 6.94-m interval of very dark gray (5Y 3/1) silty clay with silt laminae was recovered between 133.80 and 140.74 mbsf (Core 944A-16X). Between 143.40 and 144.58 mbsf (Core 944A-17X), thin beds and laminae of fine to medium sand are interbedded with very dark gray (5Y 3/1) silty clays. The interval between 153.10 and 153.42 mbsf (Core 944A-18X) consists of olive gray (5Y 4/2) fine to medium silt with two centimeter-thick mud clasts, and the interval between 162.70 and 163.23 mbsf consists of very dark gray (5Y 3/1) silty clay with thin to medium beds of very fine to coarse sand. The fluctuation in grain size and bed thickness downhole is best defined by gamma-ray and resistivity logs; these logs indicate sandy deposits from 115 to 182 mbsf, which could account for the poor recovery in this interval.

Subunit IID

This subunit extends from 182 to 191.60 mbsf (interval 944A-21X-1, 0 cm, through -22X-1, 0 cm) and consists of dark olive gray (5Y 3/2) silty clay that contains thin beds and laminae of silt; some beds are cross-laminated (Fig. 7). Groups of fining- and thinning-upward fine sand beds, between 1 and 3 cm thick, occur throughout this interval.

Unit III

Interval: 155-944A-22X-1, 0 cm, through -30X-1, 0 cm
Age: late Pleistocene
Depth: 191.60 to 268.70 mbsf

No core was recovered between 185.03 and 191.60 mbsf. The upper boundary of lithostratigraphic Unit III is placed at the top of Core 944A-22X because downhole logs constrain the boundary between 188 mbsf and 193 mbsf (see "Downhole Logging" section, this chapter). Unit III consists of 77.10 m of clays and silty clays ranging through dark gray (5Y 4/1, 5Y 3/1, 10Y 3/1), dark olive gray (5Y 3/2), dark greenish gray (5GY 3/1, 5GY 4/1, 5GY 5/1), and black (5GY 2.5/1, 5Y 2.5/1, N2/0). The carbonate content is generally low (1%–2%) throughout the unit, although some carbonate-rich intervals do occur.

The limited lithologic evidence indicates the sediment within Unit III have been affected by soft-sediment deformation and redeposition

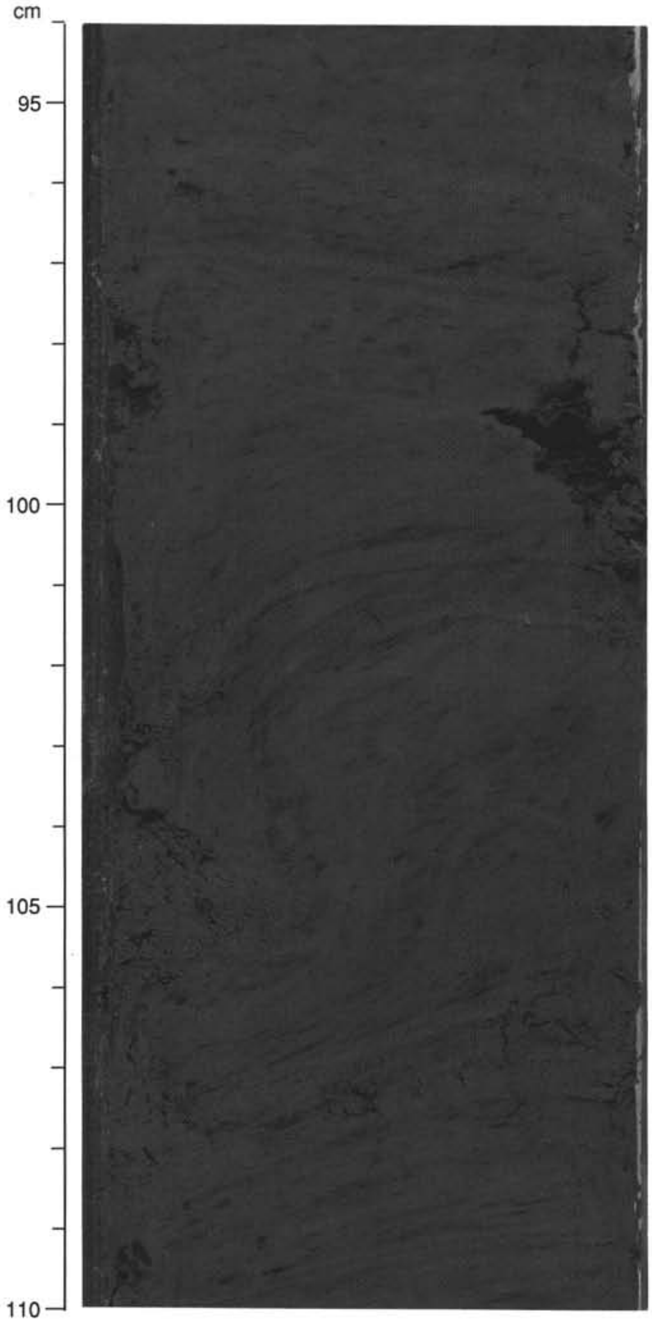

Figure 5. Small-scale slump as inferred from contorted laminae in Subunit IIC (155-944A-6H-2, 94–110 cm).

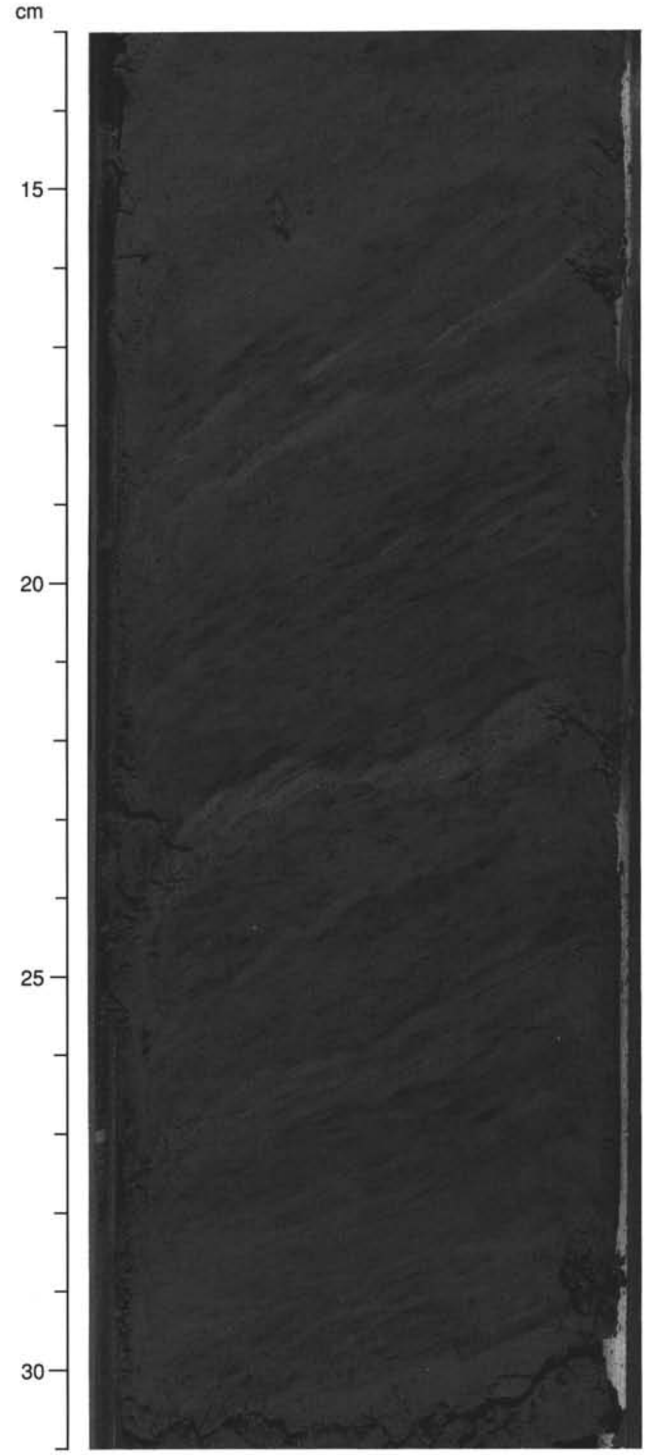

Figure 6. Dipping beds offset by small-scale faults highlighted by color-banded laminae in Subunit IIC (155-944A-7H-5, 13–31 cm).

as evidenced by abrupt changes in lithology and color, folds (Fig. 8), discordant stratal relationships between dipping laminae, beds, and lithologic contacts (Fig. 9), and the occurrence of clasts of various sizes. Light-colored clasts (Figs. 10 and 11) are found in several intervals in this unit (944A-22X-5, 0–70 cm; -23X-2, 23 cm, through -23X-3, 9 cm; -23X-4, 33–43 cm; 25X-5, 90–160 cm; and 25X-6, 56–60 cm). These clasts are carbonate-rich (32% carbonate in Sample 944A-25X-5, 94–95 cm). No clear lithologic subdivisions could be identified in the unit. The dipping beds and folded strata in Unit III are broken into 1- to 2-cm-thick "drilling biscuits" as a result of rotary coring with the XCB system, producing multiple apparent-dip directions that define a "wood-grain" structure in several cores (Fig. 12; see "Lithostratigraphy" section in the "Explanatory Notes" chapter, this volume).

Unit IV

Interval: 155-944A-30X-1, 0 cm, through -39X-1, 0 cm
Age: middle Pleistocene
Depth: 268.70 to 355.40 mbsf

Lithologic Unit IV is 86.70 m thick and consists of terrigenous, very dark gray (5Y 3/1) silty clay with silt laminae and thin beds of silt and sand. In general, carbonate content is low with an average of approximately 3.5%. The unit has been divided into two subunits on the basis of the occurrence of silt laminae and beds of silt and sand.

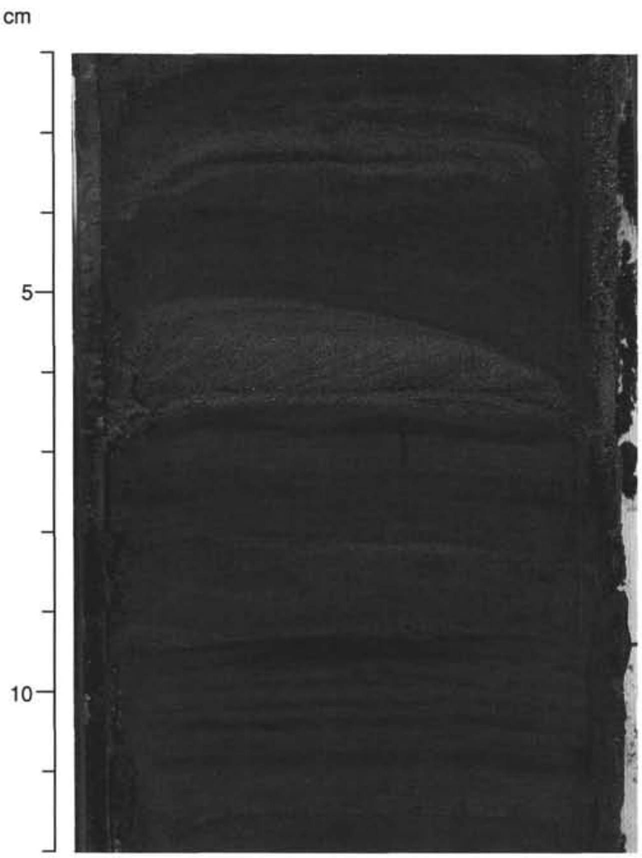

Figure 7. Silt laminae and thin beds of silt in Subunit IID. The bed located between 5 and 7 cm is cross-laminated (155-944A-21X-CC, 2–12 cm).

Subunit IVA

Subunit IVA consists of 24.37 m (268.70 to 293.07 mbsf; Section 944A-30X-1 through -32X-4, 110 cm) of very dark gray (5Y 3/1) silty clay, with black (N2/0) color banding and moderate levels of bioturbation. The interval from the top to 271.23 mbsf is distinct from the lower part of this subunit, in that it contains numerous discontinuous silt laminae together with streaked intervals of hydrotroilite staining. This fabric may have resulted as a consequence of deformation during the deposition of the mass transport deposit of Unit III. Below 271.23 mbsf, silt laminae and rare thin beds of silt occur. Some of the silt beds have irregular ?scoured bases and truncated tops; the latter may be an artifact of drilling (Fig. 13). A maximum of 105 laminae and beds per meter occurs in Section 944A-30X-3; average values for the interval are between 30 and 50 per meter.

Subunit IVB

Subunit IVB is a 62.33-m-thick interval (293.07 to 355.40 mbsf; Section 944A-32X-4, 110 cm, through -39X-1 at 0 cm) of very dark gray (5Y 3/1) silty clay that contains numerous silt laminae and thin beds of silt and sand. The uppermost boundary of the subunit is placed at the first fine sand bed. The frequency and thickness of silt and sand beds increase downhole (Fig. 2). Many of the beds are parallel- or cross-laminated. The use of downhole logging data has enabled extrapolation of this lithologic unit downhole through the 47-m-thick interval of virtually no recovery between 308 mbsf and the next interval of sediment recovery at 355 mbsf. The wireline log data indicate that the base of this subunit is at approximately 350 mbsf.

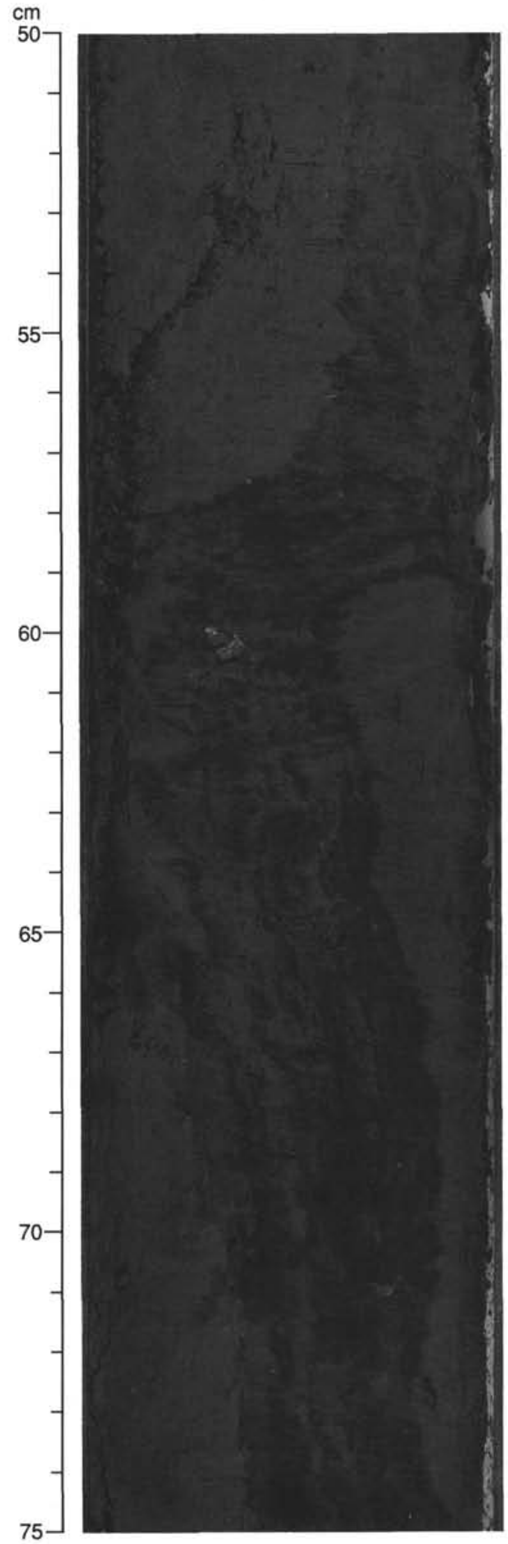

Figure 8. Folded and contorted bedding from Unit III (155-944A-25X-3, 50–75 cm), which is inferred to be a mass-transport deposit (Unit R).

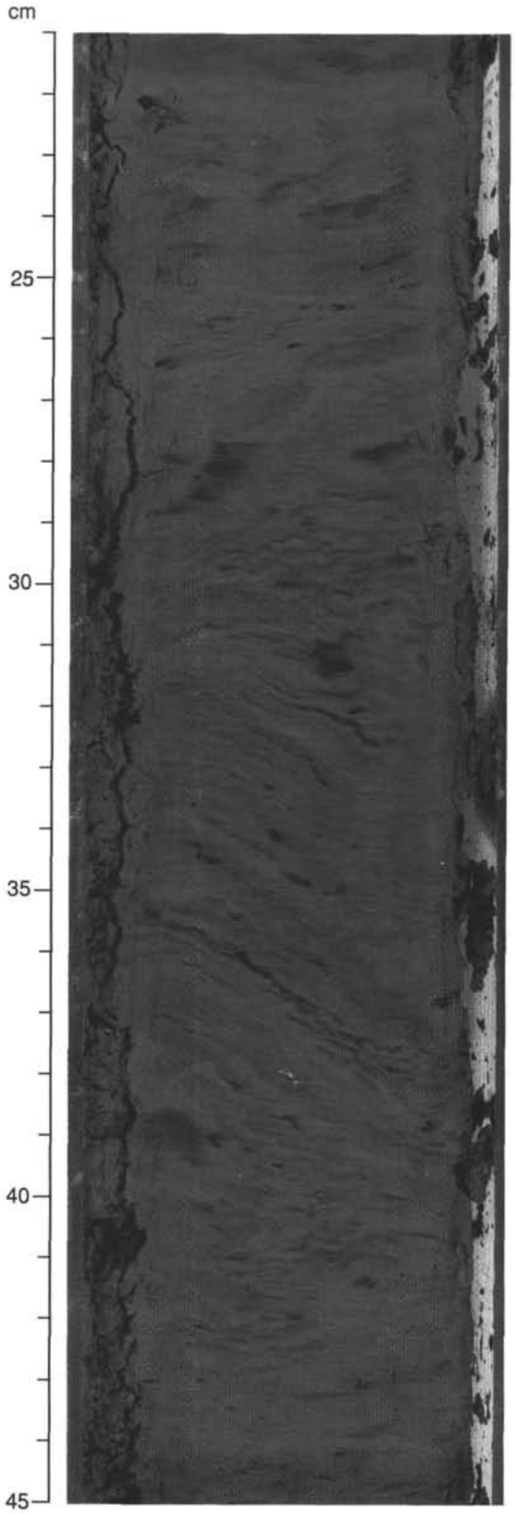

Figure 9. Dipping and contorted bedding within the inferred mass-flow deposit of Unit III (Unit R) (155-944A-23X-1, 21–45 cm).

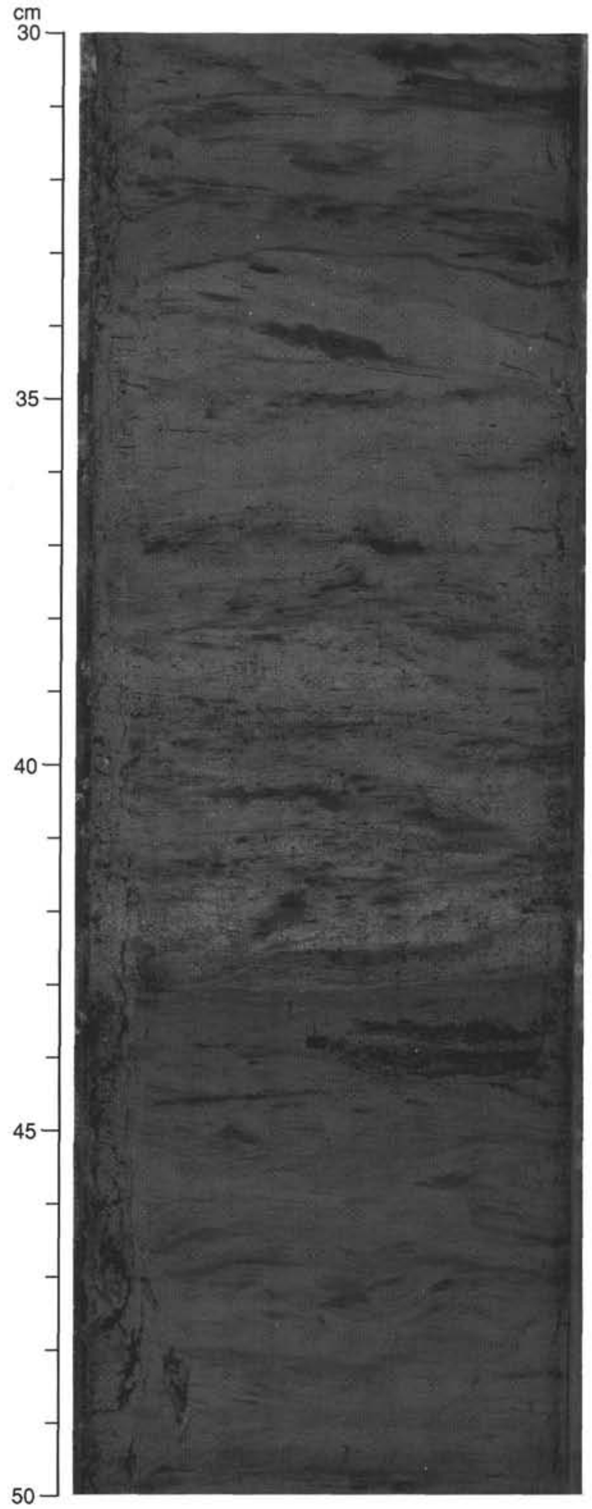

Figure 10. Carbonate-rich clast (lighter colored sediment between 33 and 43 cm) within the inferred debris-flow deposit of Unit III (155-944A-23X-4, 30–50 cm).

Unit V

Interval: 155-944A-39X-1, 0 cm, through -39X-2, 63 cm
Age: middle Pleistocene
Depth: 355.40 to 357.53 mbsf

Drilling operations seriously disrupted this 2.13-m interval of very dark gray (5Y 3/1) silty clay and lighter colored calcareous clay. Carbonate content in the recovered interval ranges from a minimum of 4.5% (Sample 944A-39X-2, 45–63 cm) to a maximum of 17.4% (Sample 944A-39X-2, 0–20 cm). The most carbonate-rich intervals, which are greenish gray (5GY 5/1), are 944A-39X-1, 77–92 cm, and 944A-39X-2, 0–30 cm.

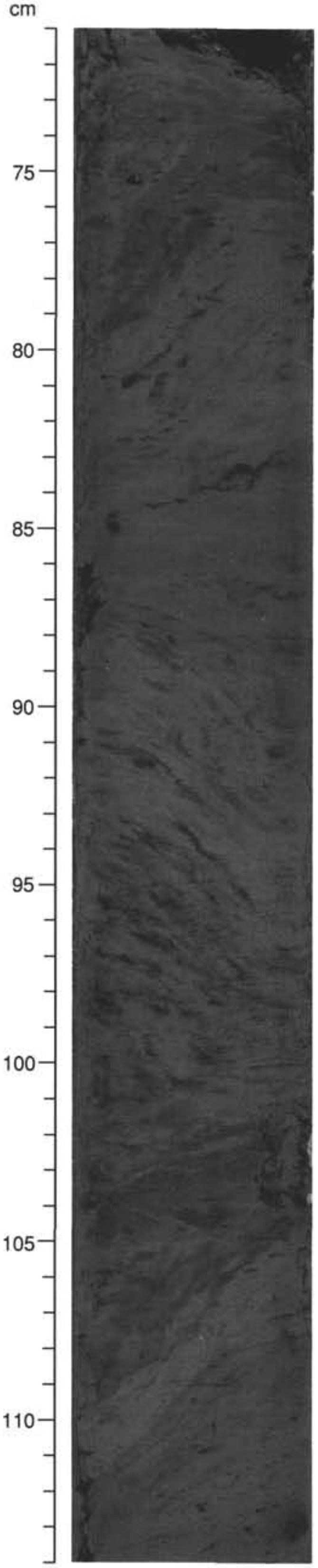

Figure 11. Carbonate-rich folded and contorted clast (lighter colored sediment between 90 and 110 cm) within the inferred debris-flow deposit of Unit III (155-944A-25X-5, 71–114 cm).

Unit VI

Interval: 155-944A-39X-2, 63 cm, through -41X-CC
Age: middle Pleistocene
Depth: 357.53 to 384.20 mbsf

Unit VI consists of very dark gray (5Y 3/1) and dark olive gray (5Y 3/2) silty clay with approximately 20 laminae and thin beds of silt per meter. The frequency of silt and sand layers does not fluctuate significantly throughout this unit. Carbonate content is 3.5% in Sample 944A-40X, 15–16 cm.

Mineralogy

Mineralogy was determined by X-ray diffraction analysis of 24 bulk samples of silty clay, together with routine semiquantitative study of smear slides. The common minerals identified by XRD are quartz, plagioclase, augite, and the clay minerals smectite, illite (+ mica), and kaolinite (Table 2). Half of the XRD samples contain minor K-feldspar; four contain hornblende. Relative to quartz, the abundances of feldspars and ferromagnesian minerals show little stratigraphic variation (Fig. 14A). The phyllosilicate mineral group with the highest relative peak intensity is illite + mica (Fig. 14B).

Spectrophotometry

Reflectance of visible light was low throughout the sediment column recovered at Site 944. Maximum reflectance levels of 35% characterize the yellowish brown (10YR 5/4) calcareous clay in Unit I. Reflectance values obtained from the dark olive gray to very dark gray silty clay, silt, and sand in all other units range from 10% to 25%. No measurements were made in Units V or VI because of poor core recovery. The ratio between spectral reflectance values for the red (650–700 nm) and the blue (450–500 nm) spectrum averages 1.12 (Fig. 1). The highest red/blue ratio was measured in the gray calcareous clay of Unit I, and is attributed to the high content of iron oxyhydroxides. Enhanced red reflectance also corresponds to the occurrence of thicker silt and sand beds in Subunits IIB and IIC (e.g., overall coarsening downward, 85 to 110 mbsf) and also in Subunits IVA and IVB. Relatively high red reflectance associated with silt and sand beds originates from iron-oxide-stained quartz grains.

The lowest values of the red/blue ratio coincide with the clays and silty clays in Subunits IIB and IIC, but a correlation between Holes 944A, 944B, and 944D is elusive because of the high-frequency variability of the reflectance record. This variability is determined by millimeter- to centimeter-scale silt laminations and thin gas-expansion cracks and by changes in the intensity and variation of color banding or mottling. Low red/blue ratios, comparable to those in Subunits IIB and IIC, were also measured in the upper part of Unit III (Cores 944A-22X through -24X). The greenish gray to dark greenish gray (5GY 3/1 to 5GY 5/1) carbonate-rich clay clasts at 225 mbsf in Core 944A-25X are marked by low (<1:1) red/blue ratios.

Discussion

A substantial proportion of the recovered sediment (Subunits IIB, IIC, IID; Units IV, VI) consists of silty clays, which contain silt laminae and thin beds of silt and fine sand. These deposits are similar to those at most other Leg 155 sites and are interpreted as levee sequences built by overbank deposition by turbidity currents. The frequency and occurrence of these layers fluctuate throughout Site 944. This variation depends on the stage of levee growth and/or the supply of material to this location on the fan (Fig. 2). The medium to coarse sand recovered in Subunit IIC may form the top of the high-amplitude reflection packet (HARP) at the base of the Brown Channel-levee System; Units IV and VI are interpreted to be the Red and

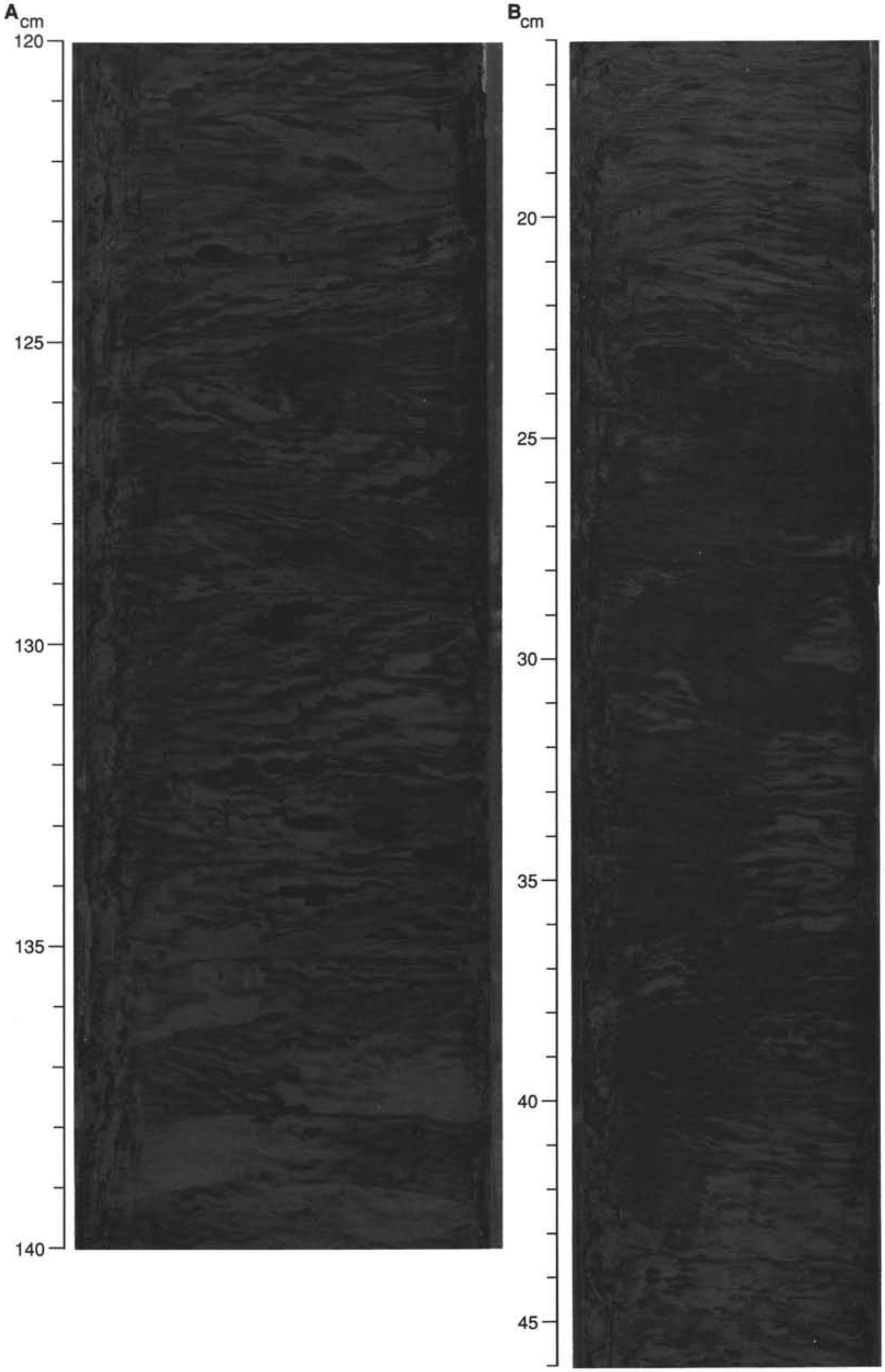

Figure 12. Two intervals of "wood-grain" fabric in Unit III that result from rotary drilling. **A.** 155-944A-22X-4, 120–140 cm. **B.** 155-944A-22X-4, 16–46 cm.

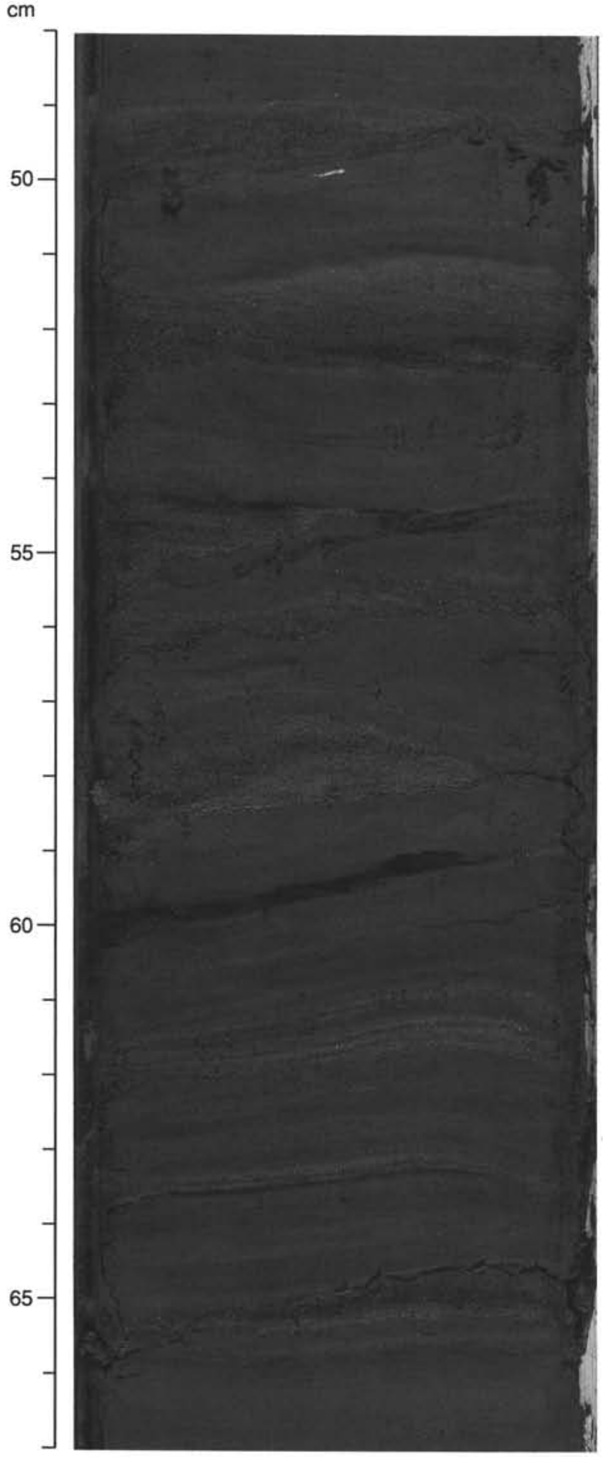

Figure 13. Laminae and thin beds of silt in Subunit IVA. Some of the beds have irregular ?scoured bases and are truncated, although the latter may be an artifact of drilling (155-944A-30X-3, 48–67 cm).

Green Channel-levee systems, respectively. Unit V is inferred to be the deposit of a high sea-level stand on top of the Green Channel-levee System. Unit III is the Unit R debris-flow deposit, which has been recovered at other Leg 155 sites. Subunit IIA and Unit I are common to all Leg 155 sites and consist of hemipelagic calcareous clay and silty clay, which are inferred to reflect the decrease in terrigenous input to the fan in response to sea-level rise during the late Pleistocene–Holocene.

BIOSTRATIGRAPHY

Calcareous Nannofossils

An abundant and well-preserved nannofossil assemblage with low diversity is present in the calcareous nannofossil and foraminifer clay (Unit I) in the mud-line sample (Table 3). Nannofossils are rare or absent in the underlying hemipelagic Unit II. The exceptions to this are in lighter colored bands in Unit IIC at 52.41 mbsf (Sample 944A-7H-1, 101 cm), which contain rare etched specimens of *Gephyrocapsa,* and at 103.44 mbsf (Sample 944A-12X-CC, 34–35 cm), where a poorly preserved nannoflora from Zone CN15 is present. Other light-colored intervals at 143.56 mbsf and at 154.22 mbsf within Unit IIC were calcareous but contained no calcareous nannofossils (Samples 944A-17X-1, 16–17 cm, and -19X-1, 8 cm).

Unit III contains calcareous nannofossils at 206.10 mbsf (Fig. 15), where nannofossil assemblages from Zone CN15 (Sample 944A-23X-4, 40 cm) and *Gephyrocapsa*-dominated assemblages at 219.26 and 226.61 mbsf (e.g., Samples 944A-24X-6, 86 cm, and -25X-5, 11 cm, respectively) are present. Nannofossils are rare or absent from 268.7 to 355.4 mbsf within Unit IV.

The carbonate-rich Unit V from 355.4 to 357.5 mbsf contains a well-preserved, highstand nannofossil assemblage dominated by species of the genus *Gephyrocapsa* (seen in samples taken at close intervals in Core 944A-39X). The assemblages lack *P. lacunosa* and *E. huxleyi,* which constrains the age to 0.26–0.46 Ma. Unit VI from 357 to 384 mbsf is barren of calcareous nannofossils.

Planktonic Foraminifers

The boundary between Ericson Zones Z and Y is at the base of Unit I, between 0.50 mbsf (Sample 944A-1H-1, 48–50 cm) and 1.32 mbsf (Sample 944A-1H-1, 130–132 cm; Table 4; Fig. 15). The occurrence of *G. menardii* and *G. tumida* in Sample 944A-1H-CC, 9–18 cm, is considered to be due to downhole contamination of core-catcher samples. Unit II from 0.54 to 191.6 mbsf has been defined as the Y Zone due to the absence of *G. tumida* (Samples 944A-1H-1, 130–132 cm [1.32 mbsf], through -21X-CC, 33 cm [185 mbsf]). The absence of *P. obliquiloculata* in Unit II suggests that the boundary between Unit II and the underlying debris-flow Unit III may be younger than 40 ka. Unit III (debris-flow Unit R) from 200 to 268.7 mbsf contains *G. tumida, G. menardii,* and *G. tumida flexuosa* (Samples 944A-22X-CC, 31 cm, through -29X-CC, 1 cm), suggesting that interglacial material of late to middle Pleistocene age has been reworked into the debris flow. Unit III contains abundant abyssal and bathyal benthic foraminifers, iron-stained foraminifers, calcareous spines, and abundant black authigenic nodules, suggesting reworking. Foraminifers are absent in Unit IV from 268.7 to 355.4 mbsf. Planktonic foraminifers are abundant and well-preserved from 355.4 to 384.2 mbsf in Units V and VI. *G. tumida flexuosa* and *G. tumida* are present, suggesting Units V and VI are from an interglacial period. The presence of *G. tumida flexuosa* constrains the age of these units to late–middle Pleistocene (see "Explanatory Notes" chapter, this volume).

Benthic Foraminifers

In Units I and II, benthic foraminifers are rare to absent from 0 to 185 mbsf (Samples 944A-1H-1 mud line, 0 cm, through -21X-CC, 33 cm). Abyssal and bathyal benthic foraminifers have relatively high abundances in Unit III from 200 to 268.7 mbsf (Samples 944A-22X-CC, 31 cm, through -29X-CC, 1 cm). Benthic foraminifers are absent from 268 to 355 mbsf in Unit IV, and rare or absent from 355 to 384 mbsf in Units V and VI.

Table 2. Relative peak intensities of the main minerals within silty clays at Site 944.

Core, section, interval (cm)	Depth (mbsf)	Relative intensity of primary peaks								
		Smectite	Mica + Illite	Kaolinite	Quartz	Plagioclase	K-feldspar	Augite	Hornblende	Calcite
155-944A-										
1H-3, 50–51	3.50	8.1	13.9	9.3	100	7.4	*	*	*	*
2H-2, 53–54	5.93	11.6	20.2	8.8	100	8.1	3.9	*	*	*
3H-5, 59–60	19.99	16.2	26.6	15.9	100	7.7	5.1	*	*	*
5H-3, 29–30	35.69	9.1	18.2	10.8	100	10.1	*	*	*	*
6H-4, 6–7	46.06	16.9	24.5	14	100	9.3	5	*	*	*
7H-4, 119–120	57.09	14	27.5	12.4	100	7.7	5.6	*	*	*
8H-4, 69–70	66.09	12.9	26.8	12.9	100	8.9	5.5	*	*	*
9H-2, 84–85	72.74	10.1	17.5	11.9	100	9	*	*	*	*
10H-1, 85–86	80.75	7.2	12.6	9.1	100	8.4	4.1	*	*	*
11H-3, 110–112	93.50	6.5	18.3	11.3	100	11.1	5	*	*	*
12X-3, 120–121	101.30	8.6	20.3	10.2	100	11.8	5.1	3.9	*	1.5
21X-1, 14–15	182.14	11.8	24.3	12.2	100	10.4	5.1	3.2	*	*
22X-3, 30–31	194.90	18.8	31.6	16.2	100	11.1	5.1	*	*	*
23X-2, 22–23	202.92	11.5	24	16.2	100	9	*	*	*	*
24X-2, 30–31	212.70	7.2	21.4	8.5	100	9.2	*	*	*	2.6
25X-6, 37–38	228.37	11.7	21.7	13.1	100	7.8	*	*	*	*
26X-4, 74–75	235.34	11	27.6	13	100	9.9	*	*	*	*
28X-4, 21–22	254.11	8.9	22.9	14.5	100	9.9	*	*	5.5	*
30X-6, 127–128	276.50	13	21.5	13.5	100	9.1	4.7	*	*	*
31X-5, 112–113	284.62	6	16.6	7.4	100	8.3	*	*	*	*
32X-3, 6–7	290.53	10.7	21.4	10.7	100	13.2	5.6	1.1	*	*
33X-4, 67–68	302.72	2.2	4.9	3.6	100	12.2	5.3	1.8	*	*
40X-1, 14–15	365.04	13.7	22.5	14.9	100	9.5	*	*	*	*
41X-2, 55–56	376.55	11.1	21.4	17	100	9.3	*	*	*	*

Notes: See "Lithostratigraphy" section in the "Explanatory Notes" chapter, this volume, for XRD methods. * = non-detection.

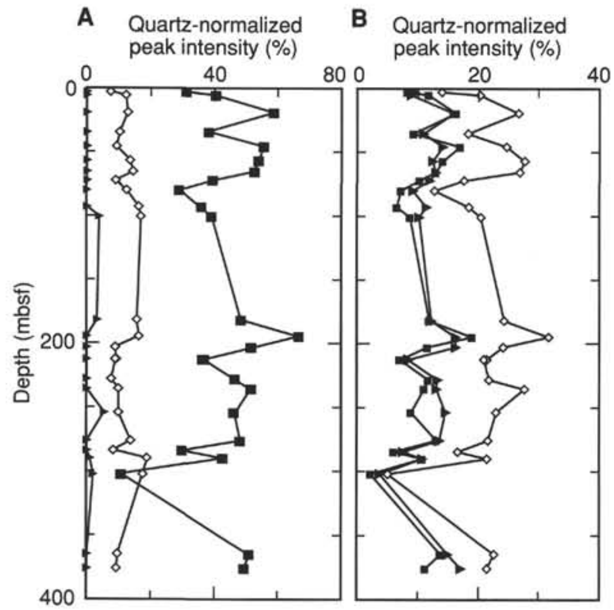

Figure 14. Relative abundances of silicate minerals in silty clay samples based on XRD analysis. **A.** Plot against depth of quartz-normalized peak intensities of the main mineral groups in Site 944 sediment. Squares = clay minerals + mica; diamonds = feldspar; triangles = augite + hornblende. **B.** Plot against depth of quartz-normalized peak intensities of clay minerals and micas. See text for discussion. Squares = smectite; diamonds = mica + illite; triangles = kaolinite.

Siliceous Microfossils

Hole 944A is barren of diatoms, except for the mud-line sample where marine diatoms occur in low abundance.

Palynology

Twelve samples were examined from Hole 944A (Table 5). The late Pleistocene pollen and spore assemblages of Unit II from 3.8 to 163.2 mbsf (Table 5) have very low to moderate abundances and poor preservation, with only Cyatheaceae and monolete spores present. Poor preservation suggests that older reworked spores may make a significant contribution to the total palynomorph assemblage in this unit. The Pleistocene pollen and spore assemblages of Units III, IV, and V have low to moderate abundances and moderate preservation, with tricolporate (TCP) type, Euphorbiaceae, Cyatheaceae, and monolete spores present. Wood particles were observed in all sample slides in low to moderate abundance. Macroscopic wood (>63 µm) was observed in three core-catcher samples at 103.3, 112.5, and 163.1 mbsf (Tables 4 and 5). Dinoflagellates are not present.

Stratigraphic Summary

Unit I contains well-preserved planktonic foraminifer assemblages indicative of the Holocene. The well-preserved nannofossil assemblages represents nannofossil Zone CN15b. The boundary between Ericson Zones Z and Y is between 0.50 mbsf and 1.32 mbsf at the base of Unit I. In Unit II the Y Zone extends from 1.3 to 185.0 mbsf. The absence of *P. obliquiloculata* in Unit II suggests that the boundary between Unit II and the underlying Unit III (debris flow) is younger than 40 ka. Unit III (debris-flow Unit R) contains *G. tumida, G. menardii,* and *G. tumida flexuosa,* suggesting there is reworked interglacial material within this unit. Unit IV is barren of foraminifers, and nannofossils are extremely rare. Units V and VI contain *G. tumida flexuosa* and *G. tumida* and a well-preserved *Gephyrocapsa*-dominated nannofossil assemblage of Zone CN14b.

PALEOMAGNETISM

Remanence Studies

Archive-half sections were measured from 22 APC cores and 17 XCB cores from Holes 944A, 944B, 944C, and 944D. Core 944A-4H, which consisted of one short section, was not run. Core 944A-3H, Cores 944A-5H through -11H, and Cores 944B-3H through -6H were oriented with the Tensor tool. For the majority of these cores, the Tensor tool performed well, although the declinations for Cores 944A-3H, -5H, and -11H and Core 944B-5H were more than 45° from the expected 0° azimuth.

Table 3. Calcareous nannofossil and siliceous microfossil abundance data for Hole 944A.

Core, section, interval (cm)	Top interval (mbsf)	Bottom interval (mbsf)	Calcareous nannofossils			Diatoms		Sponge spicules	Radiolarians	Ericson Zone (inferred from foraminifers)	Age (inferred from foraminifers)
			Abundance	Preservation	Zone	Marine	Fresh water				
155-944A-											
1H-Ml, 0–0	0.00	0.00	a	g	CN15b	—	—	—	—	Z	Holocene
1H-1, 0–1	0.00	0.01	a	g		—	—	—	—		
1H-CC, 18–19	3.86	3.87	b	—		—	—	—	—	Y	late Pleist.
2H-CC, 20–21	9.48	9.49	b	—		—	—	—	—		
3H-CC, 33–34	23.62	23.63	b	—		—	—	—	—		
4H-CC, 9–10	23.31	23.32	b	—		—	—	—	—		
6H-CC, 91–92	51.54	51.55	b	—		—	—	—	—		
7H-1, 51–51	51.91	51.91	b	—		—	—	—	—		
7H-1, 101–101	52.41	52.41	tr	—		—	—	—	—		
7H-CC, 55–56	61.54	61.55	b	—		—	—	—	—		
9H-CC, 54–55	80.82	80.83	b	—		—	—	—	—		
10H-CC, 61–62	88.89	88.90	b	—		—	—	—	—		
11H-CC, 35–36	97.12	97.13	b	—		—	—	—	—		
12X-CC, 34–35	103.44	103.45	r	—		—	—	—	—		
13X-CC, 38–39	112.60	112.61	b	—		—	—	—	—		
14X-CC, 0–1	124.09	124.10	b	—		—	—	—	—		
15X-CC, 29–30	124.68	124.69	b	—		—	—	—	—		
16X-CC, 12–13	140.73	140.74	b	—		—	—	—	—		
17X-1, 16–17	143.56	143.57	b	—		—	—	—	—		
17X-CC, 22–23	144.57	144.58	b	—		—	—	—	—		
18X-CC, 31–32	153.41	153.42	b	—		—	—	—	—		
19X-CC, 22–23	163.22	163.23	b	—		—	—	—	—		
20X-CC, 0–1	181.99	182.00	b	—		—	—	—	—		
21X-CC, 33–34	185.02	185.03	b	—		—	—	—	—		
22X-CC, 40–41	200.36	200.37	b	—		—	—	—	—	RW X	late Pleist.
23X-1, 40–40	201.60	201.60	b	—		—	—	—	—		late Pleist.
23X-2, 40–40	203.10	203.10	tr	—		—	—	—	—		
23X-3, 30–30	204.50	204.50	vr	—		—	—	—	—		
23X-4, 7–7	205.77	205.77	tr	—		—	—	—	—		
23X-4, 40–40	206.10	206.10	c		CN15	—	—	—	—		
23X-4, 67–67	206.37	206.37	vr	—		—	—	—	—		
23X-4, 120–120	206.90	206.90	tr	—		—	—	—	—		
23X-5, 103–103	208.23	208.23	tr	—		—	—	—	—		
23X-6, 7–7	208.77	208.77	r			—	—	—	—		
23X-CC, 39–40	209.40	209.41	b	—		—	—	—	—	RW X	late Pleist.
24X-6, 86–86	219.26	219.26	f			—	—	—	—		
24X-CC, 21–22	220.51	220.52	b	—		—	—	—	—	RW X	late Pleist.
25X-4, 123–123	226.23	226.23	c	g		—	—	—	—		
25X-5, 11–11	226.61	226.61	a	g		—	—	—	—		
25X-5, 82–82	227.32	227.32	c	g	CN15a?	—	—	—	—		
25X-6, 56–58	228.56	228.58	c	g		—	—	—	—		
25X-6, 62–62	228.62	228.62	f	g		—	—	—	—		
25X-CC, 31–32	230.36	230.37	c	g		—	—	—	—	RW X	late Pleist.
26X-1, 30–30	230.40	230.40	b	—		—	—	—	—		
26X-CC, 32–33	237.35	237.36	f	g		—	—	—	—	RW X	late Pleist.
27X-CC, 9–10	239.79	239.80	vr	—		—	—	—	—	RW X	late Pleist.
28X-2, 40–40	251.30	251.30	b	—		—	—	—	—		
28X-CC, 37–38	255.63	255.64	r	p		—	—	—	—	RW X	late Pleist.
30X-CC, 49–50	278.30	278.31	vr	—		—	—	—	—	?	
31X-CC, 53–54	287.54	287.55	tr	—		—	—	—	—	X?	
32X-CC, 56–57	297.65	297.66	r	—		—	—	—	—	?	
33X-CC, 90–91	305.41	305.42	tr	—		—	—	—	—	?	
34X-CC, 17–18	308.29	308.30	b	—		—	—	—	—	?	
38X-CC, 9–10	346.31	346.32	vr	—		—	—	—	—	?	
39X-1, 8–8	355.48	355.48	c	g	CN14b	—	—	—	—		
39X-1, 39–39	355.79	355.79	a	g		—	—	—	—		
39X-1, 83–83	356.23	356.23	a	g		—	—	—	—		
39X-1, 90–90	356.30	356.30	a	g		—	—	—	—		
39X-1, 126–126	356.66	356.66	c	g		—	—	—	—		
39X-1, 144–144	356.84	356.84	c	g		—	—	—	—		
39X-2, 12–12	357.02	357.02	a	g		—	—	—	—		
39X-2, 14–14	357.04	357.04	a	g		—	—	—	—		
39X-2, 19–19	357.09	357.09	a	g		—	—	—	—		
39X-2, 39–39	357.29	357.29	c	g		—	—	—	—		
39X-2, 59–59	357.49	357.49	r	p		—	—	—	—	X?	mid. Pleist.
39X-CC, 5–5	357.58	357.58	b	—		—	—	—	—		mid Pleist.
39X-CC, 26–27	357.79	357.80	b	—		—	—	—	—	X?	mid. Pleist.
40X-CC, 9–10	365.51	365.52	vr	—		—	—	—	—	X?	mid. Pleist.
41X-CC, 32–33	378.05	378.06	b	—		—	—	—	—	X?	mid. Pleist.

Short wavelength oscillations in inclination, declination, and remanence intensity were recorded throughout the APC cores in all holes. Representative samples of this cyclicity, which we interpret as geomagnetic secular variation, are shown for Core 944A-3H (Fig. 16) and Core 944C-1H (Fig. 17). In general, two to four cycles per meter are present in the cores from Site 944.

Remanence intensity, measured after AF demagnetization, shows considerable variation with depth at Site 944. In Hole 944A, a large increase in intensity occurs in the vicinity of the boundary between Units IIB and IIC (37 mbsf). The lowest remanence values are associated with Unit III (debris flow) from 192 to 269 mbsf (Fig. 18).

No anomalous behavior of remanence direction or intensity, which could be interpreted as a geomagnetic excursion, was observed in the APC cores from Site 944. XCB cores in general retained a significant amount of drill stem overprint after AF demagnetization, and so the identification of geomagnetic events within them was not possible.

Magnetic Susceptibility Studies

Whole-core and discrete-sample magnetic susceptibilities were measured on all cores collected from Site 944. Discrete-sample data

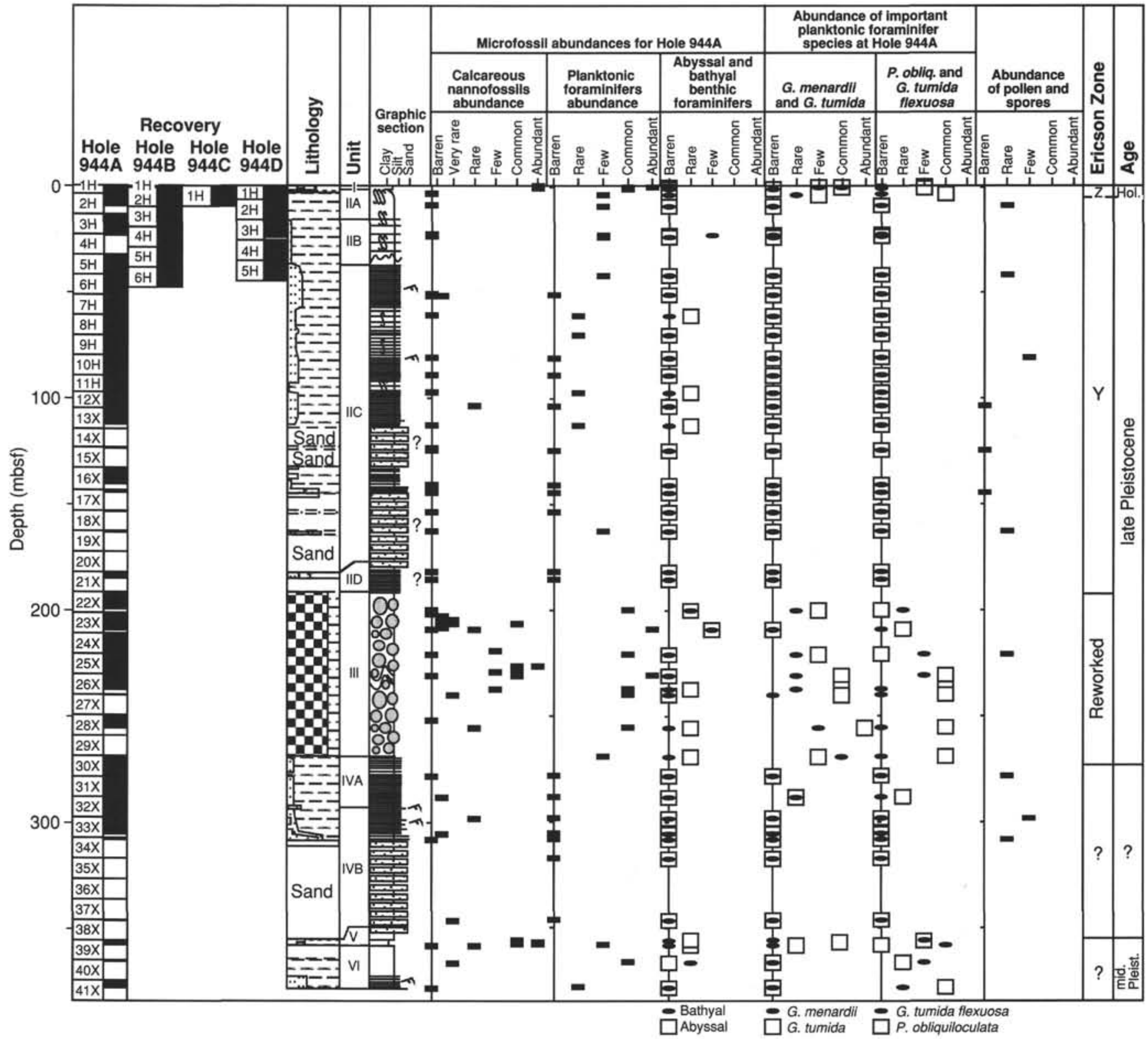

Figure 15. Biostratigraphic summary for Site 944.

from Hole 944A are used to represent the site in Figure 19. Susceptibilities in general correlate with remanence intensity (Fig. 18), with the highest whole-core susceptibility values associated with the top of Subunit IIC. The lowest whole-core values are within carbonate-rich Units I and V. The debris flow, Unit III, is marked by a zone of relatively low values from 192 to 269 mbsf.

ORGANIC GEOCHEMISTRY

Volatile Hydrocarbons

Headspace methane concentrations increase rapidly below the sediment surface to a value of 16,835 ppm at 6.90 mbsf (Table 6; Fig. 20). Methane concentrations remain relatively constant below this depth, ranging from ~3200 ppm to ~9000 ppm, except for a high value of 19,800 ppm at 144.35 mbsf. Vacutainer methane values are considerably higher than headspace concentrations (Fig. 20), ranging from 95,000 to 926,000 ppm in the top 100 mbsf. Methane concentrations ranging from 70,000 to 472,000 ppm were also measured in vacutainer samples from 275.23 to 302.07 mbsf in Hole 944A. Higher molecular weight hydrocarbons were not detected, indicating a predominantly biogenic methane source at Site 944.

Carbon, Nitrogen, and Sulfur Concentrations

Carbonate (calculated as $CaCO_3$) concentrations are high (>25%) in the top 0.42 mbsf and in a gray clast at 227.44 mbsf (Table 7; Fig. 21). In addition, moderately high carbonate contents, ranging from ~6% to ~17%, were measured in several samples of nannofossil-rich clay in Unit V between 356.00 and 357.29 mbsf. In other samples from Hole 944A, carbonate concentrations are between 1% and 5%.

Most TOC concentrations range between 0.7% and 1%. Lower values (<0.7%) were observed in the carbonate-rich clay layers discussed above and in silt laminae and beds. Total nitrogen concentrations mostly range from 0.08% to 0.12%. Similar to TOC values, relatively low TN values (<0.08%) were found in carbonate-rich

Table 4. Foraminifer abundance data for Hole 944A.

Core, section, interval (cm)	Top interval (mbsf)	Bottom interval (mbsf)	*Globorotalia menardii*	*Globorotalia tumida*	*Globorotalia tumida flexuosa*	*Pulleniatina obliquiloculata*	*Globigerinoides ruber* (white)	*Globigerinoides ruber* (pink)	*Globorotalia hexagonus*	*Neogloboquadrina dutertrei*	*Globorotalia trilobus trilobus*	*Globorotalia inflata*	*Globorotalia truncatulinoides*	*Globigerina bulloides*	*Globigerinoides trilobus sacculifer*	*Globorotalia fimbriata*	*Bolliella adamsi*	*Hastigerinella digitata*	*Globigerina calida calida*	*Globorotalia crassaformis hessi*	*Globorotalia crassaformis viola*	*Globorotalia tosaensis*	*Globorotalia crassaformis crassaformis*	Other planktonic foraminifers	Vivianite nodules	Overall foraminifer abundance	Preservation	Abundance of bathyal benthic foraminifers	Abundance of abyssal benthic foraminifers	Comments	Ericson Zone	Age
155-944A-																																
1H-MI, 0–0	0.00	0.00	C	F	B	F	C	F	B	R	C	B	B	B	C	F	B	B	B	B	B	B	B	B	B	A	G	B	B	OS	Z	Holocene
1H-1, 48–50	0.48	0.50	F	C	B	F	C	R	B	C	F	B	R	B	F	B	B	B	B	B	B	B	B	B	B	C	G	B	B		Z	Holocene
1H-1, 130–132	1.30	1.32	B	B	B	F	C	R	B	C	B	B	C	F	B	B	B	B	R	B	B	B	B	B	B	C	G	B	B		Y	late Pleist.
1H-CC, 9–18	3.77	3.86	R	F	B	C	C	B	B	B	C	B	F	B	F	B	B	B	B	R	B	B	B	B	B	F	G	B	B	BN,SP	Y	late Pleist.
2H-CC, 11–20	9.39	9.38	B	B	B	B	C	B	B	C	B	B	F	B	F	B	B	B	B	B	B	B	B	B	R	F	M	B	B	RN,IS,SP,OS	Y	late Pleist.
3H-CC, 24–33	23.53	23.62	B	B	B	B	C	R	B	C	F	F	B	B	F	B	B	B	B	R	B	B	B	B	F	F	M	B	B	IS,M	Y	late Pleist.
4H-CC, 0–9	23.22	23.31	B	B	B	B	C	R	B	C	C	B	B	B	F	B	B	B	B	B	B	B	B	B	C	F	M	F	B	M,IS	Y	late Pleist.
5H-CC, 23–32	42.49	42.58	B	B	B	B	C	B	B	B	C	B	B	B	C	B	B	B	B	B	B	B	B	B	C	F	M	B	B	RN	Y	late Pleist.
6H-CC, 82–91	51.45	51.54	B	B	B	B	B	B	B	B	B	B	B	B	B	B	B	B	B	B	B	B	B	B	A	B	B	B	B	M	Y	late Pleist.
7H-CC, 46–55	61.45	61.54	B	B	B	B	C	R	B	F	A	B	B	B	B	B	B	B	B	B	B	B	B	B	C	R	M	B	R	M,IS	Y	late Pleist.
8H-CC, 2–11	70.26	70.35	B	B	B	B	C	B	B	C	C	B	B	B	R	B	B	B	B	B	B	B	B	B	A	R	M	B	B	M	Y	late Pleist.
9H-CC, 45–54	80.73	80.82	B	B	B	B	B	B	B	B	B	B	B	B	B	B	B	B	B	B	B	B	B	B	A	B	B	B	B	M,RN	Y	late Pleist.
10H-CC, 52–61	88.80	88.89	B	B	B	B	B	B	B	B	B	B	B	B	B	B	B	B	B	B	B	B	B	B	A	B	B	B	B	M	Y	late Pleist.
11H-CC, 26–35	97.03	97.12	B	B	B	B	C	B	B	C	C	B	B	B	C	B	B	B	B	B	B	B	B	B	A	R	G	B	R	M,S	Y	late Pleist.
12X-CC, 25–34	103.35	103.44	B	B	B	B	B	B	B	B	B	B	B	B	B	B	B	B	B	B	B	B	B	B	B	B	B	B	B	M,S,W	Y	late Pleist.
13X-CC, 29–38	112.51	112.60	B	B	B	B	F	B	B	C	C	B	C	B	B	B	B	B	B	R	B	B	B	B	A	R	M	B	R	M,W	Y	late Pleist.
15X-CC, 20–29	124.59	124.68	B	B	B	B	B	B	B	B	B	B	B	B	B	B	B	B	B	B	B	B	B	B	R	B	B	B	B	S	Y	late Pleist.
16X-CC, 3–12	140.64	140.73	B	B	B	B	B	B	B	R	B	B	B	B	B	B	B	B	B	B	B	B	B	B	F	B	B	B	B	S,BN	Y	late Pleist.
17X-CC, 13–22	144.48	144.57	B	B	B	B	B	B	B	B	B	B	B	B	B	B	B	B	B	B	B	B	B	B	R	B	B	B	B	M,FO	Y	late Pleist.
18X-CC, 22–31	153.32	153.41	B	B	B	B	B	B	B	B	B	B	B	B	B	B	B	B	B	B	B	B	B	B	R	B	B	B	B	S,FO	Y	late Pleist.
19X-CC, 13–22	163.13	163.22	B	B	B	B	F	B	B	C	C	B	C	B	F	B	B	B	B	B	B	B	B	B	B	F	G	B	B	W	Y	late Pleist.
20X-CC, 0–1	181.99	182.00	B	B	B	B	B	B	B	B	B	B	B	B	B	B	B	B	B	B	B	B	B	B	B	B	B	B	B		Y	late Pleist.
21X-CC, 24–33	184.93	185.02	B	B	B	B	B	B	B	B	R	B	B	B	B	B	B	B	B	B	B	B	B	B	B	B	M	B	B	S,IS	Y	late Pleist.
22X-CC, 31–40	200.27	200.36	R	F	R	B	C	B	B	C	F	R	B	B	R	B	B	B	B	B	R	B	B	B	B	C	G	R	R	BN,SP,OS	RW X	late Pleist.
23X-CC, 30–39	209.31	209.40	B	B	B	R	C	F	B	C	C	B	F	B	F	B	B	B	B	B	B	B	B	B	F	A	G	F	F	SP,FO,BN	RW X	late Pleist.
24X-CC, 12–21	220.42	220.51	R	F	F	B	C	B	B	C	C	B	B	B	C	B	B	B	B	B	R	B	B	B	F	C	G	B	B	BN,SP	RW X	late Pleist.
25X-CC, 22–31	230.27	230.36	R	C	F	C	F	B	B	F	F	B	R	B	F	B	B	B	B	B	B	B	B	B	B	A	G	B	B	BN	RW X	late Pleist.
26X-CC, 23–32	237.26	237.35	R	C	B	C	F	B	B	F	F	B	F	B	F	B	B	B	B	B	B	B	B	B	A	C	G	B	R	BN,IS	RW X	late Pleist.
27X-CC, 0–9	239.70	239.79	B	C	B	C	F	B	B	F	F	B	F	B	B	B	B	B	R	B	B	B	B	B	A	C	G	B	B	BN,IS	RW X	late Pleist.
28X-CC, 28–37	255.54	255.63	F	A	B	C	F	B	B	F	F	B	B	B	B	B	B	B	B	B	B	B	B	B	A	C	G	B	R	BN	RW X	late Pleist.
29X-CC, 0–1	268.69	268.70	C	F	B	C	R	B	B	R	F	F	F	B	B	B	B	B	B	B	B	B	B	B	F	F	G	B	R	S,M,BN	RW X	mid. Pleist.
30X-CC, 40–49	278.21	278.30	B	B	B	B	B	B	B	B	B	B	B	B	B	B	B	B	B	B	B	B	B	B	B	B	B	B	B	M	?	mid. Pleist. ?
31X-CC, 44–53	287.45	287.54	R	R	B	R	B	B	B	B	B	B	B	B	B	B	B	B	B	B	B	B	B	B	C	B	B	B	B		X ?	mid. Pleist. ?
32X-CC, 47–56	297.56	297.65	B	B	B	B	B	B	B	B	B	B	B	B	B	B	B	B	B	B	B	B	B	B	R	B	B	B	B	M,BN	?	?
33X-CC, 81–90	305.32	305.41	B	B	B	B	B	B	B	B	B	B	B	B	B	B	B	B	B	B	B	B	B	B	B	B	B	B	B	S,M	?	?
34X-CC, 8–17	308.20	308.29	B	B	B	B	B	B	B	B	B	B	B	B	B	B	B	B	B	B	B	B	B	B	B	B	B	B	B	S	?	?
35X-CC, 0–2	316.90	316.92	B	B	B	B	B	B	B	B	B	B	B	B	B	B	B	B	B	B	B	B	B	B	B	B	B	B	B	S	?	?
38X-CC, 0–9	346.22	346.31	B	B	B	B	B	B	B	B	B	B	B	B	B	B	B	B	B	B	B	B	B	B	B	B	B	B	B	M,S	?	?
39X-2, 18–20	356.20	356.22	B	C	F	F	F	B	R	C	F	B	B	B	F	B	B	B	R	B	B	B	B	B	B	A	G	B	R		X ?	mid. Pleist.
39X-CC, 17–26	357.70	357.79	B	R	C	B	F	F	B	C	C	B	R	B	R	B	B	B	B	B	B	B	B	B	B	F	G	B	R	IS,M	X ?	mid. Pleist.
40X-CC, 0–9	365.42	365.51	B	B	F	R	F	C	B	C	B	B	B	B	C	B	B	B	B	B	B	B	B	B	A	C	M	R	B	IS,S	X ?	mid. Pleist.
41X-CC, 23–32	377.96	378.05	B	B	R	C	B	B	B	F	C	B	B	B	R	B	B	B	B	B	B	B	B	B	F	R	M	B	B	M,S	X ?	mid. Pleist.

Notes: Key to Comments section: Sediment composition: S = sand, M = mica, BN = black nodules, RN = red nodules, indicators of reworking: FO = fine organics, W = wood fragments, OS = ostracod shells, SP = sponge spicules or spines, IS = iron-stained foraminifers. Note also the occurrence of bathyal benthic foraminifers.

Table 5. Spores and pollen data for Hole 944A.

Core, section, interval (cm)	Top interval (mbsf)	Bottom interval (mbsf)	Pollen and spores: Abundance	Preservation	Major types recorded	Dinocysts	Wood/ carbonized particles	Ericson Zone (inferred from forams.)	Age (inferred from forams.)
155-944A-									
1H-CC, 18–19	3.86	3.87	r	p	Cyatheaceae	b	r	Y	late Pleist.
2H-CC, 20–21	9.48	9.49	r	m	Cyatheaceae, monolete spore	b	f	Y	late Pleist.
5H-CC, 32–33	42.58	42.59	r	p	Monolete spore	b	c	Y	late Pleist.
9H-CC, 54–55	80.82	80.83	f	p	Cyatheaceae, monolete spore	b	c	Y	late Pleist.
12X-CC, 34–35	103.44	103.45	b			b	f	Y	late Pleist.
15X-CC, 29–30	124.68	124.69	b			b	r	Y	late Pleist.
17X-CC, 22–23	144.57	144.58	b			b	c	Y	late Pleist.
19X-CC, 22–23	163.22	163.23	r	m	Monolete spore	b	c	Y	late Pleist.
24X-CC, 21–22	220.51	220.52	r	m	Monolete spore	b	f	RW X	late Pleist.
30X-CC, 49–50	278.30	278.31	r	m	Tricolporate	b	f	?	?
32X-CC, 56–57	297.65	297.66	f	m	Euphorbiaceae, Cyatheaceae	b	f	?	?
34X-CC, 17–18	308.29	308.30	r	m		b	r	?	?

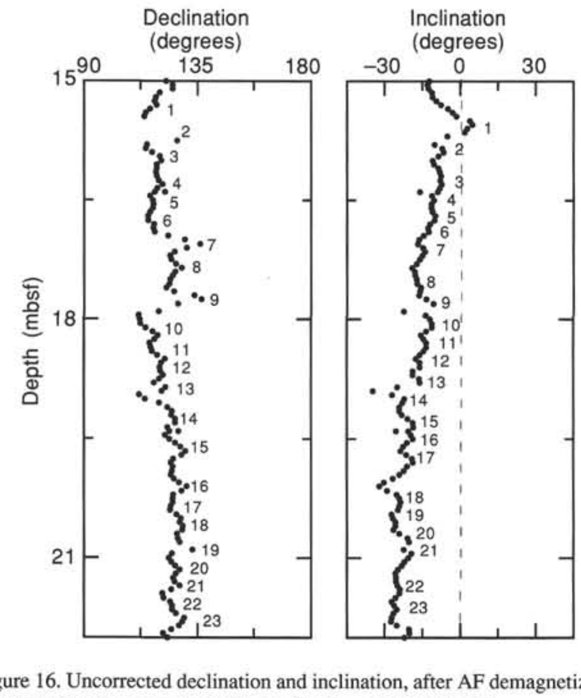

Figure 16. Uncorrected declination and inclination, after AF demagnetization to 20 mT, for the interval 15–22 mbsf in Core 155-944A-3H.

clays and silt layers. Exceptions are the carbonate-rich clay samples between 356.00 and 357.20 mbsf, which have relatively high TN concentrations of 0.09%.

In general, total sulfur concentrations are low (<0.2%) throughout. Unlike at previous sites, there are not elevated TS concentrations below Unit I. However, high TS contents (>1%) were measured in the debris-flow unit (Unit III) and in the lower part of Unit V near the deep carbonate-rich layer. The [C/N]a ratios generally range between 7 and 14 despite an unusually high value of 29 at 0.42 mbsf. In addition, low ratios (3 to 6) are observed between 356.00 and 357.2 mbsf in lithologic Unit VI.

INORGANIC GEOCHEMISTRY

Interstitial Water Analysis

Interstitial waters were collected from 32 sediment samples at Site 944, 12 from Hole 944A and 20 from Hole 944D, which was offset from Hole 944A by approximately 300 m. In Hole 944A, samples were taken approximately every 10 m for the upper 20 mbsf and approximately every 30 m thereafter to a depth of 284.90 mbsf, with one additional sample from 377.32 mbsf (Table 8 and Fig. 22). The interval between 284.90 and 377.32 mbsf could not be sampled because of poor core recovery. In Hole 944D, a high-resolution suite of samples was taken with a sample interval of approximately 1.5 m for the first 19 mbsf, and approximately 3 m thereafter to 40.84 mbsf (Table 8). The geochemical gradients observed in the two holes are generally similar. For some pore-water constituents, the higher resolution sampling in Hole 944D shows features not observable in the more widely spaced samples of Hole 944A; for example, peaks in the concentrations of alkalinity and phosphate (Figs. 23A and 23C).

Salinities of the water samples range from 32.0 to 35.0 (Fig. 22A). In the shallowest sample from each hole, the salinity is between 34.5 and 35.0. Salinity decreases fairly quickly with depth and, at approximately 6 to 8 mbsf, has decreased to between 32.0 and 32.5. Below 8 mbsf, the salinity remains within this range.

Chloride concentrations initially increase with depth in the holes, from 551 mM at 0.50 mbsf to 559 mM at about 40 mbsf (Fig. 22B). Below 40 mbsf, chloride concentrations slowly decrease with depth, to about 552 mM near the bottom of Hole 944A.

Pore-water pH values range from 7.39 to 7.82. These values vary irregularly with depth in Hole 944D (Fig. 22C). Below 40 mbsf, pH values are more constant, generally between 7.4 and 7.6.

Alkalinity increases quickly in the upper 5 mbsf (Fig. 23A), from 9.12 mM at 0.50 mbsf to 22.23 mM at 4.40 mbsf. Alkalinity then decreases to 10.96 mM at 9.50 mbsf, and generally remains near 10 mM throughout the remainder of both holes. There is a slight increase to 14.87 mM at 183.40 mbsf in Hole 944A (Fig. 22D).

Magnesium concentrations decrease over the upper 5 mbsf, from about 49 mM between 0.5 and 1.45 mbsf, to 40.5 mM at 4.40 mbsf (Fig. 23E). The concentration then increases slightly, to about 43 mM at 11.00 mbsf, and continues in the range of 42 to 44 mM through 138.20 mbsf (Fig. 22E). Below 138.20 mbsf, the concentration decreases to about 40 mM and remains so downhole. Calcium concentrations decrease somewhat more slowly with depth than do those of magnesium, from 9.8 mM at 0.50 mbsf to 4.5 mM at 9.50 mbsf (Fig. 23F). From 9.50 to 93.80 mbsf, calcium concentrations are between 4.4 and 5.0 mM. Below 93.80 mbsf, the concentrations increase to about 6 mM (Fig. 22F).

Pore-water sulfate concentrations are 20.2 mM at 0.50 mbsf and have fallen to zero by 4.40 mbsf (Fig. 23B). Values generally remain at or near zero for most of the remainder of the hole. Values above zero were measured at 138.20 mbsf (2.0 mM), and in the three lowermost samples of Hole 944A (up to 4.6 mM). All of these samples, and also the great majority of similar samples from other holes, were taken with the extended core barrel (XCB). The XCB appears occasionally either to contaminate the samples with seawater or somehow to enhance post-sampling re-oxidation of sulfide minerals.

Ammonium concentrations increase regularly with depth in the uppermost 10 mbsf, from 0.7 mM at 0.50 mbsf to 6.6 mM at 11.00 mbsf (Fig. 23D). From 11.00 to about 40 mbsf, the concentrations in-

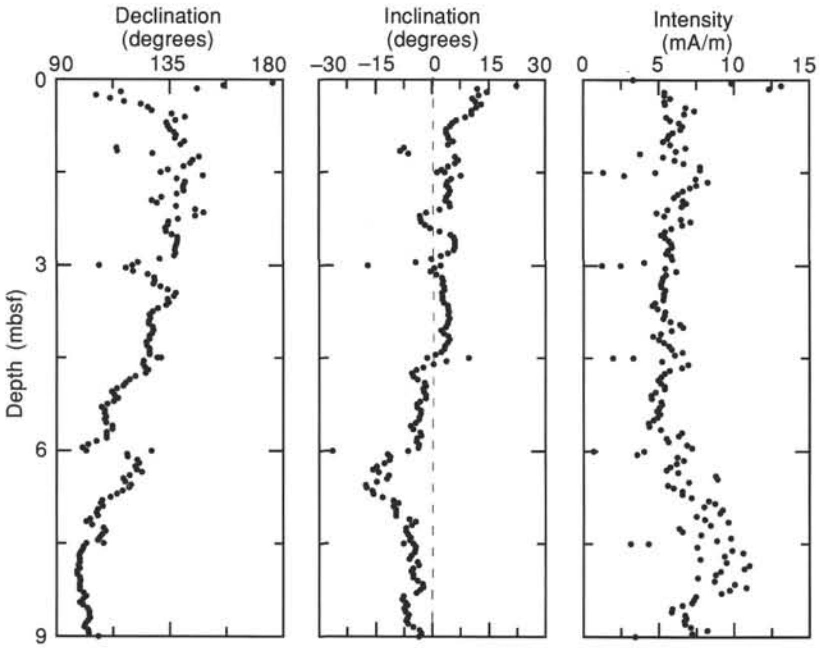

Figure 17. Uncorrected declination, inclination, and remanence intensity, after AF demagnetization to 20 mT, for Core 155-944C-1H.

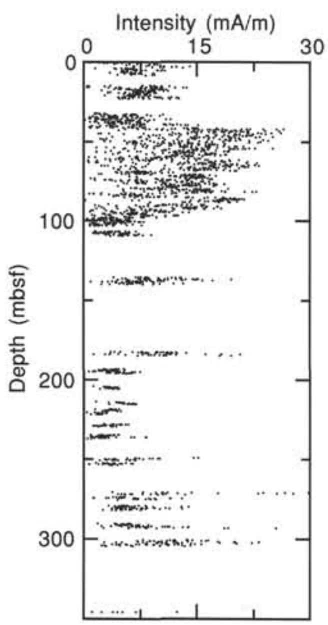

Figure 18. Intensity of remanent magnetization, after AF demagnetization to 20 mT, for Hole 944A.

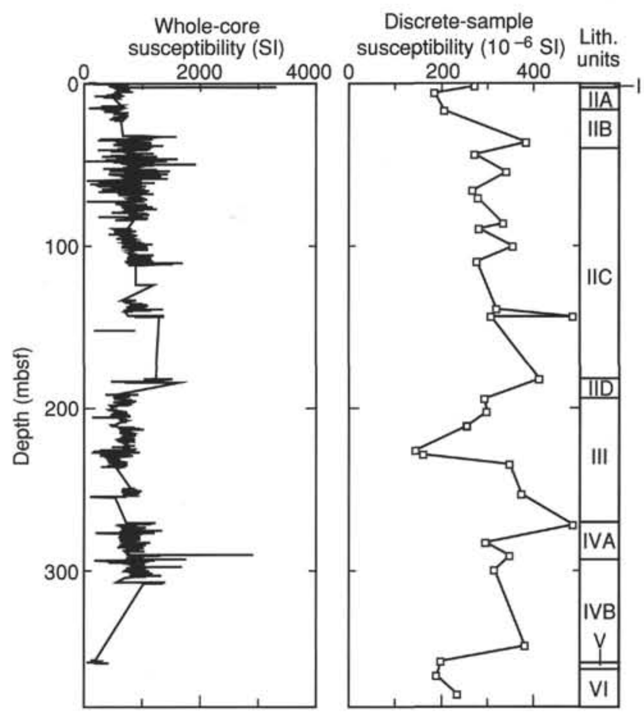

Figure 19. Whole-core and discrete-sample magnetic susceptibilities for Site 944.

crease more slowly, reaching 8.3 mM at 40.84 mbsf. The concentrations remain from 7 to 8 mM down to 93.80 mbsf, then decrease to between 4.8 and 5.7 mM over the interval 138.20–252.30 mbsf (Fig. 22H). The concentrations increase again in the two lowermost samples, reaching 8.3 mM at 377.82 mbsf.

Pore-water phosphate concentrations increase rapidly in the upper few meters. The concentrations are about 50 to 60 µM near the sediment surface and increase to 392 µM at 4.40 mbsf. As with the two previous high-resolution surveys, the peak in phosphate concentration is coincident with the depth of complete sulfate reduction. From 4.40 to 8.00 mbsf, the phosphate concentration decreases quickly, falling to 16.7 µM at 8.00 mbsf. From 8.00 to 252.30 mbsf, phosphate concentrations remain below 20 µM. The concentrations increase slightly in the two lowermost samples, to 39.4 µM near the bottom of the hole.

Dissolved silica concentrations are highly variable in Hole 944D, ranging from 225 to 367 µM, and show no trend downhole (Fig. 22J). In Hole 944A, the concentrations increase from 287 µM at 1.45 mbsf to 389 µM at 20.85 mbsf. Below 20.85 mbsf, the concentrations tend to increase slowly downhole, with the lowermost samples having 533 µM silica.

Table 6. Gas concentrations in sediments from Site 944.

Core, section, interval (cm)	Depth (mbsf)	Sed. temp.* (°C)	Methane HS (ppm)	Methane VAC (ppm)
155-944A-				
1H-2, 0–5	1.50	2	4	
2H-3, 0–5	6.90	2	16,835	113,692
3H-6, 0–5	20.90	3	6,021	571,124
4H-1, 0–5	22.90	3	5,279	
5H-6, 0–5	39.90	3	5,585	335,498
6H-6, 0–5	49.00	4	3,907	262,847
7H-5, 0–5	57.40	4	6,372	
8H-6, 0–5	68.17	4	5,081	475,006
9H-6, 5–6	77.90	4	915	926,557
10H-1, 145–150	81.35	5	4,799	95,971
11H-4, 0–5	93.90	5	7,121	307,245
12X-3, 0–5	100.10	5	7,180	
13X-3, 0–5	107.90	5	5,414	
16X-4, 0–5	138.30	6	7,770	
17X-7, 0–5	144.35	7	19,817	
19X-1, 0–5	162.70	7	9,401	
21X-2, 0–5	183.50	8	6,941	
22X-5, 0–5	197.60	8	6,902	
23X-5, 0–5	207.20	9	7,031	
24X-6, 0–5	218.40	9	7,394	
25X-3, 0–5	223.50	9	3,236	
26X-3, 0–5	233.10	9	3,482	
28X-3, 0–5	252.40	10	8,372	
30X-6, 0–5	275.23	11	5,704	76,541
31X-7, 0–5	286.50	11	7,629	112,649
32X-4, 0–5	291.97	11	8,959	472,606
33X-4, 0–5	302.05	12	8,598	70,583
34X-1, 77–82	308.07	12	5,088	
40X-1, 0–5	364.90	14	5,949	
41X-3, 0–5	377.42	14	6,730	

Notes: HS = headspace; VAC = vacutainer. Geothermal gradient = 39°C/km. Bottom-water temperature = 2°C. *See "In-situ Temperature Measurements" section, this chapter.

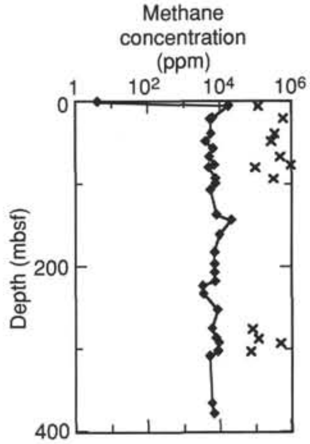

Figure 20. Methane concentrations at Site 944. Headspace (diamond) and vacutainer (×) samples are plotted.

Pore-water potassium and sodium concentrations show similar changes downhole. The concentrations decrease from 12 mM potassium and 471 mM sodium near the sediment surface to about 7 mM potassium and 455 mM sodium at about 10 mbsf (Figs. 22K and 22L). The concentrations are fairly constant to 138.20 mbsf, then increase to 10.1 mM potassium and 464 mM sodium at 183.40 mbsf. Thereafter, the potassium concentrations tend to decrease slightly to 7.0 mM potassium in the lowermost sample, while sodium concentrations remain between 464 and 461 mM.

Dissolved iron concentrations are highly variable in Hole 944D, ranging between 6.2 and 114 µM (Fig. 22M). In the upper 10 m of the hole, iron tends to vary inversely with phosphate. Below 10 mbsf, there is no clear trend downhole. In Hole 944A, the concentrations vary from 13.4 to 105 µM, again with no clear trend downhole, although the samples with the lowest concentrations are found from 183.40 to 284.90 mbsf, in or near the debris flow, Unit III.

Manganese concentrations are highest, around 35 µM, in the shallowest sample in each hole (Fig. 22N). The concentrations decrease quickly, to less than 5 µM by 4.40 mbsf. The values remain less than 5 µM downhole.

In general, the pore-water geochemical profiles at this site change more rapidly with depth, compared with the other two high-resolution sites (931 and 939). The peak in alkalinity and phosphate, and depth to total sulfate depletion are all several meters shallower at Site 944. These differences may reflect different sedimentation rates or different organic carbon oxidation rates.

PHYSICAL PROPERTIES

Index Properties

Index properties were determined for intact, predominantly clayey sediment intervals in Hole 944A (Table 9). Unlike at previous Leg 155 sites, there is a wide scatter of index values in the upper part of the hole. The single sample from the foraminifer-nannofossil clay of Unit I has a water content of 48.5%. Within the silty clay of Unit II, water content decreases with depth from 52% to about 28% (Fig. 24). Water content values in the lower part of Subunit IIB and the uppermost part of Subunit IIC are lower than those expected from the general trend. The lower values may be the result of lower sedimentation rates, increased compaction rates, or consequences of soft-sediment deformation. The increase of 3% to 4% in the water content and porosity profiles at 97 mbsf coincides with the change from APC to XCB coring.

Unit III is divided at 213 mbsf into an upper part in which water content decreases from 28% to 23% and a lower part in which water contents are lower (19%–28%) and more variable with no clear trend (Fig. 24). Water contents are slightly higher in Unit IV than in Unit III. They remain constant within Subunit IVA at about 24% but increase overall downhole within Subunit IVB from 21% to 26%. The downhole water content increase in Subunit IVB suggests an increase in sedimentation rate downhole or enhanced compaction at the top of Subunit IVB.

Grain density averages 2.75 g/cm^3 with most of the values scattered between 2.68 and 2.85 g/cm^3 (Table 9). Grain densities increase downhole from about 2.68 to 2.75 g/cm^3 near the seafloor to about 2.75 to 2.85 g/cm^3 at 90 mbsf. Below 90 mbsf, values decrease downhole to about 2.68 to 2.77 g/cm^3 at 220 mbsf. The trend reverses below 220 mbsf, and grain density values are between 2.75 and 2.83 g/cm^3 at 290 mbsf. Lower values below 300 mbsf suggest a third trend reversal. Six samples of sandy sediment were measured. The grain density of this sediment is not significantly different from that of the adjacent clayey sediment (Fig. 24).

Wet-bulk density increases from 1.5 to 1.9 g/cm^3, from near the seafloor to the base of Unit II. Values increase gradually within the upper part of Unit III to about 2.1 g/cm^3 at 212 mbsf, and remain nearly constant within the lower part of Unit III. Below Unit III wet-bulk density decreases slightly to 2.0 g/cm^3 at the base of Hole 944A. Comparison of the discrete-sample wet-bulk densities with the GRAPE bulk density profile provides a qualitative measure of the expansion experienced by the cores. The difference between the two data sets increases over the upper 10 m from 0.1 to 0.3 g/cm^3 (Fig. 24). Below this depth, the GRAPE densities are between 0.3 and 0.4 g/cm^3 less than the discrete sample values but display trends similar to those of the discrete samples.

Compressional-wave Velocity

Compressional-wave velocity measurements were made with the PWL on whole-round cores from Holes 944A, 944B, 944C, and 944D. Pervasive microfractures in sediment affected by gas expansion restricted PWL measurements to the interval from the seafloor

Table 7. Elemental and organic carbon compositions of sediments from Site 944.

Core, section, interval (cm)	Depth (mbsf)	IC (%)	$CaCO_3$* (%)	TC (%)	TOC (%)	TN (%)	TS (%)	[C/N]a	Lith. unit
155-944A-									
1H-1, 7–8	0.07	4.59	38.2	4.93	0.34	0.05	0.18	8	I
1H-1, 42–43	0.42	3.02	25.2	3.85	0.83	0.03	0.14	29	
1H-1, 84–85	0.84	0.24	2.0	0.74	0.50	0.05	0.12	11	
1H-3, 60–61	3.60	0.15	1.2	0.98	0.83	0.07	0.18	14	
2H-3, 53–54	7.43	0.29	2.4	1.21	0.92	0.09	0.09	13	
2H-3, 97–98	7.87	0.32	2.7	1.23	0.91	0.09	0.05	11	
3H-4, 18–19	18.08	0.26	2.2	1.02	0.76	0.08	0.05	11	
5H-3, 112–113	36.52	0.26	2.2	0.96	0.70	0.07	0.04	12	
5H-4, 70–71	37.60	0.29	2.4	1.24	0.95	0.10	0.15	11	
6H-4, 53–54	46.53	0.35	2.9	1.18	0.83	0.09	0.05	11	
6H-7, 8–10	49.49	0.20	1.7	0.50	0.30	0.04	0.02	9	
7H-3, 121–122	55.61	0.30	2.5	1.30	1.00	0.11	0.06	11	II
7H-3, 138–139	55.78	0.17	1.4	0.76	0.59	0.05	0.03	15	
8H-5, 61–62	67.28	0.42	3.5	1.32	0.90	0.10	0.05	11	
9H-2, 10–11	72.00	0.27	2.2	1.30	1.03	0.11	0.02	11	
9H-4, 41–42	75.31	0.35	2.9	1.29	0.94	0.10	0.04	11	
10H-3, 49–50	83.39	0.33	2.7	0.75	0.42	0.07	0.02	7	
10H-3, 70–71	83.60	0.26	2.2	0.73	0.47	0.06	0.03	9	
11H-2, 100–101	91.90	0.26	2.2	1.11	0.85	0.09	0.04	11	
11H-4, 94–95	94.84	0.27	2.2	1.14	0.87	0.10	0.02	11	
12X-3, 122–123	101.32	0.32	2.7	1.34	1.02	0.10	0.00	12	
13X-5, 1–2	110.87	0.49	4.1	1.46	0.97	0.12	0.17	9	
16X-5, 40–41	140.20	0.57	4.7	1.36	0.79	0.09	0.08	10	
21X-2, 103–104	184.53	0.35	2.9	1.35	1.00	0.09	0.06	13	
22X-1, 27–28	191.87	0.33	2.7	0.86	0.53	0.08	0.05	8	
22X-4, 76–77	196.86	0.15	1.2	0.82	0.67	0.08	0.36	9	
23X-4, 22–23	205.92	0.19	1.6	0.65	0.46	0.08	0.12	7	
24X-5, 116–117	218.06	0.17	1.4	0.81	0.64	0.09	0.28	8	
25X-5, 94–95	227.44	3.82	31.8	4.26	0.44	0.08	0.14	7	III
25X-6, 54–55	228.54	0.43	3.6	1.16	0.73	0.10	0.11	8	
25X-6, 67–68	228.67	0.55	4.6	1.41	0.86	0.12	1.22	9	
26X-3, 74–75	233.84	0.30	2.5	1.02	0.72	0.09	0.58	9	
28X-4, 102–103	254.92	0.30	2.5	1.13	0.83	0.11	0.17	9	
30X-4, 59–60	272.82	0.19	1.6	0.63	0.44	0.05	0.14	10	
30X-4, 136–137	273.59	0.44	3.7	1.10	0.66	0.08	0.12	10	
31X-5, 60–61	284.10	0.42	3.5	1.20	0.78	0.09	0.06	10	IV
32X-3, 8–9	290.55	0.49	4.1	1.04	0.55	0.08	0.05	8	
33X-3, 71–72	301.31	0.47	3.9	1.21	0.74	0.10	0.04	9	
39X-1, 60–80	356.00	1.11	9.2	1.32	0.21	0.09	0.05	3	
39X-1, 100–120	356.40	0.66	5.5						
39X-1, 120–140	356.60	1.40	11.7	1.74	0.34	0.09	0.55	4	
39X-1, 140–150	356.80	1.26	10.5						V
39X-2, 0–20	356.90	2.09	17.4	2.33	0.24	0.09	1.31	3	
39X-2, 30–45	357.20	1.26	10.5						
39X-2, 45–63	357.35	0.54	4.5	0.99	0.45	0.09	1.44	6	
40X-1, 15–16	365.05	0.42	3.5	1.12	0.70	0.09	0.09	9	VI

Note: * = calculated assuming all IC is calcite.

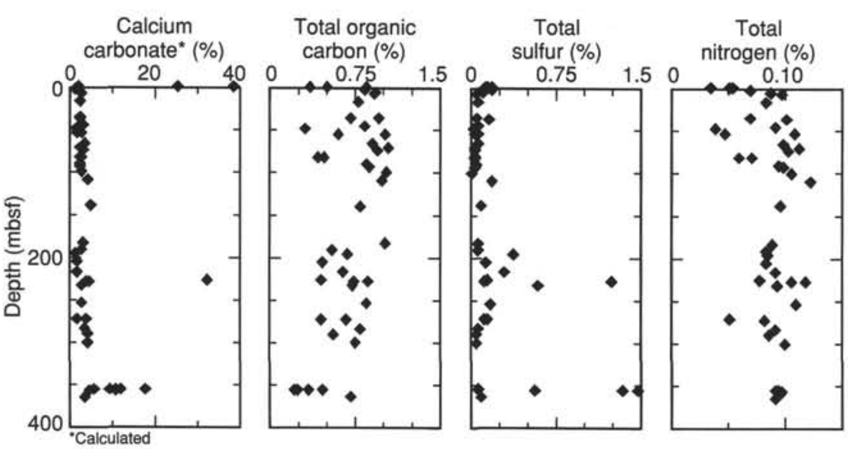

Figure 21. Concentration profiles of carbonate, total organic carbon, total sulfur, and total nitrogen at Site 944.

Table 8. Interstitial water chemistry, Site 944.

Core, section, interval (cm)	Depth (mbsf)	Salinity	pH	Alkalinity (mM)	Cl^- (mM)	Mg^{2+} (mM)	Ca^{2+} (mM)	K^+ (mM)	HPO_4^{2-} (μM)	SO_4^{2-} (mM)	NH_4^+ (mM)	H_4SiO_4 (μM)	Na^+ (mM)	Fe^{2+} (μM)	Mn^{2+} (μM)
155-944A-															
1H-1, 145–150	1.45	35.0	7.69	9.27	552	49.4	9.8	12.5	50.8	20.4	0.6	287	471	31.6	31.2
2H-2, 145–150	6.85	32.5	7.55	12.81	554	42.1	5.3	7.9	9.7	0.1	4.9	364	460	88.3	3.6
3H-5, 150–155	20.85	32.5	7.39	9.76	556	43.4	4.7	6.9	5.2	0.0	7.3	389	455	58.2	5.2
5H-5, 140–150	39.80	32.0	7.52	9.86	559	44.4	4.8	6.7	6.5	0.1	7.4	377	456	74.9	4.4
8H-5, 140–150	68.07	32.0	7.54	9.43	557	43.9	4.8	6.3	2.0	0.2	7.2	421	456	37.5	5.2
11H-3, 140–150	93.80	32.0	7.44	7.76	556	42.2	5.0	7.3	6.7	1.0	7.8	377	456	89.9	4.4
16X-3, 140–150	138.20	32.5	7.59	9.68	554	43.4	5.8	8.0	5.2	2.0	5.3	362	456	95.8	4.5
21X-1, 140–150	183.40	32.5	7.56	14.87	555	40.3	5.5	10.1	7.1	0.7	4.8	454	464	19.8	3.6
24X-5, 140–150	218.30	32.0	7.72	12.63	552	39.6	5.6	8.9	7.5	0.3	4.8	359	461	13.4	3.8
28X-2, 140–150	252.30	32.0	7.44	9.75	552	40.5	6.1	8.1	5.4	3.1	5.7	466	461	22.7	3.4
31X-6, 140–150	284.90	32.5	7.62	11.98	553	40.5	6.6	8.0	25.7	4.6	7.0	404	465	36.5	3.2
41X-2, 132–142	377.32	32.5	7.53	11.979	552	39.4	5.8	7.0	39.4	2.8	8.31	533	464	105	4.2
155-944D-															
1H-1, 50–55	0.50	34.5	7.51	9.12	551	48.8	9.8	12.1	64.8	20.2	0.7	317	471	57.0	35.6
1H-1, 140–145	1.40	34.0	7.61	12.50	551	47.6	9.4	11.5	96.1	14.7	1.1	367	467	18.4	17.3
1H-2, 140–145	2.90	33.5	7.82	20.45	553	46.9	8.4	11.8	368.0	4.8	1.8	317	460	10.9	6.0
1H-3, 140–145	4.40	33.0	7.82	22.23	553	40.5	6.5	10.2	392.0	0.2	2.7	340	469	11.9	4.2
1H-4, 140–145	5.90	33.0	7.68	19.05	552	41.3	6.2	9.6	61.7	0.3	3.5	340	464	37.0	3.0
2H-1, 140–145	8.00	32.0	7.61	11.78	553	42.5	4.9	7.9	16.7	0.4	4.7	335	458	84.6	3.1
2H-2, 140–145	9.50	32.0	7.57	10.96	554	42.1	4.5	8.3	14.0	0.4	5.4	346	459	114.2	2.7
2H-3, 140–145	11.00	32.0	7.56	9.98	554	42.9	4.6	7.7	1.2	0.2	6.6	356	455	47.6	3.8
2H-4, 140–145	12.50	32.0	7.44	9.96	555	42.7	4.6	7.4	5.6	0.1	6.7	333	456	66.4	3.2
2H-5, 140–145	14.00	32.0	7.53	9.28	556	42.9	4.5	7.8	6.2	0.2	7.0	275	456	55.6	2.2
2H-6, 108–113	15.18	32.0	7.65	9.15	556	42.8	4.6	7.5	9.8	0.4	6.9	298	457	88.2	3.5
3H-1, 140–145	17.50	32.0	7.57	9.25	556	43.8	4.9	7.0	12.1	0.5	7.3	359	455	88.9	4.4
3H-2, 110–115	18.70	32.0	7.68	9.22	555	43.8	4.4	7.0	7.3	0.4	6.8	348	455	58.9	4.2
3H-4, 132–137	21.51	32.0	7.69	9.61	556	43.9	4.4	6.7	18.0	0.2	7.2	385	456	102.2	4.6
3H-6, 60–65	23.62	32.0	7.70	9.33	557	44.2	4.4	7.3	4.1	0.2	7.5	240	455	18.4	3.4
4H-2, 140–145	27.84	32.0	7.56	9.09	559	43.3	4.6	7.1	4.9	0.2	7.2	319	458	24.5	3.2
4H-4, 132–137	30.76	32.0	7.43	9.16	559	42.5	4.5	7.1	5.8	0.2	7.3	327	460	47.4	3.5
4H-6, 132–137	33.49	32.0	7.72	8.13	558	42.1	4.4	7.8	4.7	0.6	8.2	235	458	6.2	3.0
5H-2, 140–145	37.84	32.0	7.60	8.42	559	43.2	4.6	7.8	3.5	1.1	7.7	225	459	11.4	2.8
5H-4, 140–145	40.84	32.0	7.56	8.55	559	43.6	4.6	7.4	11.3	1.0	8.3	243	458	45.3	3.4

to 3.6 mbsf. The average transverse velocities range between1439 m/s and 1484 m/s. Longitudinal and transverse velocity measurements were made using the DSV from seafloor to 3.34 mbsf in Hole 944A. A longitudinal velocity of 1532 m/s was measured at 0.31 mbsf in Unit I. Longitudinal velocities range from 1497 to 1500 m/s for the upper 2 m of Unit II. Transverse velocities in Unit II range from 1474 to 1491 m/s.

Shear Strength

Measurements of undrained shear strength were made using the motorized shear vane on most cores from Hole 944A (Table 10). Below 52 mbsf, compressive strengths were determined using a pocket penetrometer.

Subunit IIA shows increasing strength downhole ranging from 3 kPa to 19 kPa (Fig. 25). Subunit IIB displays two parts; from 15.38 to 23.1 mbsf, shear strength values generally decrease downhole to 10 kPa, and from 33.6 to the base of the subunit, shear strength is about 25 kPa. Within Subunit IIC, the magnitude and variability of shear strength increase with depth. The change from APC to XCB coring is accompanied by a drop of about 25 kPa and a greater divergence between shear strength measured by the lab vane and that estimated from compressive strength (Fig. 25). A single measurement of 43 kPa for Subunit IID should be considered a minimum value because the test failed by a major fracture across the core.

The upper part of Unit III (191.6 to ~213 mbsf) is characterized by a general increase in shear strength from 43 to 166 kPa. Shear strength is generally higher in the lower part of Unit III and commonly over 200 kPa. This pattern in Unit III is similar to that noted at Sites 935 and 936 for the same seismic unit, Unit R. The wide scatter of measurements in the lower part of the unit is partially the result of premature fracturing during shear strength tests. Lower shear strengths (typically 50 to 135 kPa) occur in Unit IV. No strength measurements were made in Unit V. The shear-strength measurements from Unit VI should be considered as minimum values because all samples failed by major (about 5 mm wide) fractures across the core.

Resistivity

Longitudinal and transverse resistivity were determined for Hole 944A (Table 11). Longitudinal resistivity increases below seafloor from 0.23 Ωm to 0.43 Ωm at 144 mbsf with a minima of 0.20 Ωm at 2 to 3 mbsf (Fig. 26). Within the upper part of Subunit IIB (19.5–23.1 mbsf), resistivity measurements are above the general trend. The higher values coincide with the zone of decreasing shear strength and constant water content and porosity. This pattern resembles that which occurs between 25 mbsf and 33 mbsf in Hole 940A. The apparent decrease in resistivity at approximately 100 mbsf coincides with the porosity increase associated with the change from APC to XCB coring. In Units III through VI resistivity varies between 0.4 Ωm and 0.6 Ωm with wide scatter. The greatest scatter and highest resistivity values occur in the lower part of Unit III.

Comparison of longitudinal and transverse resistivities indicates that the sediment in Hole 944A is slightly anisotropic. The resistivity anisotropy is generally negative in the upper 145 m of the hole, similar to other levee deposits sampled during Leg 155. No consistent trends in anisotropy exist below 145 mbsf.

DOWNHOLE LOGGING

Logging Operations and Quality of Logs

In preparation for logging, we conditioned the hole by circulating sepiolite mud mixed with seawater and by tripping the drill pipe for reaming the borehole to remove debris. No fill was encountered in the bottom of the hole (total depth [TD] = 384.2 mbsf). An additional se-

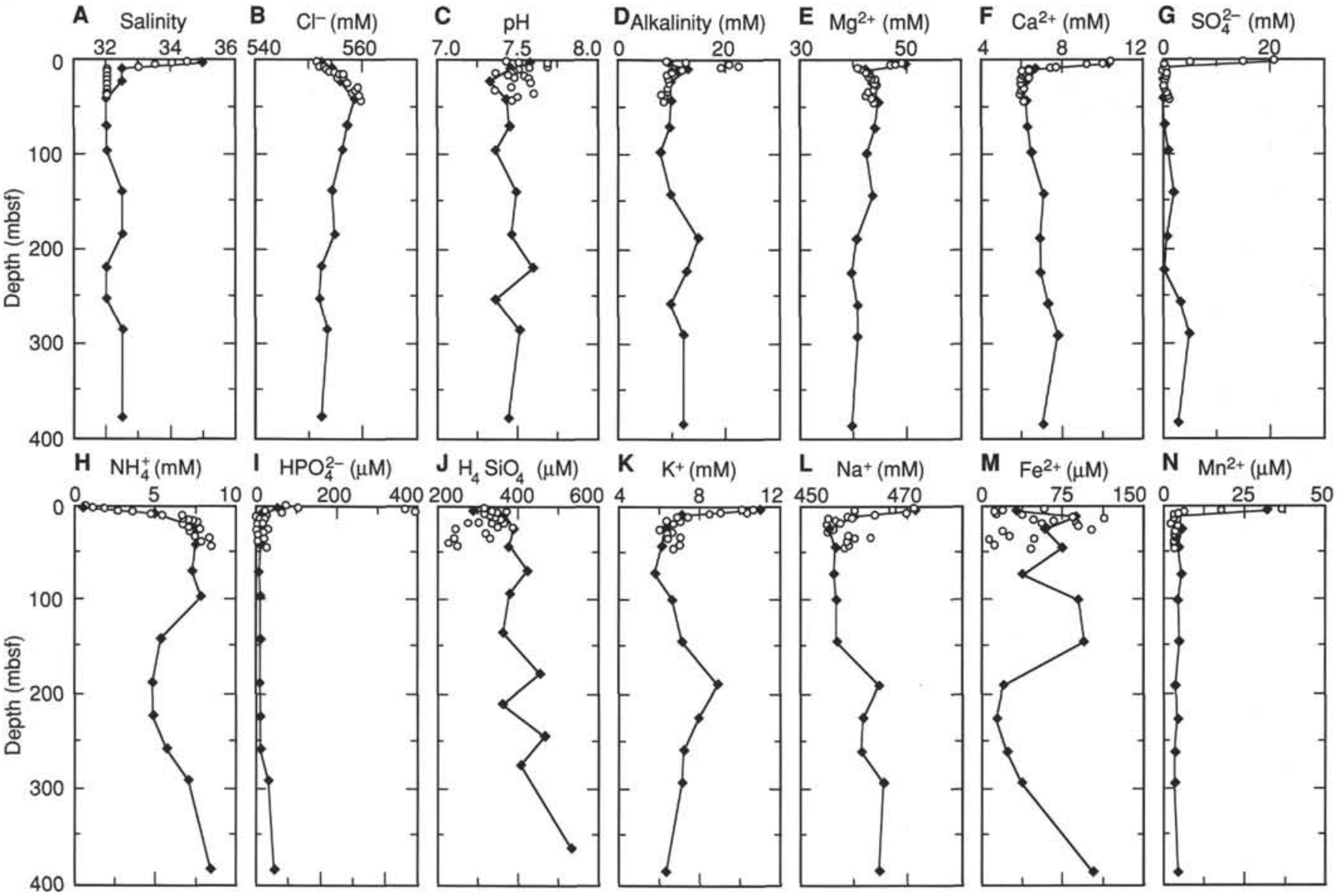

Figure 22. Downhole variation in pore-water chemistry for Hole 944A (solid diamonds) and Hole 944D (open circles). **A.** Salinity. **B.** Chloride. **C.** pH. **D.** Alkalinity. **E.** Magnesium. **F.** Calcium. **G.** Sulfate. **H.** Ammonium. **I.** Phosphate. **J.** Silica. **K.** Potassium. **L.** Sodium. **M.** Iron. **N.** Manganese.

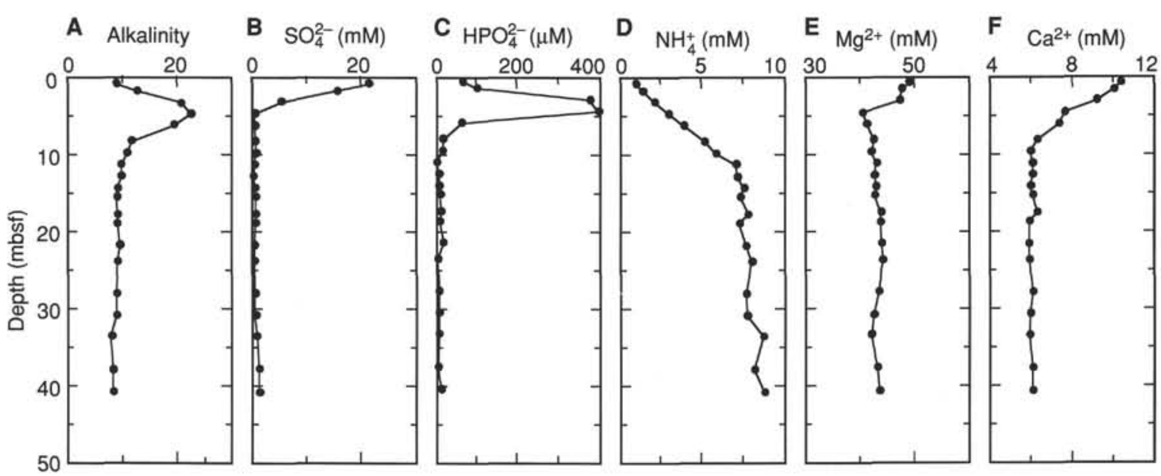

Figure 23. Pore-water chemistry of the upper 50 mbsf for Hole 944D. **A.** Alkalinity. **B.** Sulfate. **C.** Phosphate. **D.** Ammonium. **E.** Magnesium. **F.** Calcium.

piolite-seawater mix having a weight of 8.8 lb/gal (1.055 g/cm^3) was circulated into the borehole to help maintain borehole stability during logging. Both the Quad-combination and FMS tool strings reached TD and obtained useful logs between 384 and 74 mbsf (Table 12).

The density (HLDT) tool caliper showed that the borehole had been severely washed out and was rugose in several intervals (Fig. 27). Borehole diameter was particularly large (greater than the maximum HLDT caliper aperture of 16 in. [41 cm]) between 305 and 350 mbsf. Bulk density (RhoB) data are particularly affected by borehole conditions and yield inaccurately low values when pad contact is lost. Similarly, the FMS tool showed that intermittent pad contact between 305 and 350 mbsf severely degraded data quality. Good results were obtained from the remainder of the borehole, except over small (1–2 m thick) intervals where the borehole diameter exceeded 15.5 in. (39

Table 9. Index properties at Site 944.

Core, section, interval (cm)	Depth (mbsf)	Water content (%)	Wet-bulk density (g/cm^3)	Grain density (g/cm^3)	Dry-bulk density (g/cm^3)	Porosity (%)	Void ratio
155-944A-							
1H-1, 31–33	0.31	48.5	1.52	2.72	0.78	71.4	2.50
1H-1, 109–111	1.09	51.9	1.49	2.67	0.70	73.7	2.81
1H-2, 61–63	2.11	52.8	1.46	2.65	0.68	74.3	2.89
1H-3, 32–34	3.32	47.9	1.55	2.75	0.79	71.2	2.47
2H-1, 43–45	4.33	44.3	1.62	2.77	0.88	68.3	2.15
2H-2, 43–45	5.83	42.6	1.63	2.69	0.91	66.1	1.95
2H-3, 43–45	7.33	41.7	1.65	2.67	0.93	65.1	1.87
2H-4, 33–35	8.73	39.3	1.68	2.68	0.99	62.8	1.69
3H-1, 43–45	13.83	39.2	1.70	2.70	1.00	63.0	1.70
3H-2, 45–47	15.35	37.5	1.69	2.67	1.04	61.0	1.56
3H-3, 49–51	16.89	39.2	1.68	2.68	1.00	62.8	1.69
3H-4, 70–72	18.60	37.0	1.73	2.73	1.06	61.1	1.57
3H-5, 83–85	20.23	36.3	1.72	2.65	1.07	59.6	1.48
3H-6, 35–37	21.25	36.7	1.73	2.75	1.07	60.9	1.56
3H-7, 67–69	23.07	36.9	1.71	2.74	1.07	61.1	1.57
4H-1, 19–21	23.09	37.6	1.71	2.66	1.04	61.0	1.56
5H-1, 126–128	33.66	32.4	1.81	2.70	1.19	55.8	1.26
5H-2, 34–36	34.24	28.6	1.87	2.72	1.32	51.5	1.06
5H-3, 106–108	36.46	33.1	1.76	2.69	1.17	56.5	1.30
5H-4, 90–92	37.80	31.7	1.83	2.77	1.23	55.6	1.25
5H-5, 72–74	39.12	32.8	1.80	2.72	1.18	56.4	1.29
5H-6, 56–58	40.46	34.7	1.78	2.78	1.14	59.1	1.44
5H-7, 56–58	41.96	33.7	1.77	2.71	1.16	57.3	1.34
6H-1, 74–76	42.64	32.9	1.81	2.79	1.19	57.2	1.34
6H-2, 76–78	43.76	33.6	1.80	2.77	1.17	57.8	1.37
6H-3, 24–26	44.74	32.1	1.78	2.72	1.21	55.6	1.25
6H-4, 115–117	47.15	32.1	1.83	2.84	1.23	56.8	1.32
6H-5, 113–115	48.63	31.9	1.85	2.85	1.24	56.6	1.30
6H-7, 71–73	50.12	32.8	1.80	2.76	1.19	56.8	1.32
6H-CC, 45–47	51.08	31.2	1.81	2.74	1.24	54.8	1.21
7H-1, 99–101	52.39	31.9	1.82	2.73	1.21	55.6	1.25
7H-2, 99–101	53.89	31.3	1.84	2.83	1.25	55.7	1.26
7H-3, 8–80	55.18	30.1	1.85	2.74	1.27	53.6	1.15
7H-4, 113–115	57.03	30.5	1.83	2.80	1.27	54.5	1.20
7H-5, 109–111	58.49	29.8	1.87	2.78	1.29	53.6	1.15
7H-6, 60–62	59.50	30.1	1.82	2.74	1.27	53.5	1.15
7H-7, 35–37	60.75	30.0	1.89	2.84	1.30	54.3	1.19
8H-1, 127–129	62.17	30.4	1.86	2.79	1.27	54.4	1.19
8H-2, 114–116	63.54	30.8	1.85	2.81	1.27	54.9	1.22
8H-3, 86–88	64.76	29.4	1.86	2.81	1.31	53.4	1.14
8H-4, 92–94	66.32	29.9	1.81	2.73	1.28	53.1	1.13
8H-5, 47–49	67.14	29.1	1.86	2.83	1.33	53.1	1.13
8H-6, 11–13	68.28	30.6	1.85	2.79	1.27	54.5	1.20
8H-7, 49–51	70.16	29.7	1.84	2.72	1.28	52.8	1.12
9H-1, 42–44	70.82	30.3	1.83	2.75	1.27	53.8	1.17
9H-2, 37–39	72.27	29.1	1.85	2.85	1.33	53.3	1.14
9H-3, 81–83	74.21	29.3	1.88	2.81	1.32	53.1	1.13
9H-4, 32–34	75.22	29.1	1.91	2.76	1.31	52.6	1.11
9H-5, 50–52	76.90	28.8	1.89	2.75	1.32	52.1	1.09
9H-6, 83–85	78.73	28.1	1.88	2.77	1.35	51.4	1.06
9H-7, 81–83	80.21	28.4	1.88	2.75	1.33	51.6	1.07
10H-1, 77–79	80.67	30.5	1.86	2.81	1.27	54.7	1.21
10H-2, 61–63	82.01	29.5	1.86	2.84	1.32	53.7	1.16
10H-3, 97–99	83.87	29.2	1.88	2.81	1.32	53.0	1.13
10H-4, 53–55	84.93	27.9	1.95	2.82	1.36	51.6	1.07
10H-5, 104–106	86.32	28.2	1.93	2.87	1.37	52.4	1.10
10H-6, 101–103	87.79	27.3	1.97	2.84	1.39	51.0	1.04
11H-1, 60–62	90.00	28.2	1.88	2.76	1.34	51.4	1.06
11H-2, 60–62	91.50	28.6	1.90	2.82	1.34	52.5	1.11
11H-3, 60–62	93.00	28.5	1.91	2.81	1.34	52.2	1.09
11H-4, 60–62	94.50	28.6	1.87	2.75	1.33	51.7	1.07
11H-5, 76–78	96.16	27.8	1.89	2.75	1.35	50.8	1.03
12X-1, 82–84	97.92	31.5	1.81	2.75	1.23	55.3	1.24
12X-1, 133–135	98.43			2.83			
12X-2, 88–90	99.48	30.6	1.84	2.75	1.26	54.2	1.18
12X-3, 92–94	101.02	30.1	1.89	2.80	1.28	54.1	1.18
12X-4, 103–105	102.63	29.4	1.86	2.77	1.30	53.0	1.13
13X-1, 82–84	105.72	30.1	1.87	2.82	1.29	54.2	1.18
13X-2, 101–103	107.41	29.9	2.01	2.77	1.29	53.6	1.15
13X-3, 115–117	109.05	31.0	1.86	2.82	1.26	55.3	1.24
13X-4, 115–117	110.51	29.9	1.87	2.78	1.29	53.7	1.16
13X-5, 98–100	111.84			2.72			
13X-5, 106–108	111.92	29.4	1.91	2.74	1.29	52.7	1.11
16X-1, 87–89	134.67	29.8	1.94	2.84	1.31	54.0	1.17
16X-2, 89–91	136.19	28.6	1.88	2.76	1.33	51.9	1.08
16X-3, 85–87	137.65	28.9	1.95	2.75	1.31	52.2	1.09
16X-4, 79–81	139.09	28.7	1.91	2.85	1.34	52.9	1.12
16X-5, 58–60	140.38	27.5	1.93	2.83	1.38	51.1	1.05
17X-1, 53–55	143.93	30.6	1.86	2.77	1.26	54.4	1.19
17X-1, 58–60	143.98			2.72			
21X-1, 100–102	183.00			2.70			
21X-1, 108–110	183.08	29.4	1.89	2.72	1.29	52.6	1.11
21X-2, 89–91	184.39	24.8	1.97	2.72	1.45	46.7	0.88
22X-1, 59–61	192.19	27.6	1.92	2.73	1.35	50.4	1.01
22X-2, 61–63	193.71	27.2	1.92	2.71	1.36	49.7	0.99
22X-3, 64–66	195.24	24.6	2.05	2.79	1.48	47.0	0.89
22X-4, 60–62	196.70	27.0	1.95	2.75	1.38	49.9	0.99

Table 9 (continued).

Core, section, interval (cm)	Depth (mbsf)	Water content (%)	Wet-bulk density (g/cm³)	Grain density (g/cm³)	Dry-bulk density (g/cm³)	Porosity (%)	Void ratio
155-944A-							
22X-5, 66–68	198.26	24.7	2.06	2.76	1.47	46.9	0.88
22X-6, 57–59	199.67	25.6	1.97	2.74	1.42	47.9	0.92
23X-1, 92–94	202.12	24.2	1.99	2.70	1.47	45.6	0.84
23X-2, 93–95	203.63	23.7	2.03	2.69	1.48	44.9	0.82
23X-3, 91–93	205.11	23.7	2.01	2.69	1.48	44.8	0.81
23X-4, 94–96	206.64	23.9	2.04	2.75	1.49	45.7	0.84
23X-5, 99–101	208.19	24.0	1.99	2.72	1.48	45.6	0.84
24X-1, 123–125	212.13	23.3	2.04	2.74	1.51	44.9	0.81
24X-2, 116–118	213.56	20.9	2.06	2.71	1.59	41.2	0.70
24X-3, 102–104	214.92	23.8	1.99	2.70	1.48	45.1	0.82
24X-4, 96–98	216.36	21.7	2.09	2.73	1.57	42.5	0.74
24X-5, 92–94	217.82	21.2	2.10	2.76	1.60	42.0	0.72
24X-6, 108–110	219.48	20.7	2.08	2.78	1.63	41.5	0.71
24X-7, 20–22	220.10	21.2	2.08	2.76	1.60	42.0	0.72
25X-1, 47–49	220.97	25.7	1.94	2.67	1.40	47.5	0.90
25X-2, 44–46	222.44	19.9	2.11	2.69	1.63	39.5	0.65
25X-2, 91–93	222.91	21.8	2.05	2.72	1.56	42.5	0.74
25X-3, 83–85	224.33	21.6	2.10	2.79	1.59	42.8	0.75
25X-3, 118–120	224.68	19.0	2.13	2.75	1.69	38.6	0.63
25X-4, 24–26	225.24	21.0	2.11	2.72	1.59	41.4	0.71
25X-4, 75–77	225.75	21.2	2.10	2.73	1.59	41.8	0.72
25X-5, 130–132	227.80	21.9	2.06	2.75	1.57	43.0	0.75
25X-6, 91–93	228.91	27.6	1.95	2.78	1.37	50.8	1.03
25X-7, 31–33	229.81	21.0	2.07	2.68	1.58	41.0	0.70
26X-1, 74–76	230.84	22.9	2.02	2.69	1.51	43.9	0.78
26X-2, 74–76	232.34	21.3	2.05	2.72	1.58	41.9	0.72
26X-3, 64–66	233.74	21.1	2.04	2.73	1.59	41.6	0.71
26X-4, 96–98	235.56	21.8	2.05	2.71	1.56	42.4	0.74
26X-5, 44–46	236.54	22.0	2.07	2.77	1.57	43.3	0.77
28X-1, 62–64	250.02	20.8	2.07	2.73	1.61	41.1	0.70
28X-2, 81–83	251.71	21.1	2.04	2.70	1.58	41.3	0.71
28X-3, 51–53	252.91	20.4	2.06	2.70	1.61	40.3	0.67
28X-4, 55–57	254.45	21.7	2.08	2.79	1.59	43.1	0.76
28X-CC, 4–6	255.30	22.1	2.09	2.74	1.56	43.2	0.76
30X-1, 94–96	269.64	24.5	1.99	2.72	1.46	46.2	0.86
30X-2, 8–10	270.28	23.8	2.02	2.78	1.51	45.8	0.85
30X-3, 27–29	271.00	24.4	1.99	2.74	1.47	46.4	0.86
30X-4, 110–112	273.33	23.1	2.03	2.80	1.54	45.1	0.82
30X-5, 50–52	274.23	24.0	2.00	2.76	1.49	46.0	0.85
30X-6, 22–24	275.45	23.2	2.03	2.74	1.52	44.6	0.81
30X-7, 92–94	277.54	21.6	2.04	2.77	1.59	42.6	0.74
31X-2, 44–46	279.44	23.8	2.02	2.79	1.51	45.9	0.85
31X-3, 32–34	280.82	24.1	2.02	2.82	1.50	46.7	0.88
31X-4, 24–26	282.24	24.1	2.05	2.73	1.48	45.8	0.84
31X-5, 25–27	283.75	24.5	2.01	2.73	1.46	46.4	0.87
31X-6, 37–39	285.37	23.4	2.05	2.86	1.54	46.0	0.85
31X-7, 13–15	286.63	22.1	2.04	2.75	1.56	43.3	0.76
32X-2, 59–61	289.56	23.5	2.02	2.80	1.52	45.7	0.84
32X-3, 48–50	290.95	22.9	2.06	2.76	1.53	44.5	0.80
32X-4, 42–44	292.39	23.8	2.05	2.77	1.50	45.8	0.85
32X-5, 42–44	293.79	22.6	2.04	2.78	1.55	44.2	0.79
32X-6, 37–39	295.24	21.1	2.17	2.79	1.61	42.2	0.73
32X-7, 62–64	296.60	21.8	2.09	2.82	1.59	43.5	0.77
33X-1, 45–47	298.05	25.1	2.00	2.76	1.45	47.5	0.90
33X-2, 47–49	299.57	24.6	2.03	2.75	1.46	46.7	0.88
33X-3, 29–31	300.89	24.7	1.99	2.74	1.46	46.8	0.88
33X-4, 25–27	302.30			2.80			
33X-4, 30–32	302.35	23.6	2.04	2.80	1.52	45.8	0.85
33X-5, 67–69	304.22	24.4	2.01	2.75	1.47	46.4	0.87
34X-1, 43–45	307.73			2.70			
40X-1, 40–42	365.30	27.1	1.95	2.74	1.37	49.8	0.99
41X-1, 20–22	374.70	24.4	1.99	2.70	1.46	46.0	0.85
41X-1, 130–132	375.80	23.7	2.02	2.67	1.47	44.7	0.81
41X-2, 48–50	376.48	23.7	2.03	2.68	1.48	44.9	0.81
41X-3, 22–24	377.64	23.0	2.03	2.69	1.51	44.0	0.79

cm). A second pass with the FMS tool provided some additional borehole coverage. Shore-based processed logs are shown at the end of this chapter and in the enclosed CD-ROM (back pocket).

Results

Logs were obtained within lithostratigraphic Subunits IIC through IID and Units III, IV, V, and VI (Fig. 27). The logging data were particularly useful in low core recovery intervals between 114 and 192, 234 and 266, and 304 and 384 mbsf (TD).

Comparison with Lithology

The interval between 75 and 138 mbsf, within lithostratigraphic Subunit IIC, shows an increase in resistivity, velocity, and density downhole. Gamma-ray values are relatively high (~80 API units), and subtle fluctuations may be related to the small-scale variations in bed thickness and grain size observed in the cores (Fig. 28A). The interval between 122 and 128 mbsf was washed out. However, it appears to display distinctly low porosity and gamma-ray values, as well as high velocity and density, suggesting a thick-bedded sand-rich interval. The low neutron porosity values probably result from a smaller contribution of clay-bound water to neutron attenuation within this sand interval.

Between 138 and 182 mbsf, lower resistivity and gamma-ray values are punctuated by fluctuations that may be caused by interbedded silty clay and sand, but also in part by borehole rugosity. Between 158 and 180 mbsf, high velocity, low gamma-ray, and low neutron porosity values suggest the presence of thick, sand-rich intervals. Between 182 and 190 mbsf, resistivity and gamma-ray values gradually

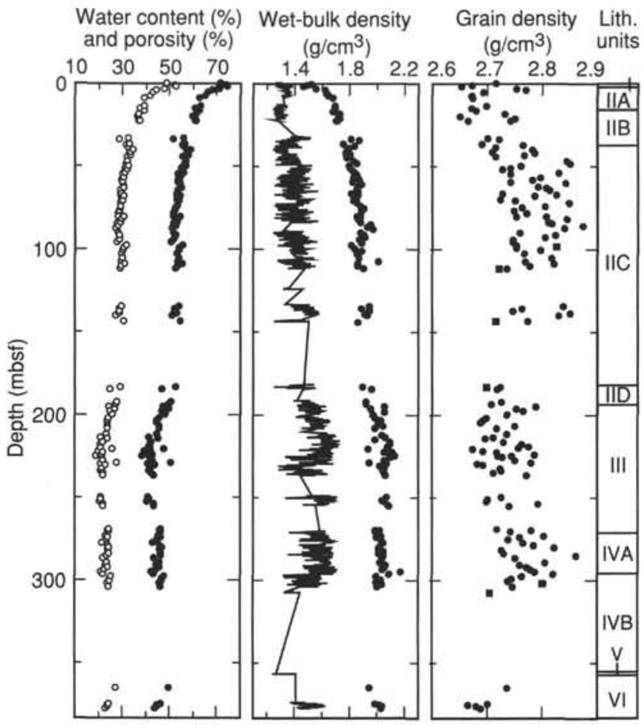

Figure 24. Water content (open circles) and porosity (solid circles), wet-bulk density as determined for discrete samples and by the GRAPE (line), and grain density for Hole 944A. Silt and sand sampled only for grain density are represented by squares.

increase downhole to overall high values within Subunit IID (Figs. 27 and 28A). The contact between Units II and III appears to occur at 190 mbsf in the logs, rather than at 192 mbsf (see the "Lithostratigraphy" section, this chapter), as suggested by increases in resistivity and velocity; this contact marks the top of the "Unit R" mass-flow deposit (see "Core-Seismic Integration" section, this chapter). The gradual change in log responses observed here contrast with the abrupt downhole increases in resistivity, density, and velocity at the top of Unit R at Site 936.

Lithostratigraphic Unit III is characterized by a uniform gamma-ray response, except for a washed-out interval between 225 and 233 mbsf that has low values (Fig. 27). The interval between 218 and 226 mbsf is characterized by high velocity, density, and resistivity and apparently correlates with the interval of mud clasts recovered in Core 944A-25X. The base of Unit III is defined by a very sharp decrease in gamma-ray, resistivity, velocity, and density values at 266 mbsf. Similar logging responses were observed at Sites 935 and 936, and these may suggest contact with an underconsolidated interval below.

Between 266 and 305 mbsf (Unit IV), logs indicate nearly constant resistivity and gamma ray, with values similar to those in Subunit IIC; both intervals are characterized by thin-bedded silty turbidites. Between 291 and 297 mbsf, short intervals of lower resistivity apparently correlate with thin packets of sand beds (Fig. 28B). A pronounced decrease in resistivity and gamma-ray values below 305 mbsf coincides with the top of a large washed-out interval that extends down to 350 mbsf (Fig. 27). Although the logs need to be corrected for borehole size, this interval shows log character similar to the basal part of Subunits IIC and IID. Both resistivity and gamma-ray data suggest the presence of coarsening-upward cycles.

Anomalously low values of velocity and density between 305 and 315 mbsf are accompanied by a high neutron porosity. This may in part result from the large borehole, but the combination with low ve-

Table 10. Undrained shear strength at Site 944.

Core, section, interval (cm)	Depth (mbsf)	Peak undrained shear strength (kPa)	Residual undrained shear strength (kPa)	Unconfined compressive strength* (kPa)
155-944A-				
1H-1, 110	1.10	3.2	2.3	
1H-2, 62	2.12	3.9	2.7	
1H-3, 33	3.33	6.5	4.9	
2H-1, 44	4.34	8.7	6.0	
2H-2, 44	5.84	12.0	8.1	
2H-3, 44	7.34	13.1	9.0	
2H-4, 34	8.74	13.9	9.4	
3H-1, 44	13.84	15.6	9.9	
3H-2, 46	15.36	18.7	11.4	
3H-3, 50	16.90	12.9	8.6	
3H-4, 71	18.61	14.8	9.5	
3H-5, 84	20.24	13.2	8.3	
3H-6, 113	22.03	12.4	7.0	
3H-7, 68	23.08	12.3	8.6	
4H-1, 20	23.10	10.2	7.5	
5H-1, 127	33.67	23.8	14.6	
5H-2, 35	34.25	29.8	15.9	
5H-3, 107	36.47	22.5	13.2	
5H-4, 91	37.81	25.0	14.4	
5H-5, 73	39.13	17.2	10.9	
5H-6, 57	40.47	21.3	14.0	
5H-7, 47	41.87	60.2	45.6	
5H-7, 57	41.97	23.8	16.6	
6H-1, 75	42.65	32.2	17.7	
6H-2, 77	43.77	19.8	11.7	
6H-3, 25	44.75	25.7	14.8	
6H-4, 116	47.16	27.2	15.8	
6H-5, 114	48.64	33.9	19.2	
6H-7, 72	50.13	39.0	21.9	
6H-CC, 46	51.09	32.5	19.3	
7H-1, 100	52.40	44.4	24.2	83.4
7H-2, 100	53.90	34.8	15.9	73.6
7H-3, 79	55.19	46.4	22.3	83.4
7H-4, 114	57.04	52.1	25.2	98.1
7H-5, 110	58.50	40.5	21.7	93.2
7H-6, 61	59.51	35.6	17.8	88.3
7H-7, 36	60.76	24.0	13.6	73.6
8H-1, 128	62.18	45.0	24.4	122.6
8H-2, 115	63.55	52.1	26.3	127.5
8H-3, 87	64.77	59.7	31.2	117.7
8H-4, 93	66.33	57.5	34.8	112.8
8H-5, 48	67.15	38.9	22.3	98.1
8H-6, 12	68.29	36.2	24.1	78.5
8H-7, 50	70.17	42.4	27.5	98.1
9H-1, 43	70.83	46.9	25.5	88.3
9H-2, 38	72.28	38.0	17.2	83.4
9H-3, 82	74.22	38.9	24.1	78.5
9H-4, 33	75.23	28.3	13.0	88.3
9H-5, 51	76.91	44.2	18.9	83.4
9H-6, 84	78.74	46.0	21.2	93.2
9H-7, 82	80.22	53.9	29.4	112.8
10H-1, 78	80.68	33.6	22.3	73.6
10H-2, 62	82.02	36.2	18.4	73.6
10H-3, 98	83.88	57.5	33.3	107.9
10H-4, 54	84.94	56.6	33.1	152.1
10H-5, 105	86.33	61.9	36.5	152.1
10H-6, 102	87.80	53.9		152.1
11H-1, 60	90.00	36.2		117.7
11H-2, 60	91.50	53.0	31.3	147.2
11H-3, 60	93.00	71.6	39.7	176.6
11H-4, 61	94.51	53.9		137.3
11H-5, 77	96.17			171.7
12X-1, 82	97.92	27.4	19.4	78.5
12X-2, 88	99.48	34.5	23.8	107.9
12X-3, 93	101.03	29.2	22.2	98.1
12X-4, 105	102.65	33.6	24.7	117.7
13X-1, 83	105.73	42.4	29.6	112.8
13X-2, 102	107.42	30.9	22.6	103.0
13X-3, 116	109.06	40.7	27.8	127.5
13X-4, 116	110.52	57.5	37.5	157.0
13X-5, 108	111.94	47.7	31.5	127.5
16X-1, 88	134.68	46.0	31.9	152.1
16X-2, 90	136.20	55.7	33.7	147.2
16X-3, 87	137.67	61.9	36.9	161.9
16X-4, 79	139.09	68.1	41.8	166.8
16X-5, 55	140.35	102.5	55.8	215.8
17X-1, 54	143.94			49.1
21X-2, 90	184.40	43.3		166.8
22X-1, 60	192.20	77.8	42.1	289.4
22X-2, 62	193.72	112.3	61.8	309.0
22X-3, 65	195.25	137.9	69.0	353.2
22X-4, 61	196.71	95.5	53.1	387.5
22X-5, 67	198.27	134.4	71.2	338.4
22X-6, 58	199.68			363.0
23X-1, 93	202.13	108.7	57.8	269.8

Table 10 (continued).

Core, section, interval (cm)	Depth (mbsf)	Peak undrained shear strength (kPa)	Residual undrained shear strength (kPa)	Unconfined compressive strength* (kPa)
23X-2, 94	203.64	87.5	54.3	294.3
23X-3, 92	205.12	108.7	62.5	318.8
23X-4, 95	206.65	130.8	67.5	304.1
23X-5, 100	208.20	152.1	73.4	382.6
24X-1, 124	212.14	146.7	73.8	343.4
24X-2, 117	213.57	166.2	89.9	358.1
24X-3, 103	214.93	147.6	79.1	407.1
24X-4, 97	216.37	210.4	97.8	416.9
24X-5, 93	217.83	171.5	83.0	>440
24X-6, 109	219.49	134.4	63.1	431.6
24X-7, 21	220.11	177.7	93.0	412.0
25X-1, 54	221.04	63.6	38.5	157.0
25X-2, 35	222.35	172.4	85.3	426.7
25X-2, 92	222.92	86.6	41.7	269.8
25X-3, 84	224.34	116.7	60.4	392.4
25X-3, 119	224.69	263.4	121.7	>440
25X-4, 25	225.25	208.6	98.1	>440
25X-4, 76	225.76	125.5	73.3	313.9
25X-5, 131	227.81	122.0	67.8	377.7
25X-6, 92	228.92	206.9	72.7	402.2
25X-7, 32	229.82	184.8	74.6	431.6
26X-1, 75	230.85			>440
26X-2, 75	232.35	165.3	76.4	416.9
26X-3, 65	233.75	137.0	67.9	431.6
26X-4, 97	235.57	133.5	76.4	358.1
26X-5, 45	236.55	123.8	75.0	318.8
28X-1, 63	250.03	121.1	71.0	274.7
28X-2, 82	251.72	152.1	77.4	323.7
28X-3, 52	252.92	176.8	92.4	338.4
28X-4, 56	254.46	152.9	80.1	309.0
28X-CC, 5	255.31			338.4
30X-1, 95	269.65	122.0	64.3	196.2
30X-2, 9	270.29			367.9
30X-3, 28	271.01	93.7	62.0	210.9
30X-4, 111	273.34	84.0	53.9	206.0
30X-5, 51	274.24	87.5	55.4	210.9
30X-6, 23	275.46	101.7	59.2	260.0
30X-7, 93	277.55			318.8
31X-2, 50	279.50	59.2	40.1	269.8
31X-3, 38	280.88	125.5	71.7	309.0
31X-4, 25	282.25	84.0	50.5	264.9
31X-5, 26	283.76	75.1	44.9	245.3
31X-6, 37	285.37	79.6	50.3	309.0
31X-7, 13	286.63	131.7	76.3	382.6
32X-2, 60	289.57	84.9	47.1	245.3
32X-3, 49	290.96	95.5	56.1	313.9
32X-4, 43	292.40	97.2	53.0	260.0
32X-5, 44	293.81	134.4	70.0	215.8
32X-6, 40	295.27	182.1		431.6
32X-7, 63	296.61	119.3	65.6	313.9
33X-1, 46	298.06	46.9	32.5	210.9
33X-2, 48	299.58	66.3	38.9	210.9
33X-3, 31	300.91	45.1	30.5	117.7
33X-4, 32	302.37	70.7		235.4
33X-5, 68	304.23	55.7		201.1
41X-1, 21	374.71	53.9		161.9
41X-1, 131	375.81	71.6		318.8
41X-2, 49	376.49	88.4		235.4
41X-3, 23	377.65	80.4		225.6

Note: *Unconfined compressive strength (q_u) can be used to approximate undrained shear strength (S_u) by the relationship $q_u = 2S_u$.

locity suggests the presence of higher gas concentrations in the formation. Although the borehole remains large, porosity is lower below 315 mbsf, down to 350 mbsf, and velocity and density increase markedly. Analogous to the base of Subunit IIC, low porosity values may result if the formation contains less clay and, consequently, less clay-bound water (hydrogen).

The carbonate-rich sediment of Unit V, observed in Core 944A-39X, can be discerned by the subtly higher resistivity interval extending between 352 and 363 mbsf (Fig. 28B). The character and values in resistivity are similar to a stratigraphically equivalent unit penetrated near the base of Hole 935A. Between 363 and 380 mbsf, gamma-ray, resistivity, and density values increase downhole, suggesting a downhole decrease in thickness and/or grain-size of silt beds.

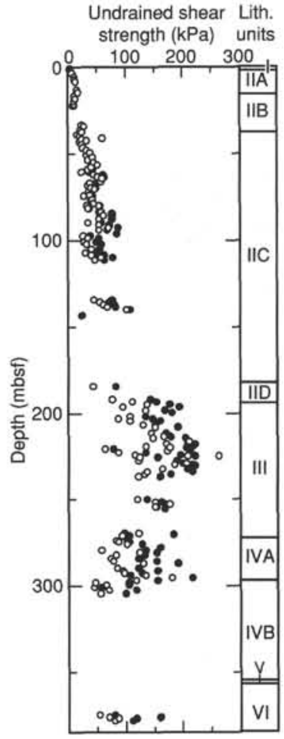

Figure 25. Undrained shear strength (open circles) and assumed undrained shear strength derived from unconfined compressive strength (solid circles) for Hole 944A.

Borehole Characteristics

The borehole was nearly vertical and had a deviation of only 1° to 1.5°. Except for the interval between 80 and 120 mbsf, borehole shape measured by the FMS calipers was nearly circular through most of the logged interval (Fig. 29). Between 80 and 120 mbsf, the borehole was elliptical with the long axis oriented approximately east-west. This interval coincides with the overbank levee deposits of the Amazon Channel. Above 95 mbsf, ellipticity is more pronounced, but this interval may have been affected by movement of the BHA during logging.

Borehole Temperature

Temperatures were measured about 3 hr after we stopped circulating seawater and mud in the borehole. The downgoing logging run of the TLT shows two large increases in temperature. The first increase is at 80 mbsf inside the BHA, immediately above the open-hole section, and the second is at 320 mbsf, within the large washed-out interval (Fig. 30). The anomaly at 320 mbsf indicates an initial temperature decrease of 0.5°C, followed by a sudden temperature increase of about 1.5°C. This increase may have resulted from the temperature tool encountering a partial obstruction in the borehole and then breaking through it (Figs. 27 and 29). The upgoing run shows a marked decrease in borehole temperature gradient at about 240 mbsf, near the base of Unit III. Although borehole temperatures are affected by seawater circulation during and after drilling, rapid changes in borehole temperature may be related to downhole variation of thermal conductivity and/or lateral fluid advection. Similar rapid variations were observed at Sites 931, 933, and 936 below mass-flow deposits.

Table 11. Electrical resistivity at Site 944.

Core, section, interval (cm)	Depth (mbsf)	Longitudinal resistivity (Ωm)	Transverse resistivity (Ωm)
155-944A-			
1H-1, 32	0.32	0.233	0.230
1H-1, 110	1.10	0.207	0.204
1H-2, 62	2.12	0.197	0.196
1H-3, 33	3.33	0.203	0.214
2H-1, 44	4.34	0.232	0.217
2H-2, 44	5.84	0.225	0.226
2H-3, 44	7.34	0.245	0.241
2H-4, 34	8.74	0.253	0.246
3H-1, 44	13.84	0.264	0.257
3H-2, 46	15.36	0.277	0.273
3H-3, 50	16.90	0.282	0.283
3H-4, 71	18.61	0.284	0.285
3H-5, 11	19.51	0.308	0.295
3H-5, 84	20.24	0.321	0.321
3H-6, 36	21.26	0.322	0.305
3H-6, 117	22.07	0.319	0.323
3H-7, 12	22.52	0.314	0.313
3H-7, 68	23.08	0.327	0.321
4H-1, 20	23.10	0.340	0.316
5H-1, 127	33.67	0.344	0.338
5H-2, 35	34.25	0.341	0.345
5H-3, 107	36.47	0.317	0.316
5H-4, 91	37.81	0.302	0.304
5H-5, 73	39.13	0.326	0.327
5H-6, 57	40.47	0.310	0.318
5H-7, 47	41.87	0.336	0.320
5H-7, 57	41.97	0.327	0.307
6H-1, 75	42.65	0.333	0.293
6H-2, 77	43.77	0.318	0.311
6H-3, 25	44.75	0.317	0.318
6H-4, 116	47.16	0.332	0.323
6H-5, 114	48.64	0.337	0.331
6H-7, 72	50.13	0.318	0.305
6H-CC, 46	51.09	0.334	0.328
7H-1, 100	52.40	0.332	0.314
7H-2, 100	53.90	0.339	0.316
7H-3, 79	55.19	0.338	0.310
7H-4, 114	57.04	0.340	0.326
7H-5, 110	58.50	0.362	0.345
7H-6, 61	59.51	0.354	0.335
7H-7, 31	60.71	0.366	0.362
8H-1, 128	62.18	0.403	0.350
8H-2, 115	63.55	0.361	0.343
8H-3, 87	64.77	0.374	0.346
8H-4, 93	66.33	0.354	0.371
8H-5, 48	67.15	0.358	0.350
8H-6, 12	68.29	0.368	0.339
8H-7, 50	70.17	0.335	0.352
9H-1, 43	70.83	0.343	0.322
9H-2, 38	72.28	0.392	0.375
9H-2, 73	72.63	0.358	0.339
9H-3, 82	74.22	0.361	0.357
9H-4, 33	75.23	0.370	0.351
9H-5, 51	76.91	0.384	0.355
9H-6, 84	78.74	0.367	0.359
9H-7, 82	80.22	0.370	0.366
10H-1, 78	80.68	0.376	0.359
10H-2, 62	82.02	0.382	0.376
10H-3, 98	83.88	0.368	0.360
10H-4, 54	84.94	0.386	0.378
10H-5, 105	86.33	0.402	0.394
10H-6, 162	88.40	0.391	0.401
11H-1, 60	90.00	0.404	0.398
11H-2, 60	91.50	0.394	0.370
11H-3, 60	93.00	0.384	0.373
11H-4, 61	94.51	0.390	0.374
11H-5, 77	96.17	0.367	0.381
12X-1, 82	97.92	0.385	0.388
12X-2, 88	99.48	0.352	0.341
12X-3, 93	101.03	0.351	0.342
12X-4, 105	102.65	0.354	0.354
13X-1, 83	105.73	0.366	0.353
13X-2, 102	107.42	0.402	0.373
13X-3, 116	109.06	0.380	0.354
13X-4, 116	110.52	0.380	0.373
13X-5, 108	111.94	0.387	0.381
16X-1, 88	134.68	0.401	0.412
16X-2, 90	136.20	0.406	0.405
16X-3, 87	137.67	0.404	0.411
16X-4, 79	139.09	0.413	0.396
16X-5, 55	140.35	0.416	0.404
17X-1, 54	143.94	0.431	0.391
21X-1, 109	183.09	0.478	0.438
21X-2, 90	184.40	0.470	0.471
22X-1, 60	192.20	0.516	0.512
22X-2, 62	193.72	0.446	0.508
22X-3, 65	195.25	0.494	0.540
22X-4, 61	196.71	0.460	0.411
22X-5, 61	198.21	0.467	0.463
22X-6, 58	199.68	0.483	0.485
23X-1, 93	202.13	0.482	0.495
23X-2, 94	203.64	0.493	0.510
23X-3, 92	205.12	0.485	0.483
23X-4, 95	206.65	0.499	0.501
23X-5, 100	208.20	0.494	0.507
24X-1, 124	212.14	0.534	0.531
24X-2, 117	213.57	0.538	0.523
24X-3, 103	214.93	0.479	0.498
24X-4, 97	216.37	0.538	0.505
24X-5, 93	217.83	0.504	0.509
24X-6, 89	219.29	0.467	0.495
24X-7, 21	220.11	0.498	0.553
25X-1, 48	220.98	0.524	0.523
25X-2, 35	222.35	0.436	0.487
25X-2, 92	222.92	0.565	0.510
25X-3, 84	224.34	0.522	0.484
25X-3, 119	224.69	0.555	0.531
25X-4, 25	225.25	0.496	0.536
25X-4, 76	225.76	0.566	0.543
25X-5, 131	227.81	0.585	0.500
25X-6, 35	228.35	0.501	0.521
25X-6, 92	228.92	0.429	0.383
25X-7, 32	229.82	0.495	0.489
26X-1, 75	230.85	0.482	0.494
26X-2, 75	232.35	0.532	0.523
26X-3, 65	233.75	0.522	0.500
26X-4, 97	235.57	0.437	0.509
26X-5, 45	236.55	0.558	0.521
28X-1, 63	250.03	0.576	0.544
28X-2, 82	251.72	0.550	0.495
28X-3, 52	252.92	0.517	0.494
28X-4, 56	254.46	0.536	0.550
28X-CC, 5	255.31	0.550	0.550
30X-1, 95	269.65	0.480	0.448
30X-2, 9	270.29	0.496	0.480
30X-3, 28	271.01	0.481	0.484
30X-4, 111	273.34	0.466	0.511
30X-5, 51	274.24	0.478	0.457
30X-6, 23	275.46	0.486	0.484
30X-7, 93	277.55	0.469	0.501
31X-2, 45	279.45	0.489	0.477
31X-3, 34	280.84	0.465	0.465
31X-4, 25	282.25	0.442	0.437
31X-5, 26	283.76	0.468	0.426
31X-6, 37	285.37	0.478	0.465
31X-7, 13	286.63	0.526	0.540
32X-2, 60	289.57	0.485	0.487
32X-3, 49	290.96	0.481	0.478
32X-4, 43	292.40	0.471	0.474
32X-5, 44	293.81	0.481	0.530
32X-6, 40	295.27	0.539	0.516
32X-7, 63	296.61	0.490	0.481
33X-1, 46	298.06	0.455	0.448
33X-2, 48	299.58	0.448	0.428
33X-3, 31	300.91	0.444	0.446
33X-4, 32	302.37	0.451	0.449
33X-5, 68	304.23	0.462	0.472
41X-1, 21	374.71	0.561	0.628
41X-1, 131	375.81	0.497	0.582
41X-2, 49	376.49	0.455	0.479
41X-2, 106	377.06	0.492	0.492
41X-3, 23	377.65	0.476	0.451

CORE-SEISMIC INTEGRATION

Hole 944A penetrated through the Amazon/Brown Channel-levee System, Unit R, the Red Channel-levee System of the Middle Levee Complex, and into the Green Channel-levee System of the Lower Levee Complex (Manley and Flood, 1988). Eight seismic-facies units are identified, the upper two on 3.5-kHz echograms (seismic-facies Units 1 and 2; Fig. 31) and the lower six on water-gun seismic profiles (seismic-facies Units 3–8; 2020UTC on 11 May 1994 during Leg 155; Fig. 32).

Preliminary correlation between the seismic-facies units and the lithologic units was made by using the velocity-depth equation determined at Site 931 and from downhole logging at this site. Seismic-facies Unit 1 (0 to 10 ms) is characterized by medium-amplitude,

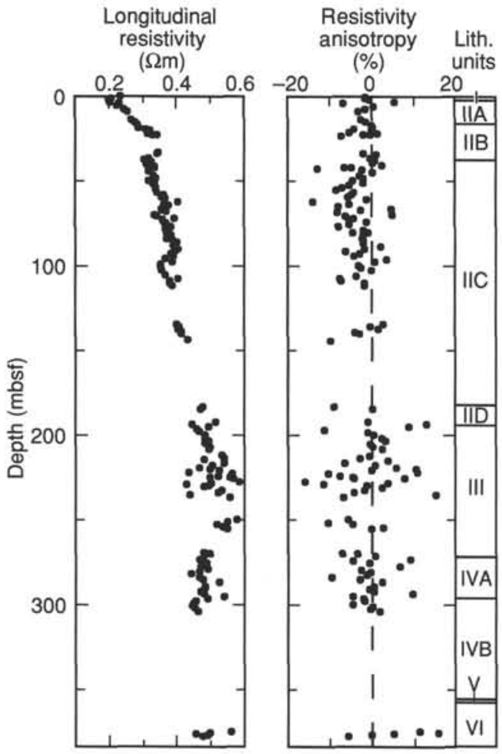

Figure 26. Longitudinal resistivity and resistivity anisotropy for Hole 944A.

continuous, parallel reflections. Seismic-facies Unit 1 correlates with lithologic Unit I, a foraminifer-nannofossil clay, and the upper 6 m of Subunit IIA, which is predominantly composed of bioturbated, hemipelagic silty clay.

Seismic-facies Unit 2 (10–35 ms) exhibits low-amplitude, divergent to transparent reflections and is correlated with lithologic Subunit IIA and the upper 10 m of Subunit IIB. This interval is composed of silty clay with silt laminae.

Seismic-facies Unit 3 (35–160 ms) is characterized by low-amplitude, continuous divergent reflections returned from sediment of the Amazon/Brown Channel-levee System. Unit 3 correlates with the lower 12 m of lithologic Subunit IIB and the upper 88 m of Subunit IIC, which are composed of silty clay containing numerous silt laminae and thin beds of silt and fine to medium sand.

High-amplitude, continuous and parallel reflections (seismic-facies Unit 4), identified as the HARP unit associated with the Amazon/Brown System and older channel-levee systems, occur between 160 and 245 ms. This interval correlates to lithologic Subunits IIC (lower 57 m) and IID, composed of thin- to medium-bedded silt and fine sand turbidites. In this interval of poor core recovery, downhole logs suggest the presence of alternating beds of sand and mud including thick sand beds at 122–128 mbsf and 158–180 mbsf.

The chaotic to hummocky reflections of seismic-facies Unit 5 (245–320 ms) correlate to lithologic Unit III, which is composed of muddy mass-flow deposits and possibly slumps. The base of Unit III does not correlate well with the seismic-facies interface between Units 5 and 6. This poor correlation is probably caused by an incorrect velocity-depth conversion for the sediment within Unit R and must await further shore-based studies to be resolved. Similar discrepancies were observed for debris flows at Sites 931 and 936. Comparison with downhole log data and the synthetic seismogram (below) suggest that the Site 931 velocity-depth profile underestimated the velocity of these debris flows by 8% to 15%.

Continuous, divergent reflections between 320 and 380 ms characterize seismic-facies Unit 6. This seismic-facies unit correlates to lithologic Subunit IVA and the upper 15 m of Subunit IVB, which are composed of silty clay with some silt laminae, and represents the levee deposits of the Red Channel-levee System.

Medium-amplitude, continuous subparallel reflections between 380 and 440 ms characterize seismic-facies Unit 7. These reflections correlate with the lower 45 m of lithologic Subunit IVB. Recovered sediment in Subunit IVB is composed of thin-bedded silt and fine sand turbidites interbedded with silty clay. Logs suggest the presence of coarsening-upward sequences. This seismic-facies unit encompasses the HARP at the base of the Red Channel-levee System and of other systems of the Middle Levee Complex.

The lower amplitude, continuous divergent reflections characteristic of seismic-facies Unit 8 (below 440 ms) originate from the overbank silt and fine sand turbidite deposits of lithologic Unit VI within the Green Channel-levee System of the Lower Levee Complex.

Synthetic Seismogram

Velocity and density profiles were determined between 74 and 385 mbsf from downhole logging. A synthetic seismogram (Fig. 33) was produced using the two-way traveltime to the first log data, based on an average constant velocity of 1540 m/s between the seafloor and 74 mbsf. The synthetic seismogram (using in-situ log velocities) is in good agreement with the seismic profile, showing the correct location of prominent reflections. A reversed polarity occurs at the base of seismic Unit 5 (Unit R; ~5.35 s two-way traveltime) due to the velocity and density decrease below the base of the Unit R Debris Flow.

IN-SITU TEMPERATURE MEASUREMENTS

Temperature gradients and heat flow were determined using two downhole measurements and the bottom-water (mud-line) temperature. Two ADARA measurements were made during Cores 944A-6H (51 mbsf) and -9H (80 mbsf) using instrument number 12. The mud-line temperature of 2.38°C measured from this instrument was used as the reference bottom-seawater temperature at Site 944. Successful measurements resulted in extrapolated equilibrium temperatures of 4.79°C at 51 mbsf, and 5.46°C at 80 mbsf.

Equilibrium temperatures, extrapolated from synthetic curves constructed to fit transient temperature data, are plotted as a function of depth (mbsf) in Figure 34. Using the ADARA mud-line temperature and the sub-bottom temperatures from the two ADARA measurements downhole, the geothermal temperature gradient can be approximated by a linear mean of 39.4°C/km. We calculated heat flow by adopting the constant geothermal temperature gradient of

Table 12. Intervals logged and tools employed in Hole 944A.

String	Run	Open hole (mbsf)	Open hole (mbrf)	In pipe (mbsf)	In pipe (mbrf)	Tools
Quad	Down	91.4–347.4	3804–4060			NGT/LSS/CNT-G/HLDT/DITE/TLT
	Up 1	380.9–247.4	4093.5–3960			
	Up 2	380.9–74	4093.5–3786.6	74–0	3786.6–3712.6	
FMS	Up 1	384.9–109.4	4097–3822			NGT/GPIT/FMS
	Up 2	384.9–78.4	4097–3791			

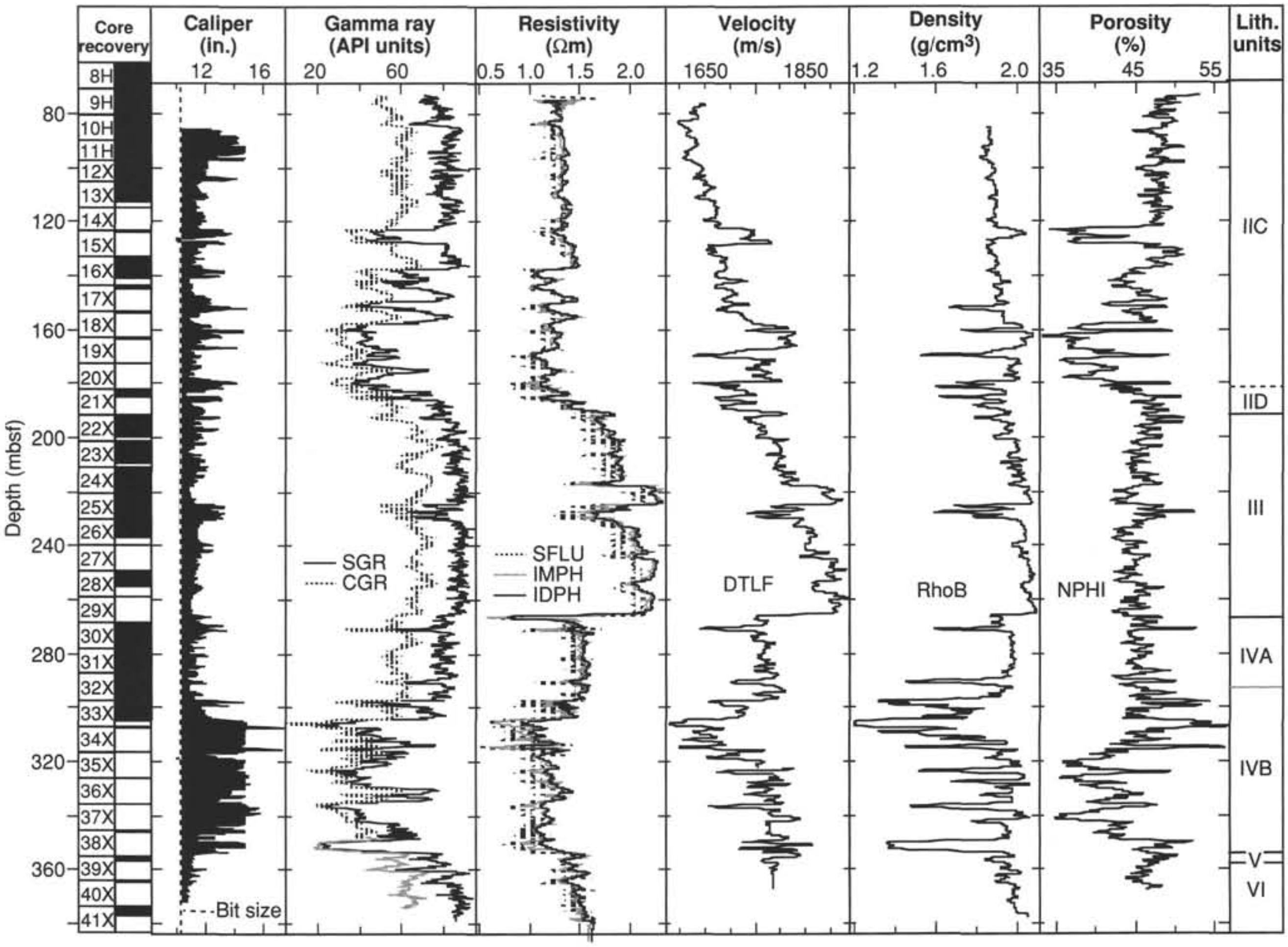

Figure 27. Summary of logging data obtained from the Quad-combination string for Hole 944A. Left to right: Core numbers and recovery; spectral (SGR) and computed (CGR = Th + K) gamma ray; shallow spherically focused resistivity (SFLU); medium (IMPH) and deep (IDPH) induction phasor resistivity; far source-receiver offset sonic velocity (DTLF); bulk density (RhoB); and neutron porosity (NPHI). On the right is the division of lithostratigraphic units.

39.4°C/km and a thermal conductivity, K, of 1.05 ± 0.15 W/(m·K), which is an average of regression estimates at 80 mbsf. This results in a calculated heat flow of 41.4 mW/m^2.

Depending on which data points are used, markedly different estimates can be made of the geothermal gradient for different intervals. Using the ADARA mud-line temperature and the one ADARA measurement at 51 mbsf, the geothermal gradient is 46.8°C/km (Fig. 34). If we use only the two sub-bottom ADARA temperatures (Fig. 34), the geothermal gradient is 23.5°C/km.

SYNTHESIS AND SIGNIFICANCE

Stratigraphic Synthesis

Holocene Surficial Foraminifer-Nannofossil Clay (Unit I)

Unit I (0–0.54 mbsf) is a Holocene, bioturbated, foraminifer-nannofossil clay, with up to 38% carbonate (Fig. 35).

Distal Levee of the Amazon/Brown Channel-levee System (Upper Part of Unit II)

The upper part of Unit II (to 122 mbsf) corresponds to the distal levee of the Amazon/Brown Channel-levee System. The mud has 2%–3% carbonate content. Subunit IIA (0.54–15.38 mbsf) comprises intensely bioturbated mud, stained to varying degrees by black hydrotroilite. Subunit IIB (15.38–37.42 mbsf) consists of mud with silt laminae. An interval of sediment deformation interpreted as a slump occurs from 32.4 to 36.9 mbsf. The upper part of Subunit IIC (37.42–122 mbsf) comprises mud with laminae and thin beds of silt and, below 111 mbsf, rare thin beds of very fine sand. Moderate bioturbation is common. Two thin intervals of contorted or dipping beds occur at 44 mbsf and 57 mbsf.

Brown, Purple, and Orange HARPs and Distal Purple Levee (Lower Part of Unit II)

The lower part of Unit II had poor recovery and corresponds in seismic-reflection profiles to a series of HARPs beneath the Amazon-Brown levee and the distal part of the Purple levee. The HARPs are tentatively correlated with the Brown, Purple, and Orange systems. The lower part of Subunit IIC (122–163.23 mbsf) comprises mud with laminae of silt and thin beds of silt, very fine, fine, and medium sand. The frequency of silt and sand beds fluctuates through the unit, but no medium sand was recovered above 143 mbsf. Log data suggest that sand is common in the interval of poor recovery in the lower half of the subunit, notably at 122–128 mbsf and 158–180 mbsf. Subunit IID (182.00–191.60 mbsf) consists of mud with thin beds and lami-

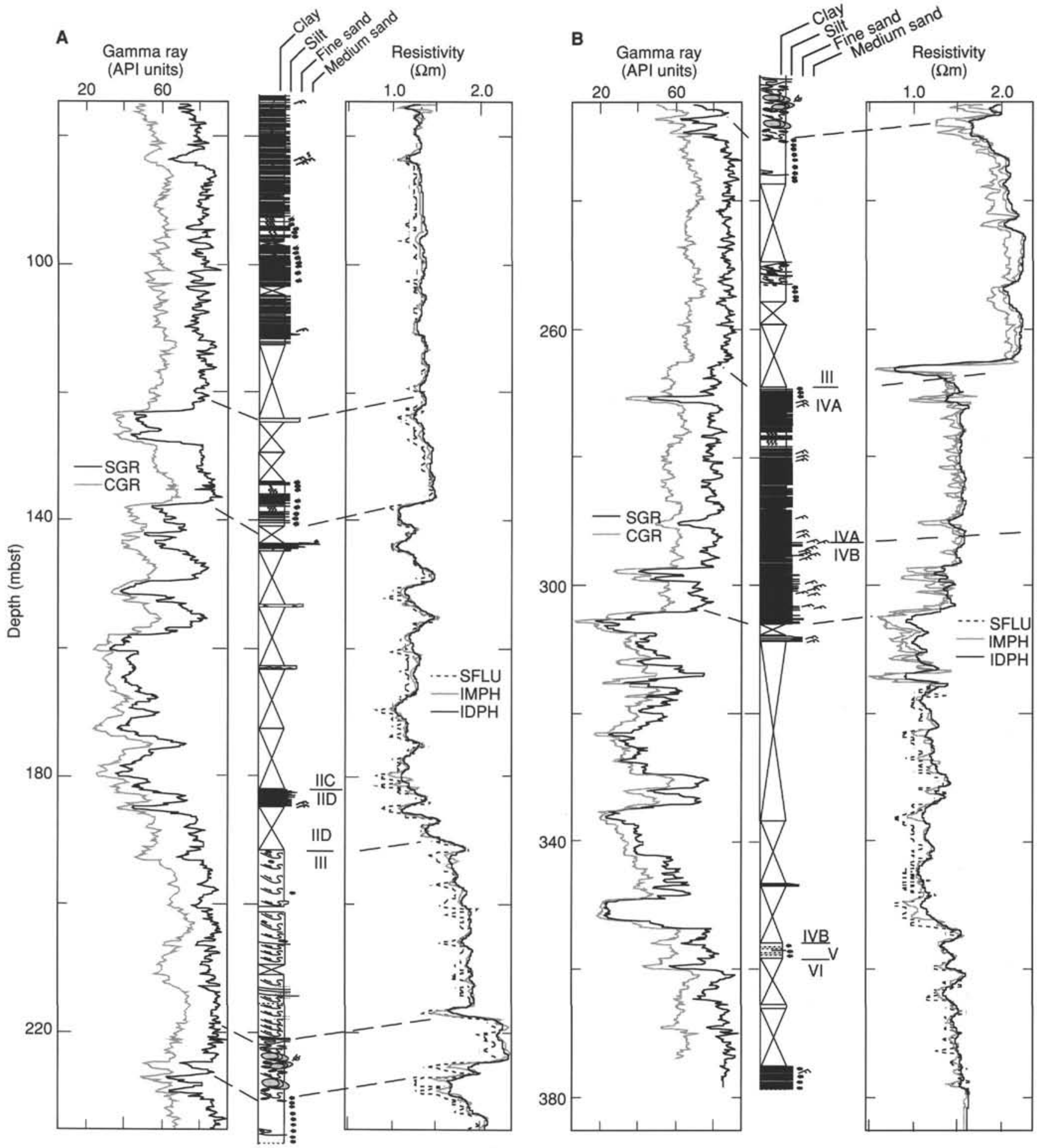

Figure 28. Comparison of gamma-ray and resistivity logs to visual core descriptions for Hole 944A. **A.** 75–235 mbsf. **B.** 225–385 mbsf.

nae of silt and thin beds of fine sand. Log data suggest that this subunit forms a coarsening-upward sequence.

Unit R Debris Flow (Unit III)

Unit III (191.60–268.70 mbsf) consists of various types of mud that appear to occur as blocks and have been affected by soft-sediment deformation. Many carbonate-rich clasts are found in the upper and middle parts of the unit. This unit is interpreted as a mass-transport deposit that correlates seismically with the Unit R Debris Flow. Log data show generally rather uniform gamma-ray response, except for a washed-out interval at 226–233 mbsf. High resistivity from 218 to 226 mbsf corresponds to an interval with large numbers of carbonate-rich clasts in cores. Color-reflectance data suggest that the interval 192–220 mbsf is compositionally different from 230–260 mbsf.

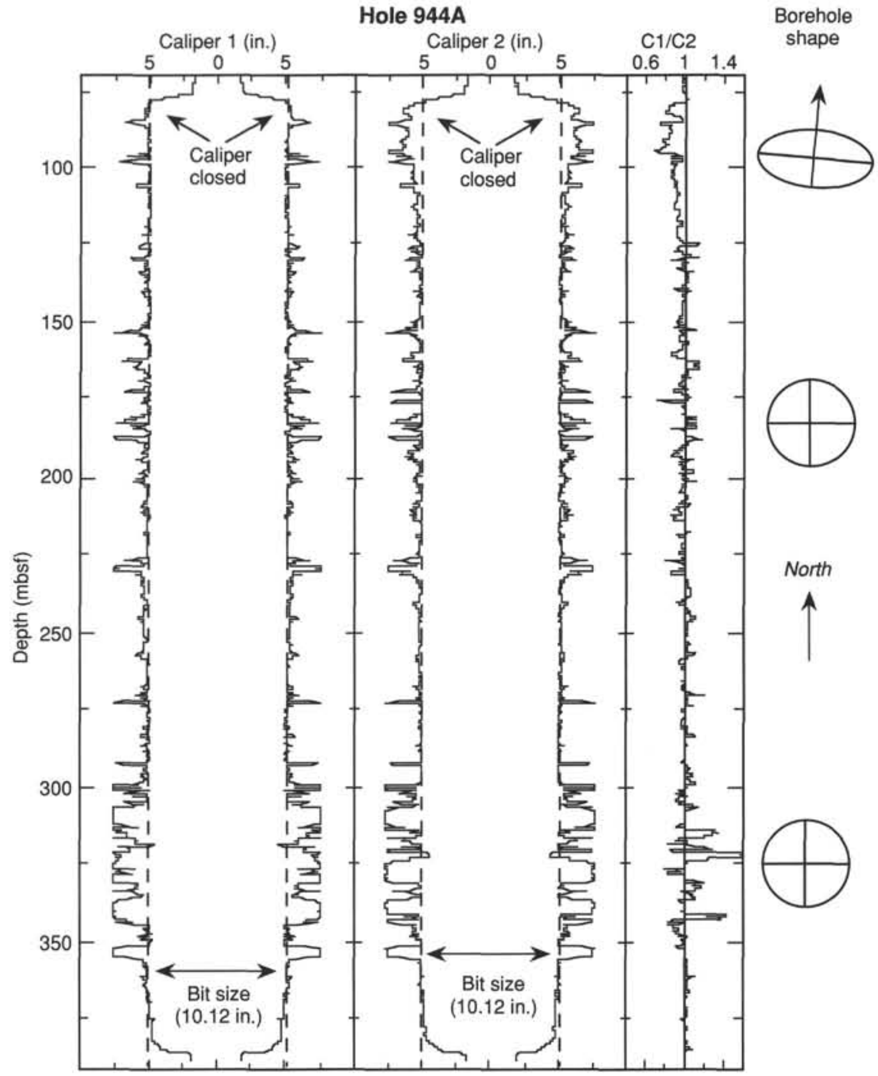

Figure 29. FMS caliper data (C1, C2, and ratio C1/C2) from Run 1, and summary of the shape and orientation of the borehole (right) determined from the azimuth of C1. (Arrow on borehole shape shows orientation of Pad 1.)

Levee of the Red Channel-levee System (Subunit IVA)

Subunit IVA (268.70–293.07 mbsf), which consists of bioturbated and color-banded mud with abundant laminae of silt, correlates seismically with the levee of the Red Channel-levee System.

HARP of the Red Channel-levee System (Subunit IVB)

The HARP underneath the Red Channel-levee System is correlated seismically with Subunit IVB (293.07–355.40 mbsf). This subunit consists of mud with numerous silt laminae and thin beds of silt and very fine sand. Only 1 m of core was recovered in the lower 47 m of this subunit, and logs suggest that the base of the subunit is at 352 mbsf. The large borehole diameter through this subunit affected the quality of log data. Log characteristics in general are similar to those in the lower part of Subunit IIC and suggest that there are several coarsening-upward sequences.

Interglacial Carbonate-rich Clay (Unit V)

Unit V (355.40–357.53 mbsf) contains two short intervals of nannofossil-foraminifer-rich clay, with up to 17% carbonate content, passing both uphole and downhole into nannofossil-bearing clay. The entire unit suffered severe coring disturbance. Wireline log data suggest that this lithology extends uphole to about 352 mbsf.

Levee of the Green Channel-levee System (Unit VI)

Unit VI (357.53–384.20 mbsf) consists of mud with laminae and thin beds of silt. It correlates seismically with the levee of the Green Channel-levee System. Log data suggest a downhole increase in the abundance of silt.

Implications

Short-wavelength oscillations in magnetic inclination, declination, and remanence intensity were detected throughout the APC cores, with generally 2–4 cycles per meter. These oscillations are interpreted as geomagnetic secular variation. No magnetic excursion was found in APC cores.

Foraminifer and nannofossil abundances are generally high in Units I and V, and in some calcareous clasts in Unit III. Otherwise, nannofossils are almost absent and foraminifers are in low abundance in Subunits IIA and IIB and Unit VI, and rare to absent in Subunits IIC and IID and Unit IV. *P. obliquiloculata* was not detected above the Unit III debris-flow deposit, but this could result from the low for-

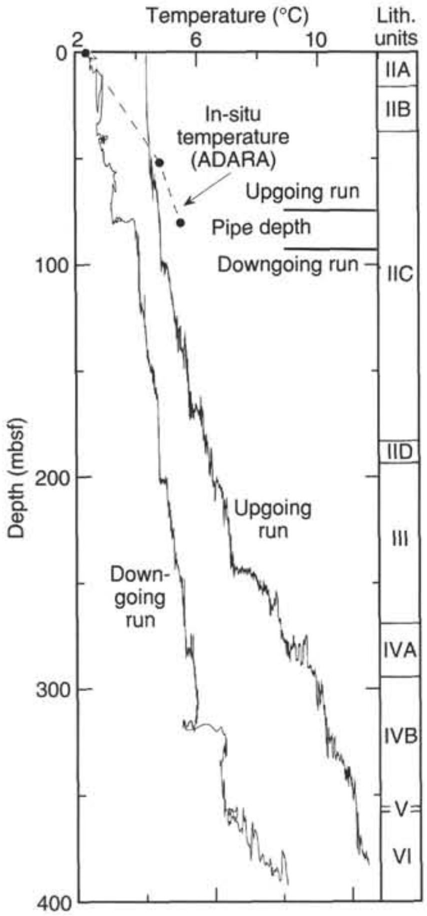

Figure 30. Borehole temperature log from the TLT and formation temperature from ADARA for Hole 944A.

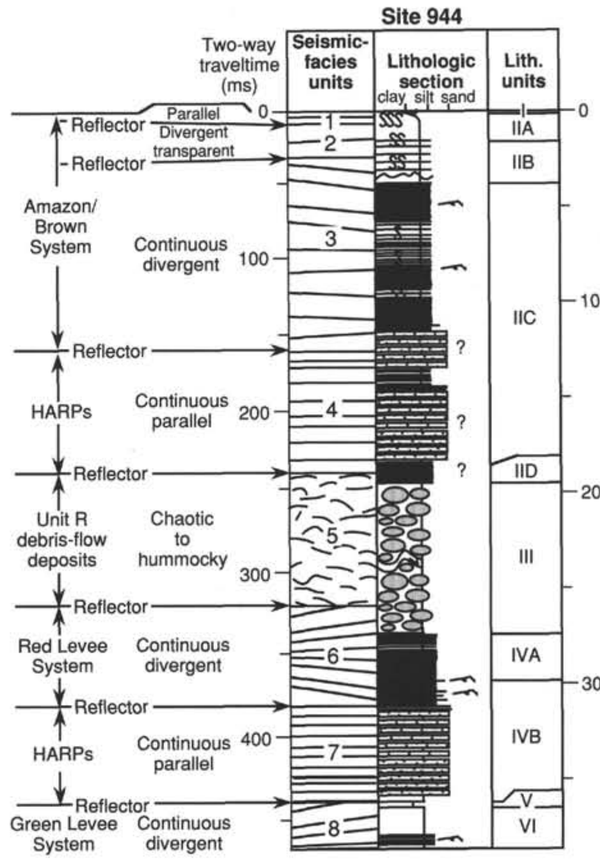

Figure 31. Correlation of lithostratigraphic observations with seismic-facies units and prominent reflections at Site 944.

aminifer abundance. Some clasts in Unit III contain well-preserved nannofossils of Zone CN15a, which indicate that the debris-flow deposit is older than 85 ka. These assemblages resemble those in Unit III of Site 942.

In Unit V, the well-preserved and abundant nannofossils, dominated by *Gephyrocapsa,* and foraminifers including *G. tumida* and *G. tumida flexuosa* indicate interglacial conditions. The nannofossils are of Zone CN14b and are similar to those sampled at depth at Sites 935 and 936. They might date from either isotopic Stage 9 or 11. Because seismic correlation indicates that Unit IV at Site 931, also from Zone CN14b, is at a deeper stratigraphic level, Unit V at Site 944 is probably from isotopic Stage 9.

Holes 944B, 944A, and 944D are spaced at about 300-m interval in a traverse down the levee flank. Hole 944B is estimated to be only 300 m from the levee crest on the outside of a meander bend. Lithologic features provide a tentative correlation between the three holes and suggest that silt laminae 5–10 mm thick in Holes 944A and 944B could be equivalent to beds 1–5 cm thick in Hole 944D. These substantial changes in silt bed thickness and abundance over distances of a few hundred meters, together with data from Site 943 in the adjacent channel, will permit analysis of turbidity-current flow dynamics and deposition.

Site 944 sampled a stratigraphic section similar to Site 936, but farther down-fan. Units II and IV, corresponding to levee and HARP sediment in the Upper and Middle Levee complexes, respectively, were sandier than at Site 936. Some Bouma T_{bcde} turbidites occur in the lower part of Subunit IIC. The Unit III mass-transport deposit is thinner and has a higher proportion of decimeter- to meter-sized blocks compared with Site 936.

A detailed pore-water profile in Hole 944D showed that alkalinity peaks at 4.4 mbsf (22 mM), decreases to 10 mM by 10 mbsf, and then remains approximately constant. Pore-water sulfate decreases to zero by 4.4 mbsf; at the same depth, phosphate peaks at 0.4 mM. Dissolved iron concentrations are variable. Pore-water geochemical profiles at this site change more rapidly with depth than at Sites 931 and 939.

Elevated total sulfur (0.5%–1.5%) was measured in the lower part of Unit III (debris flow) and the lower part of Unit V. Total organic carbon decreases from about 0.9% in Unit II to 0.7% in Unit VI. Log data show anomalously low values of velocity from 305 to 315 mbsf, which may indicate higher concentrations of gas in the formation. Cores from this interval had an unusual number of gas-filled voids.

An interval from 17 to 22 mbsf shows almost constant water content and does not appear to have undergone normal compaction. Similar intervals were identified near the top of holes at Sites 939 and 940. The detailed samples of reactive iron minerals taken at this site may help determine if these zones of constant water content are related to diagenesis.

There is a wide scatter of index values in the upper part of Hole 944A. Mean grain density increases downhole from 2.71 g/cm³ at the mud line to 2.80 g/cm³ at 90 mbsf and appears independent of sand abundance.

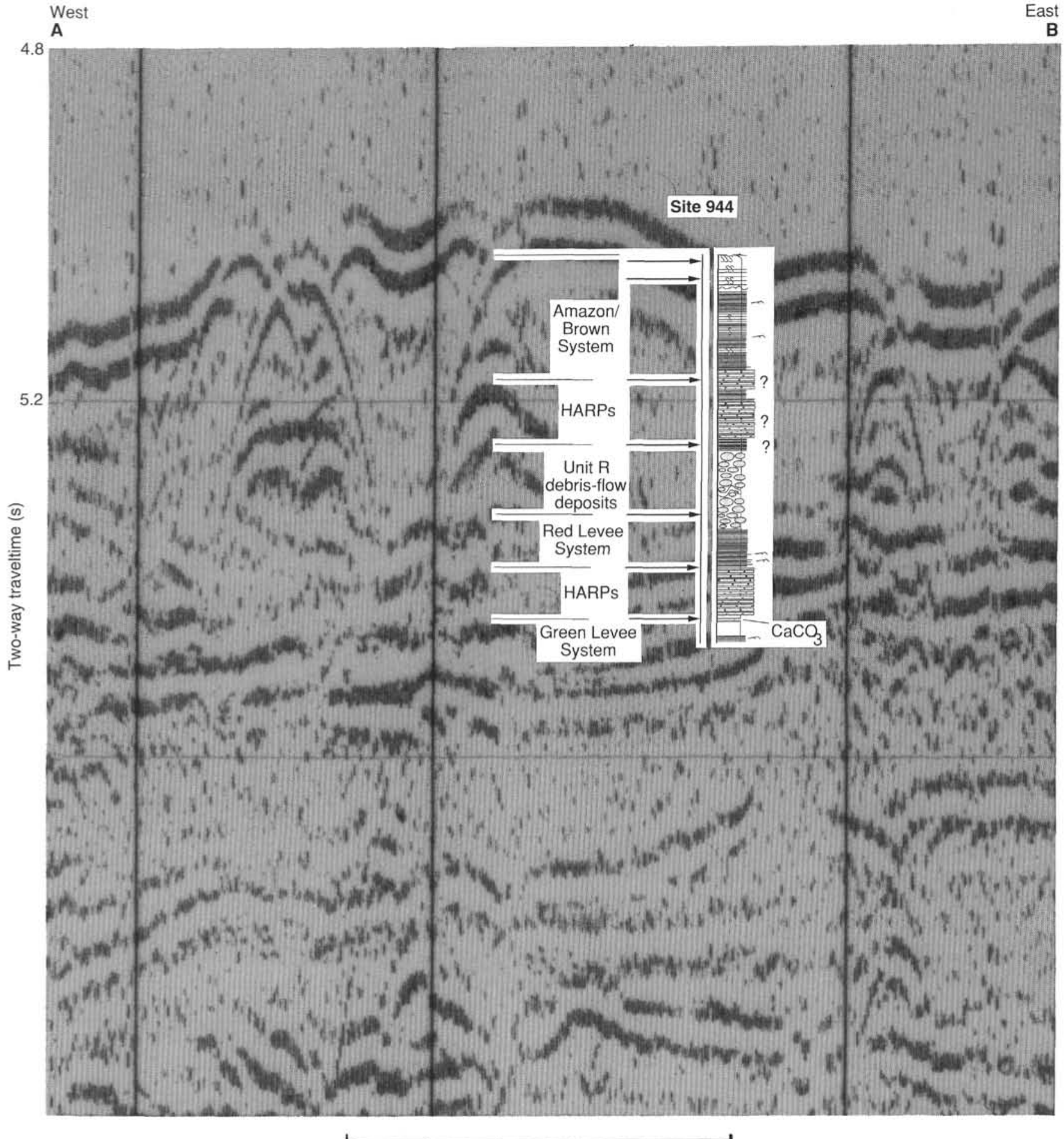

Figure 32. Seismic-reflection profile showing the location of Site 944, corresponding lithostratigraphic section and prominent reflections (arrows) that bound the seismic-facies units (Fig. 31). Question marks indicate intervals of poor recovery where lithology is inferred from logging data. Carbonate-rich zone near the base of the hole is indicated. Location of profile shown in Figure 1, "Site 943" chapter, this volume.

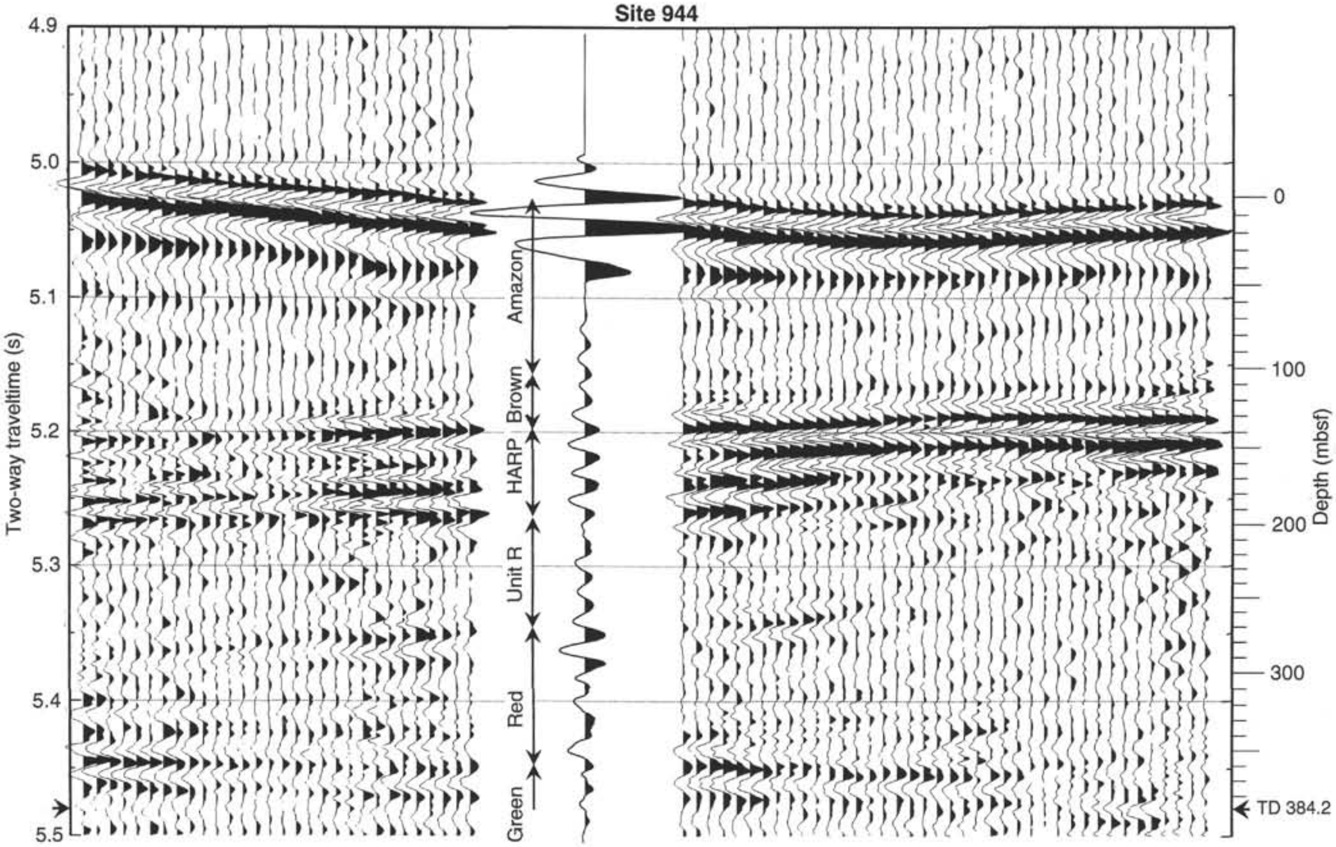

Figure 33. Synthetic seismogram for Site 944.

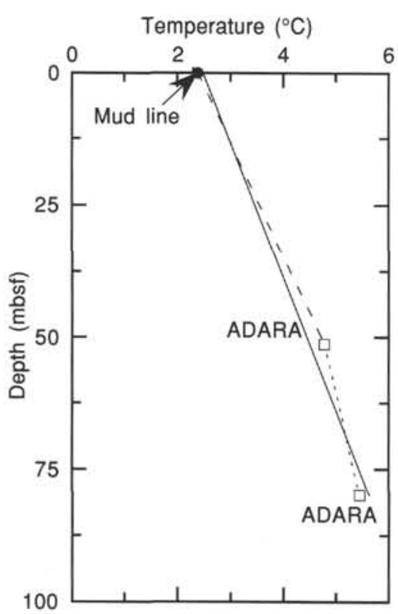

Figure 34. Estimated equilibrium temperatures in Hole 944A. A linear curve fit (solid line) through the data suggests that reliable equilibrium temperatures were acquired that indicate a geothermal gradient of 39.4°C/km. A geothermal temperature gradient of 46.75°C/km is calculated (dashed line) by using the ADARA mud-line temperature, and the one ADARA measurement at 51.4 mbsf. A geothermal temperature gradient of 23.47°C/km is calculated (dotted line) by using both ADARA measurements.

REFERENCES*

Bouma, A.H., 1962. *Sedimentology of Some Flysch Deposits: A Graphic Approach to Facies Interpretation:* Amsterdam (Elsevier).

Damuth, J.E., 1977. Late Quaternary sedimentation in the western equatorial Atlantic. *Geol. Soc. Am. Bull.,* 88:695–710.

Flood, R.D., Manley, P.L., Kowsmann, R.O., Appi, C.J., and Pirmez, C., 1991. Seismic facies and late Quaternary growth of Amazon submarine fan. *In* Weimer, P., and Link, M.H. (Eds.), *Seismic Facies and Sedimentary Processes of Submarine Fans and Turbidite Systems:* New York (Springer), 415–433.

Manley, P.L., and Flood, R.D., 1988. Cyclic sediment deposition within Amazon deep-sea fan. *AAPG Bull.,* 72:912–925.

Pirmez, C., 1994. Growth of a submarine meandering channel-levee system on the Amazon Fan [Ph.D. thesis]. Columbia Univ., New York.

*Abbreviations for names of organizations and publications in ODP reference lists follow the style given in *Chemical Abstracts Service Source Index* (published by American Chemical Society).

Ms 155IR-120

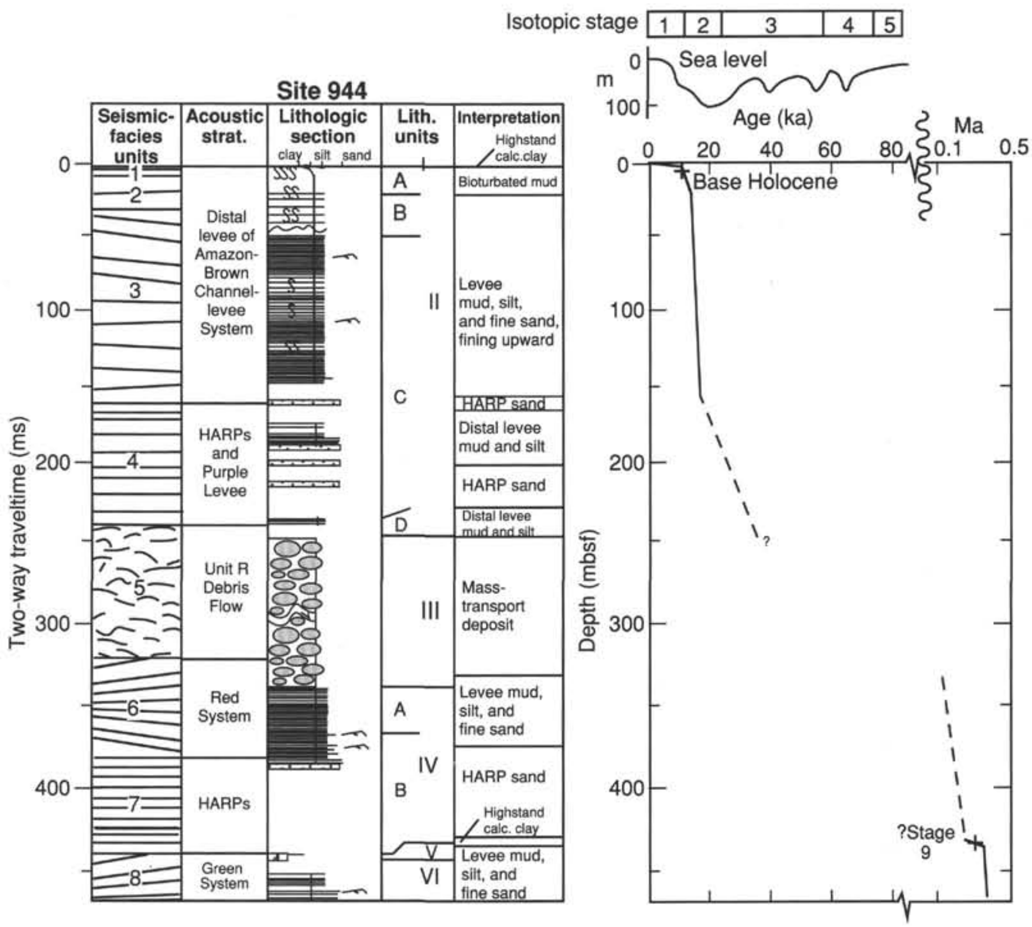

Figure 35. Summary of Site 944 showing (left to right) seismic-facies units, acoustic stratigraphy, schematic lithologic column, lithologic units, interpreted sediment facies, chronological picks, and interpreted age-depth curve (+ = datums; variations in slope between these points are interpreted, based on dated intervals of similar facies at other sites).

NOTE: For all sites drilled, core-description forms ("barrel sheets") and core photographs can be found in Section 4, beginning on page 703. Forms containing smear-slide data can be found in Section 5, beginning on page 1199. GRAPE, index property, magnetic susceptibility, and natural gamma data are presented on CD-ROM (back pocket).

SHORE-BASED LOG PROCESSING

Hole 944A

Bottom felt: 3712.6 mbrf
Penetration: 384.2 mbsf
Total core recovered: 208.01 (54%)

Logging Runs

Logging string 1: DIT/LSS/HLDT/CNT/NGT
Logging string 2: FMS/GPIT/NGT (two passes)
Wireline heave compensator was used to counter ship heave.

Bottom-hole Assembly (BHA)

The following BHA depths are as they appear on the logs after differential depth shift (see **Depth shift** section below) and depth shift to the seafloor. As such, there might be a discrepancy with the original depths given by the drillers on board. Possible reasons for depth discrepancies are ship heave, use of wireline heave compensator, and drill string and/or wireline stretch.

DIT/HLDT/LSS/CNTG/NGT: BHA at ~75.5 mbsf.
FMS/GPIT/NGT: BHA at ~74.5 mbsf.

Processing

Depth shift: All original logs have been interactively depth shifted with reference to NGT from FMS/GPIT/NGT (pass 2), and to the seafloor (–3711.6 m). The amount used to depth shift the data to the seafloor corresponds to the seafloor depth observed on the FMS logs used as depth reference. It differs 1 m from the bottom-felt depth. A list of the amount of differential depth shifts applied at this hole is available upon request.

Gamma-ray processing: NGT data have been processed to correct for borehole size and type of drilling fluid.

Acoustic data processing: No re-processing necessary due to the good quality of the logs.

Quality Control

During the processing, quality control of the data is mainly performed by cross-correlation of all logging data. Large (>12 in.) and/or irregular borehole affects most recordings, particularly those that require eccentralization and a good contact with the borehole wall (CNTG, HLDT). Due to the irregular nature of the borehole, the density data are of generally low quality, particularly below 268 mbsf.

Hole diameter was recorded by the hydraulic caliper on the HLDT tool (CALI), and the caliper on the FMS string (C1 and C2). As the HLDT caliper started closing at about 88 mbsf, no density data could be corrected for borehole size between this depth and the bottom of the pipe at 75.5 mbsf, and therefore is not presented.

Data recorded through pipe (such as the CNTG and NGT data above 75 mbsf) should be used only qualitatively because of the attenuation on the incoming signal. Erroneous NGT spikes were detected at 59–60 mbsf.

Note: Details of standard shore-based processing procedures are found in the "Explanatory Notes" chapter, this volume. For further information about the logs, please contact:

Cristina Broglia
Phone: 914-365-8343
Fax: 914-365-3182
Email: chris@ldeo.columbia.edu

Elizabeth Pratson
Phone: 914-365-8313
Fax: 914-365-3182
Email: beth@ldeo.columbia.edu

944A Natural Gamma Ray-Resistivity-Velocity Logging Data

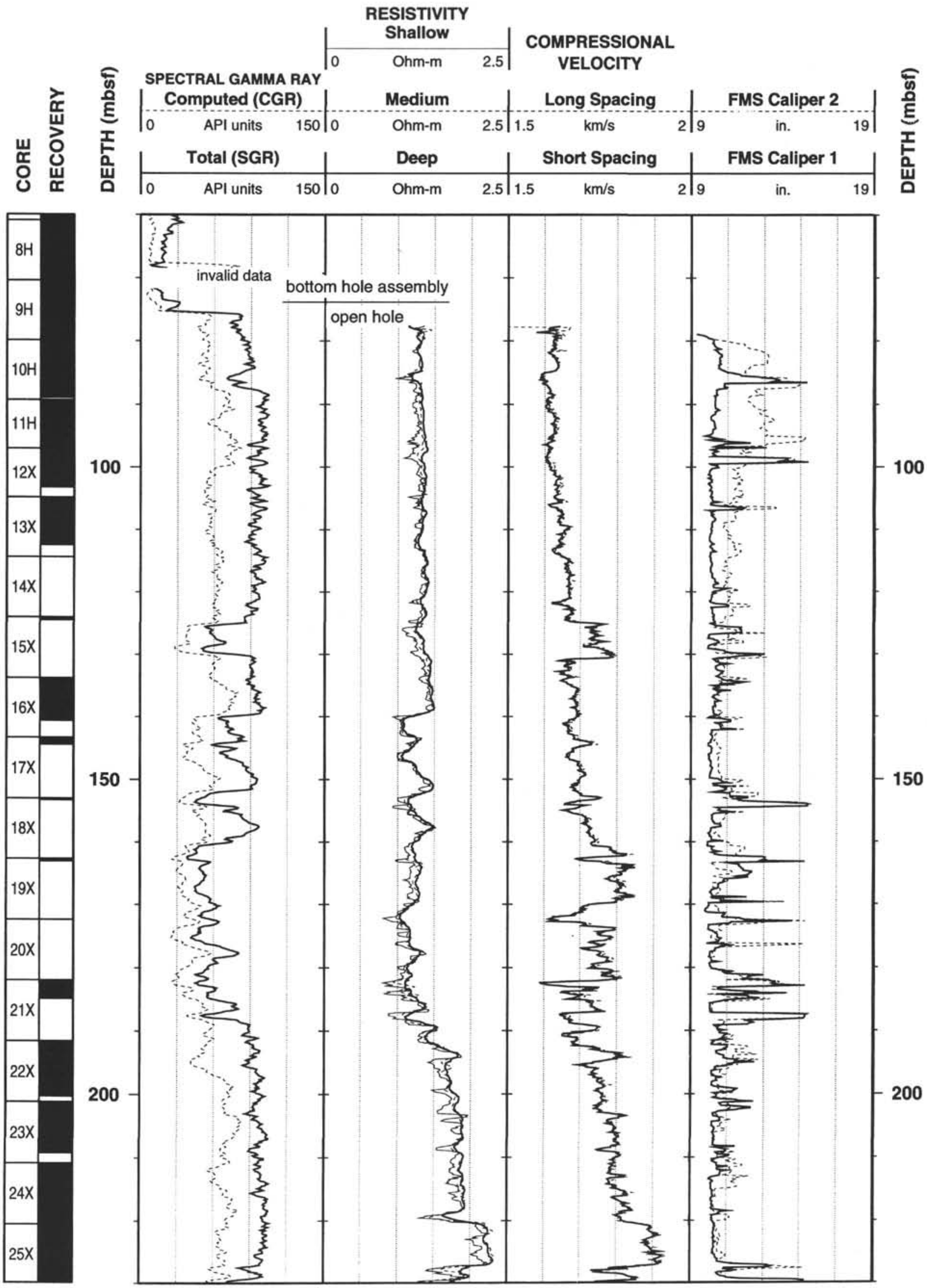

944A Natural Gamma Ray-Resistivity-Velocity Logging Data (cont.)

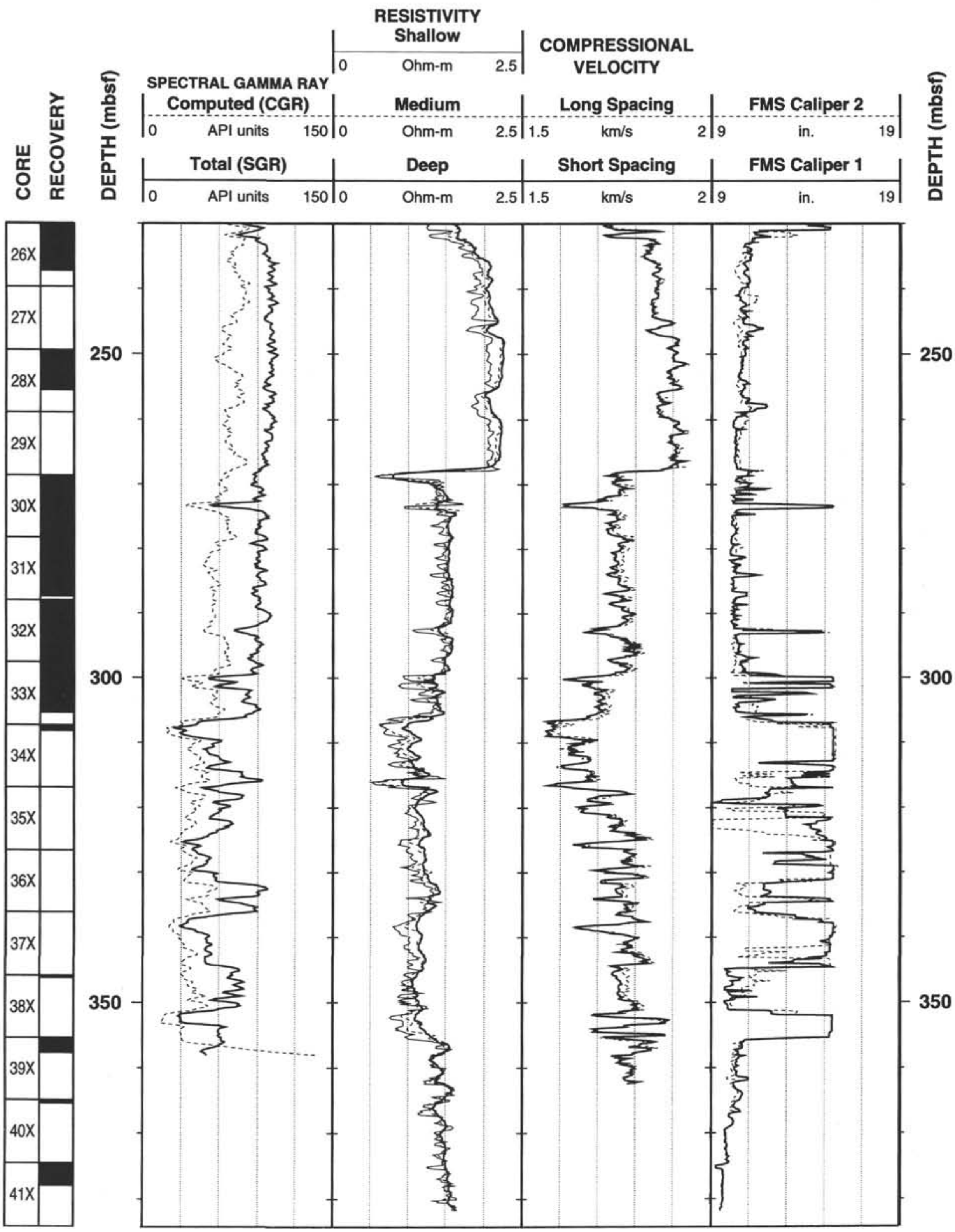

944A Natural Gamma Ray-Density-Porosity Logging Data

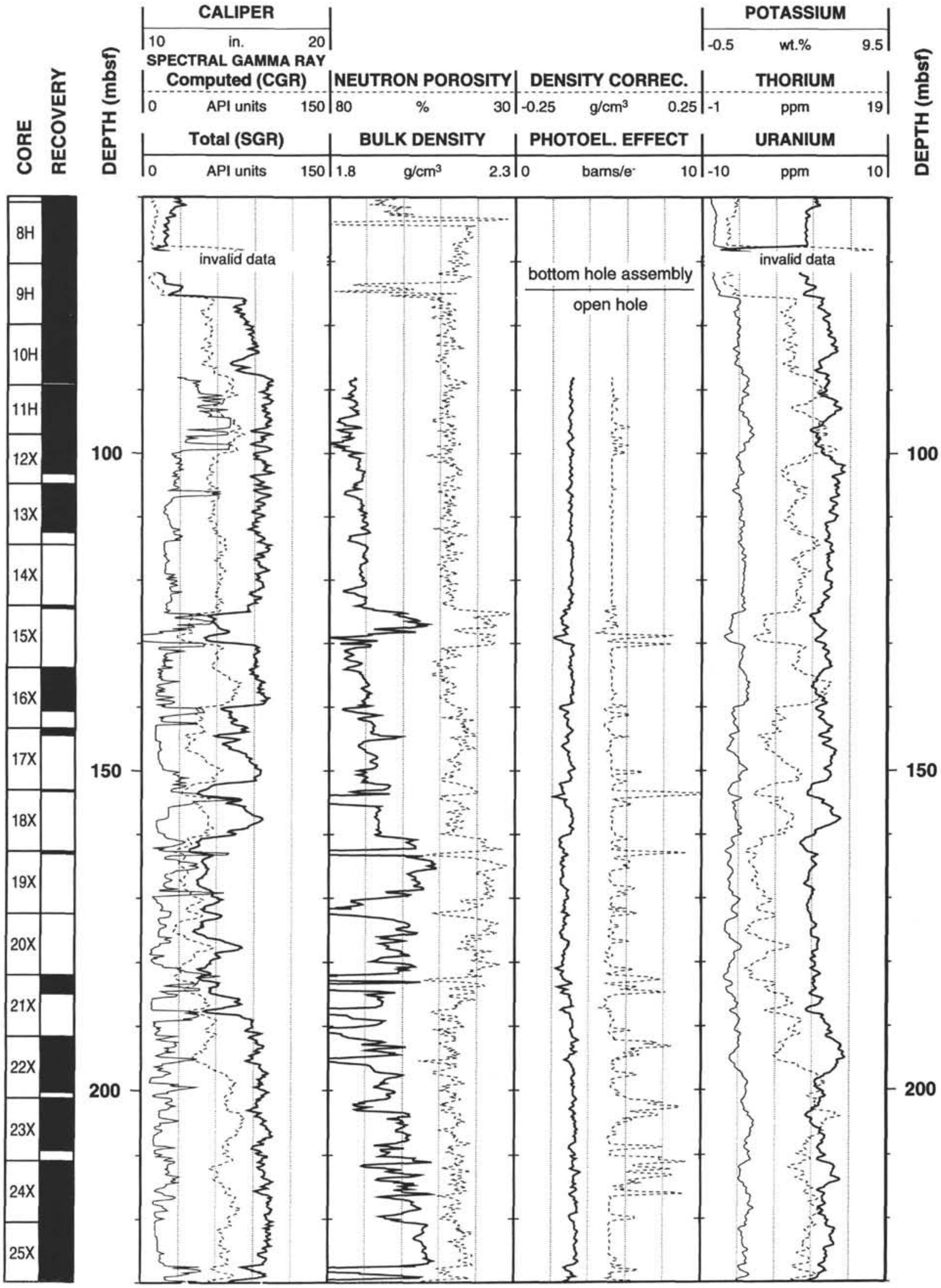

944A Natural Gamma Ray-Density-Porosity Logging Data (cont.)